

## Insights into the application of carbon materials in heterojunction solar cells



Youtian Mo <sup>a,c</sup>, Xi Deng <sup>a,c</sup>, Peixin Liu <sup>a,c</sup>, Jiansen Guo <sup>a,c</sup>, Wenliang Wang <sup>a,c,\*</sup>, Guoqiang Li <sup>a,b,c,\*</sup>

<sup>a</sup> State Key Laboratory of Luminescent Materials and Devices, School of Materials Science and Engineering, South China University of Technology, Guangzhou 510640, China

<sup>b</sup> Guangdong Choicore Optoelectronics Co., Ltd., Heyuan 517003, China

<sup>c</sup> Department of Electronic Materials, School of Materials Science and Engineering, South China University of Technology, Guangzhou 510640, China

### ARTICLE INFO

#### Keywords:

Carbon materials  
Solar cells  
Heterojunction  
CNTs  
Large-area  
Flexible

### ABSTRACT

The design of carbon material-based heterojunction solar cells (HJSCs) provides a promising approach to convert and collect solar energy. With unique photonic, electronic and mechanical properties, versatile carbon materials have attracted considerable attention in the design of heterojunction structures because of the multi-functional applications of carbon materials in the booming field of photovoltaics (PVs). Significant effort has been devoted to enhancing the light absorption capacity and charge/carrier transporting ability to obtain state-of-the-art HJSCs. This review presents the basic application of various carbon materials for PVs and the basic principles of carbon materials in HJSCs. Several optimisation methods for carbon nanotube (CNT) film modification and cell performance, such as optical property and Fermi level tuning, as well as morphological design and interface engineering, are highlighted in a summary of the state-of-art progress of CNT-based HJSCs. Moreover, the representative applications of carbon materials based flexible HJSCs are discussed. Finally, promising pathways and prospects of CNTs in HJSCs and their advanced devices are proposed using film modification, mechanism modulation, and device design to achieve cost-effective, high-performance, and flexible solar cells (SCs).

### 1. Introduction

Photovoltaic (PV) devices based on solar energy conversion have made marked advances as an effective solution to the problem of energy exhaustion [1]. The first PV device was fabricated in the mid-20th century with a photovoltaic conversion efficiency (PCE) of only 6%, which was the prelude to the research and exploitation of solar cells (SCs) [2]. From large-scale power plants to domestic roof SCs, and the energy supply system of aircraft, their field of application is constantly expanding [2]. Various PV devices have emerged as a result of continuous research. The most commonly used PV devices are perovskite SCs (PSCs), which have a PCE of more than 25% [3]. Si-based SCs lead the solar energy market and have a PCE of more than 26.7% [4].

Dye-sensitized SCs (DSSCs) are suitable for indoor application environments [5] and copper-based DSSCs show an impressive PCE of 13.5% [6]. Organic SCs (OSCs) can achieve > 19% PCE because of the refined double-fibril network morphology [7]. Cu<sub>2</sub>ZnSnS<sub>4</sub> SCs have a best reported PCE of 12.6% [8] in the literature. Notably, III-V compound semiconductor-based SCs such as single GaAs-based SCs, have the highest PCE of 29.1% [9], which is close to the highest theoretical PCE of 33.7% [10]. Moreover, their hybrid multi-junction SCs (Si/III-V or Ge/III-V) [11], termed tandem SCs (TSCs), which are expected to break through the Shockley-Queisser limit, such as GaAs/perovskite, Si/perovskite, GaTe/perovskite, organic-inorganic perovskite TSCs [12], and flexible thin film SCs [13], have been widely investigated recently.

In recent years, carbon materials as versatile materials in PV devices,

**Abbreviations:** HJSCs, heterojunction solar cells; CNTs, carbon nanotubes; PVs, photovoltaics; PCE, photovoltaic conversion efficiency; SCs, solar cells; PSCs, perovskite SCs; DSSCs, dye-sensitized SCs; OSCs, organic SCs; TSCs, tandem SCs; CQDs, carbon quantum dots; *a*-C, amorphous carbon; CNFs, carbon nanofibers; ARC, antireflection coating; MJSCs, multi-junction SCs; QDSCs, quantum dot sensitised SCs; *V*<sub>oc</sub>, open circuit voltage; *J*<sub>sc</sub>, short-circuit current density; FF, fill factor; *V*<sub>bb</sub>, built-in voltage; EQE, external quantum efficiency; *R*<sub>s</sub>, sheet resistive; CVD, chemical vapor deposition.

\* Correspondence to: State Key Laboratory of Luminescent Materials and Devices, School of Materials Science and Engineering, South China University of Technology, Guangdong Choicore Optoelectronics Co., Ltd., Department of Electronic Materials, School of Materials Science and Engineering, South China University of Technology, Guangzhou 510640, China.

E-mail addresses: [wenliangwang@scut.edu.cn](mailto:wenliangwang@scut.edu.cn) (W. Wang), [msgli@scut.edu.cn](mailto:msgli@scut.edu.cn) (G. Li).

<https://doi.org/10.1016/j.mser.2022.100711>

Received 21 November 2022; Received in revised form 3 December 2022; Accepted 10 December 2022

Available online 26 December 2022

0927-796X/© 2022 Elsevier B.V. All rights reserved.

with extraordinary efficiency and low-cost fabrication, have attracted considerable attention because of their excellent electrical, chemical, and physical characteristics. The application of graphene, fullerene, porous carbon, carbon quantum dots (CQDs), amorphous carbon ( $\alpha$ -C), carbon nanofibers (CNFs), and carbon nanotubes (CNTs) can significantly improve the performance and stability of PVs [14]. Historically, the design of carbon materials/semiconductor heterojunctions was first reported in 1979 [15], providing an ideal path to break through the technical bottleneck of the increased energy level and lattice mismatch; the complex fabrication process; and the increasing cost of homogeneous junction SCs [16]. Representative carbon materials, such as graphene [17] and CNT thin films [18], were used as a carrier transport layer to prepare heterojunction solar cells (HJSCs) and substantial progress has been achieved. For example, an Si/graphene HJSC [19] with a PCE of 1.5% and a GaAs/graphene HJSC [20] with a PCE of 1.95% were first reported in 2010 and 2013, respectively. However, direct contact with the n-type absorber to form heterojunction would cause insufficient light absorption and excessive carrier recombination, which limits the photon-generated carrier injection/extraction.

Insufficient light absorption, band misalignment and interface defects have been considered the predominant factors responsible for poor performance. To optimise the carriers' transportation and mitigate their recombination losses, several empirical approaches, such as incident light management, band alignment optimization, and interface engineering have been considered. Currently, Si/graphene and GaAs/graphene HJSCs have been improved to the highest PCEs of 15.6% [21] and 18.5% [22], respectively, by adding antireflection coating (ARC) and applying electronic gating, respectively. CNTs with a high electron mobility of  $10^5 \text{ cm}^2/(\text{Vs})$  and conductivity of up to  $10^6 \text{ S/cm}$  [14] have already been employed in HJSC devices, showing an excellent PCE Si/CNTs and their highest PCE so far has reached 22.04% [23]. An increasing number of studies have confirmed the effectiveness of top-down engineering for high-efficiency carbon material-based HJSCs. For example, surface optical property tuning, Fermi level tuning, surface electrical property tuning, and interface engineering between the carbon materials and a semiconductor substrate. In particular, the advantages of carbon materials ensure their application toward large-area and flexible devices. However, functional layer optimization, junction design, and mechanism exploration for HJSCs or multi-junction SCs (MJSCs), as well as the technology promotion for large-area, flexible and stable HJSCs, should be a research focus. This review primarily summarizes the key role of various carbon materials in PV applications and their top-down optimization strategies for HJSCs, including incident light management, film optimization, and interface engineering. Furthermore, we introduce the prospects and challenges for advanced PV devices.

## 2. Key role of allotrope carbon materials in SCs

### 2.1. Common application strategies

Based on their unique configuration, the allotropes of carbon with different valencies can be divided into 0D, 1D, 2D and 3D. Therefore, the two most common application strategies for using carbon materials in SCs, one is to be used as substrate or dopant for functional composite layers, and another way is direct application in thin film for charge collector and carrier transporter. Fullerene, CQDs [24] and CNTs [25], as 0D and 1D carbon materials, could be used as an additive to prepare a functional layer, optimize the conductivity of pristine layers and modulate their carrier transporting process. On the other hand, carbon materials film, such as graphene, CNFs, CNTs,  $\alpha$ -C and their composites, can serve as electrode and carrier transporter. For instance, in Si/CNTs [26], GaAs/graphene [27] and Si/ $\alpha$ -C [28] HJSCs, carbon materials serve as a multi-functional layer for separating and transporting photo-generated carriers by forming the heterojunction with the semiconductor substrate [29]. Moreover, CNTs as charge collector has been

extensively used in PSCs [30], OSCs [31], thin-film SCs [32], DSSCs [33], quantum dot sensitised SCs (QDSCs) [34] and GaAs-based SCs [35], which is attributed to their high conductivity, high transmission and low interlayer resistant [36]. Such as Si/CNTs-CNTs strips HJSC [37], CNFs/Bi<sub>2</sub>S<sub>3</sub> in DSSCs [38] and GaAs/graphene/Al<sub>2</sub>O<sub>3</sub>/graphene HJSC [22]. In this section, the key role of various carbon allotropes for SCs will be introduced in detail, and the comparison of their corresponding PCE are listed in Table 1.

#### 2.1.1. Carbon material film as charge collectors in SCs

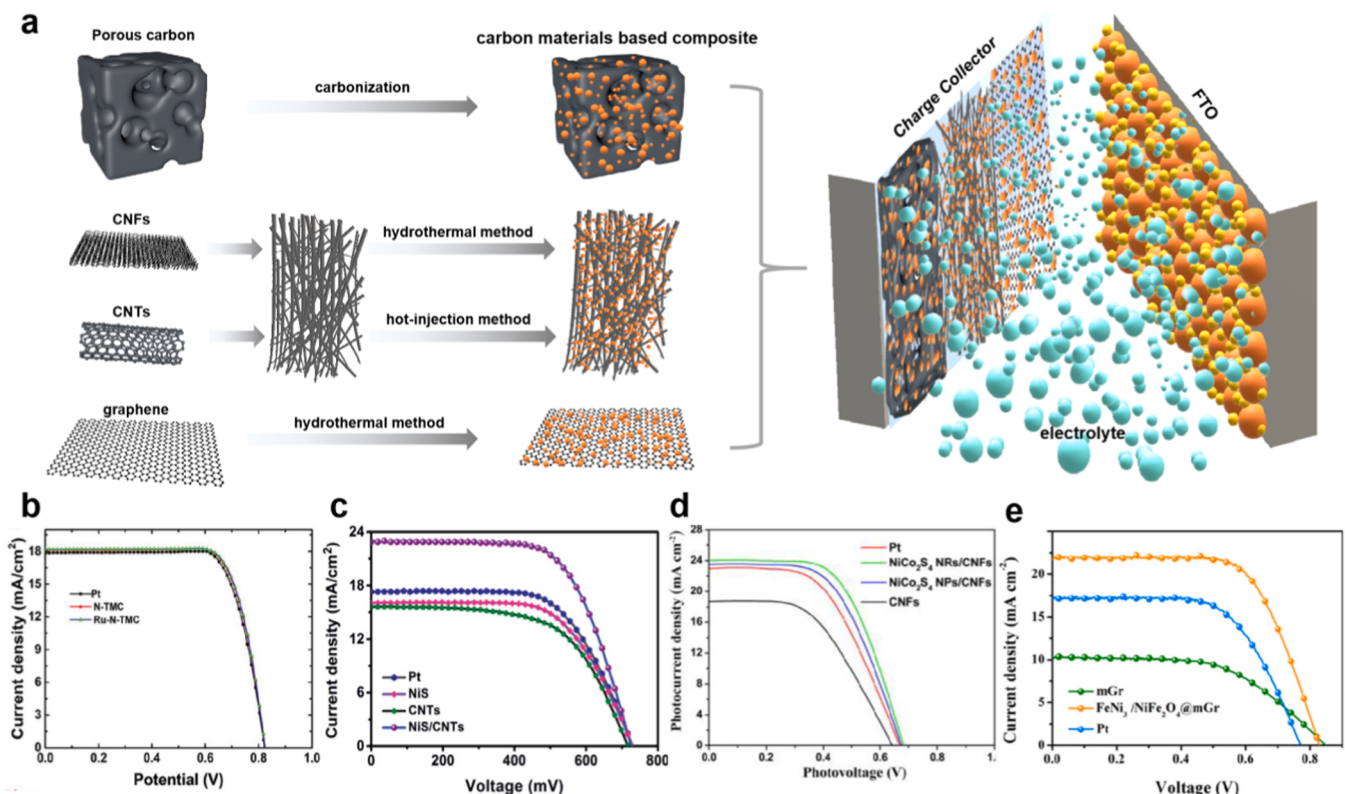
Increasing demands for deformable electronic technology, particularly flexible substrates and electrode materials that are essential for the mechanical flexibility of the device, are being presented with the development of flexible wearable electronic and energy storage devices. Metal nanowires, conductive polymers and carbon materials as well as their composites can be used as excellent electrodes in flexible SCs, instead of conventional metal oxide transparent conductors like indium-tin oxides, and hard glass substrate [39]. Porous carbon [40], CNTs [41], CNFs [42] and graphene [43] can be used for high catalytic particles deposition, replacing platinum electrodes in the electrochemical catalysis of DSSCs with the help of their excellent electrical conductivity and large specific surface area, as shown in Fig. 1a. For DSSCs, transition metal compounds with a poor conductivity and carbon materials with a poor catalytic activity could not achieve a satisfactory PCE and a perfect counter electrode with excellent electrocatalytic activity, high electrical conductivity and good durability. Therefore, several investigations focus on the carbon material-based composite counter electrode electrocatalysts [41]. N-doped carbon materials substrates reveal better conductivity and electrocatalytic activity because of electron transfer facilitated by the lone pair of electrons generated by N atoms and other atoms [44]. Kim et al. prepared Ru- and N-doped template-free mesoporous carbon (Ru-N-TMC) by direct carbonisation of ruthenium (III) acetylacetone [Ru(acac)<sub>3</sub>] with poly(butyl acrylate)-b-polyacrylonitrile (PBA-b-PAN) [40]. The PBA block was decomposed and transferred into the porous template during the carbonisation and stabilisation process. The PAN block eliminated as N-doped semi-graphitic carbon and Ru(acac)<sub>3</sub> was reduced to Ru particles anchored to N and O heteroatoms on a carbon substrate. In Fig. 1b, the slight  $J_{sc}$  boosts resulted from the ultra-low charge transfer resistance, Ru-N-TMC counter electrode exhibits a superior PCE of 11.42% compared to Pt (11.16%) in SGT-021/Co(bpy)<sub>3</sub><sup>2+</sup> based DSSCs [40].

Although the metal particles encapsulated into carbon materials prepared by pyrolysis protocol have received wide attention due to their excellent catalytic activity and stability, the types, size, amount and distribution of metal (alloy) as well as their compounds are difficult to control [41]. The facile *in situ* growth for a well-defined composite counter electrode structure is a good strategy to overcome it. Such as NiS nanoparticles embedded in CNTs are synthesised *via* hot-injection method, and its corresponding counter electrode exhibits superior catalytic activity to I<sub>3</sub><sup>-</sup> reduction with a PCE of 10.82% (Fig. 1c). The improved charge transfer mainly is ascribed to the stronger bonding between NiS nanoparticles and CNTs and the electron delocalisation from NiS to CNTs [41]. Moreover, various nanostructures have been prepared on carbon materials *via* electrospinning and hydrothermal or solvothermal strategy. NiCo<sub>2</sub>S<sub>4</sub> nanorods/CNFs and NiCo<sub>2</sub>S<sub>4</sub> nanoparticles/CNFs are prepared using a simple hydrothermal or solvothermal reaction. Vertically nanorods can expose more catalytic active sites from Ni and Co ions and facilitate faster electron transporting, thus obtaining a higher PCE of 9.47%, which is higher than of NiCo<sub>2</sub>S<sub>4</sub> nanoparticles (8.63%), Pt (8.18%) and CNFs (6.06%) [42], as shown in Fig. 1d. Heterogeneous FeNi<sub>3</sub>/NiFe<sub>2</sub>O<sub>4</sub> nanoparticles are the first to be reported as a catalytic site for carbon materials in I<sub>3</sub><sup>-</sup> reduction, and achieved a significant PCE of 12.14% (Fig. 1e) by modifying graphene *via* thermal solution method. The results show that the inserted nanoparticles can prevent the aggregation of nanosheets, provide additional catalytic active sites and enhance electrolyte diffusion. The

**Table 1**

Comparison of carbon materials in different types of SCs.

Role of carbon materials	Carbon materials	Configuration	Type of SCs	PCE (%)	Year	Refs.
Charge collector	mesoporous carbon	Ru-N-TMC	DSSCs	11.42	2020	[40]
	CNTs	NiS/CNTs	DSSCs	10.82	2019	[41]
	CNFs	NiCo <sub>2</sub> S <sub>4</sub> NRs/CNFs	DSSCs	9.47	2021	[42]
	Graphene	FeNi <sub>3</sub> /NiFe <sub>2</sub> O <sub>4</sub> @mGr	DSSCs	12.14	2021	[43]
	porous carbon nanocage	Co <sub>3</sub> S <sub>8</sub> /Ni <sub>3</sub> S <sub>8</sub> @C-N	DSSCs	8.91	2021	[44]
	Graphene	GaAs/G/Al <sub>2</sub> O <sub>3</sub> /G	GaAs	18.5	2015	[22]
	CNTs	n-GaAs/p-GaAs/CNTs	GaAs	11.5	2020	[45]
Carrier transportor (film)	CNTs	n-GaAs/CNTs (simulated)	GaAs	7.76	2016	[87]
	CNTs	n-GaAs/CNTs	GaAs	11.24	2022	[57]
	Graphene	n-GaAs/G/Al <sub>2</sub> O <sub>3</sub> /G	GaAs	18.5	2015	[22]
	Graphene	n-Si/MoS <sub>2</sub> /G	Si	15.8	2018	[50]
	CNTs	n-Si/CNT film	Si	18.9	2020	[48]
	Amorphous carbon	Si/CN-900/Ag nanowires	Si	7.67	2021	[54]
	Graphene	p-Si/G/HF/AlO <sub>x</sub>	Si	12.5	2018	[58]
Additive for active layer	Graphene	p-InP/G	InP	5.6	2015	[59]
	CNTs	Si/Nafion: CNTs	Si	22	2022	[23]
	CQDs	CQD/VAE	Si	17.86	2019	[69]
	CQDs	CQDs/CNTs	DSSCs	9.4	2021	[73]
	CQDs	CQDs/ZnO	Polymer SCs	9.64	2018	[71]
	CQDs	N,S-CQDs/ZnO	OSCs	9.31	2019	[77]
	Fullerene	D18-Cl: Y6: PC <sub>71</sub> BM	OSCs	17.97	2021	[83]
Fullerene	PM6: PY-IT: Tech-PCBM	all-Polymer SCs	16.16	2022	[82]	
	Fullerene	PC <sub>61</sub> B-TEG/ FA <sub>0.65</sub> MA <sub>0.35</sub> PbI <sub>x</sub> Cl <sub>3-x</sub>	PSCs	23.34	2022	[79]
	CQDs	CQDs/CH <sub>3</sub> NH <sub>3</sub> PbI <sub>3</sub>	PSCs	19.38	2019	[72]

**Fig. 1.** (a) Schematic diagrams and (b-e) J-V curves of porous carbon, CNTs, CNFs and graphene used as charge collectors in DSSCs.

Reproduced with permission [40]. Copyright 2020, The Royal Society of Chemistry. Reproduced with permission [41]. Copyright 2019, The Royal Society of Chemistry. Reproduced with permission [42]. Copyright 2021, Elsevier. Reproduced with permission [43]. Copyright 2021, Elsevier.

carbon material-based composite mentioned above could be further developed as an environmentally friendly, cost-effective and high-efficiency counter electrode for DSSCs.

Graphene and CNT films are also reported as top electrodes, which is ascribed to their high transmittance and excellent photoelectric performance. For the first time, CNT film has been used as top contact for GaAs SCs with an enhancement PCE from 10.6% to 11.5%, showing

better photocurrent collection ability and lower parasitic light absorption of the emitter layer than the metal contact grid. Moreover, avoiding the deposition of metal grid demand technologically energy-consuming process could significantly decrease the final device cost[45]. For GaAs/graphene HJSCs with graphene-dielectric-graphene structure, the top graphene layer serves as the gating electrode and the bottom graphene serves as hole transport layer. Combining the advantages of

antireflection property of  $\text{Al}_2\text{O}_3$  dielectric layer and electronic gating strategy, thus obtaining the highest PCE of 18.5% for GaAs/graphene system[22]. For conventional metal electrode, graphene and CNTs electrode with high transmittance could be regarded as effective alternatives to PV devices.

### 2.1.2. Carbon material film as carrier transportor in SCs

Among Si-based and III-V compound-based HJSCs,  $a\text{-C}$ , graphene and CNTs serve as carrier transportor for heterojunction structure, as shown in Fig. 2a. As a representative 1D carbon material, CNTs with a high theoretical specific surface area, high conductivity macroscopic quantum tunnelling effect and stable electrochemical properties are successfully used in solar photoelectric conversion systems at the end of the 20th century[46,47]. As shown in Fig. 2b, the first reported Si/CNTs HJSC with only a PCE of 1.31%[18]. The photogenerated current density is weak when solar light irradiates only CNT films without the presence of an n-Si substrate. The J-V curve in the dark shows a typical diode behaviour, indicating the creation of p-n junction of Si/CNTs heterojunction configuration. In particular, the characteristics of adjustable band gap and band alignment of CNTs enable it to prepare HJSCs. The use of CNT film is more operable and suitable for the preparation of large-size device, which has been confirmed in relevant studies[48]. Si/CNT film with back-junction design shows the highest PCE of 18.9%[48], allowing the entire wafer to be used as the active

area. The further development and the breakthrough of Si/CNT-based HJSCs would be introduced in detail in the later section.

Graphene has attracted the scientific community's attention since 2004, investigations on graphene/semiconductors have increased in recent years owing to their unique physical and chemical characteristics, high electron mobility, high current carrying capacity, good thermodynamic performance and strong chemical stability, particularly its energy band structure. The Dirac point in the graphene band structure is located at the Fermi level, so the internal electron is equal to the hole concentration[49]. The graphene surface will adsorb oxygen and water molecules in the air due to oxygen atoms' strong electron absorption ability. Graphene is in a state of electron loss, namely p-doping, which improves the conductivity in favour of the preparation of the device. As shown in Fig. 2c, 0.1  $\text{cm}^2$  and 0.5  $\text{cm}^2$  Si/graphene HJSCs are measured by a PCE of 1.65% and 1.34%[19], respectively. Recently, the introduction of the  $\text{MoS}_2$  layer functions as an electron blocking layer to suppress the carrier's recombination at graphene/n-Si interfaces, thus achieving a remarkable PCE of 15.8%[50].

$a\text{-C}$  has been extensively studied in the semiconductor field with low cost, low friction coefficient, high mechanical strength, high corrosion resistance and tunable band gap[51]. Several studies of  $a\text{-C}$  to combine with Si to form Schottky junction have been reported in the past few years[28,52]. The structural diagram of  $a\text{-C}$  based Schottky junction is shown in Fig. 2a and the first reported  $a\text{-C}$  was come up to be prepared

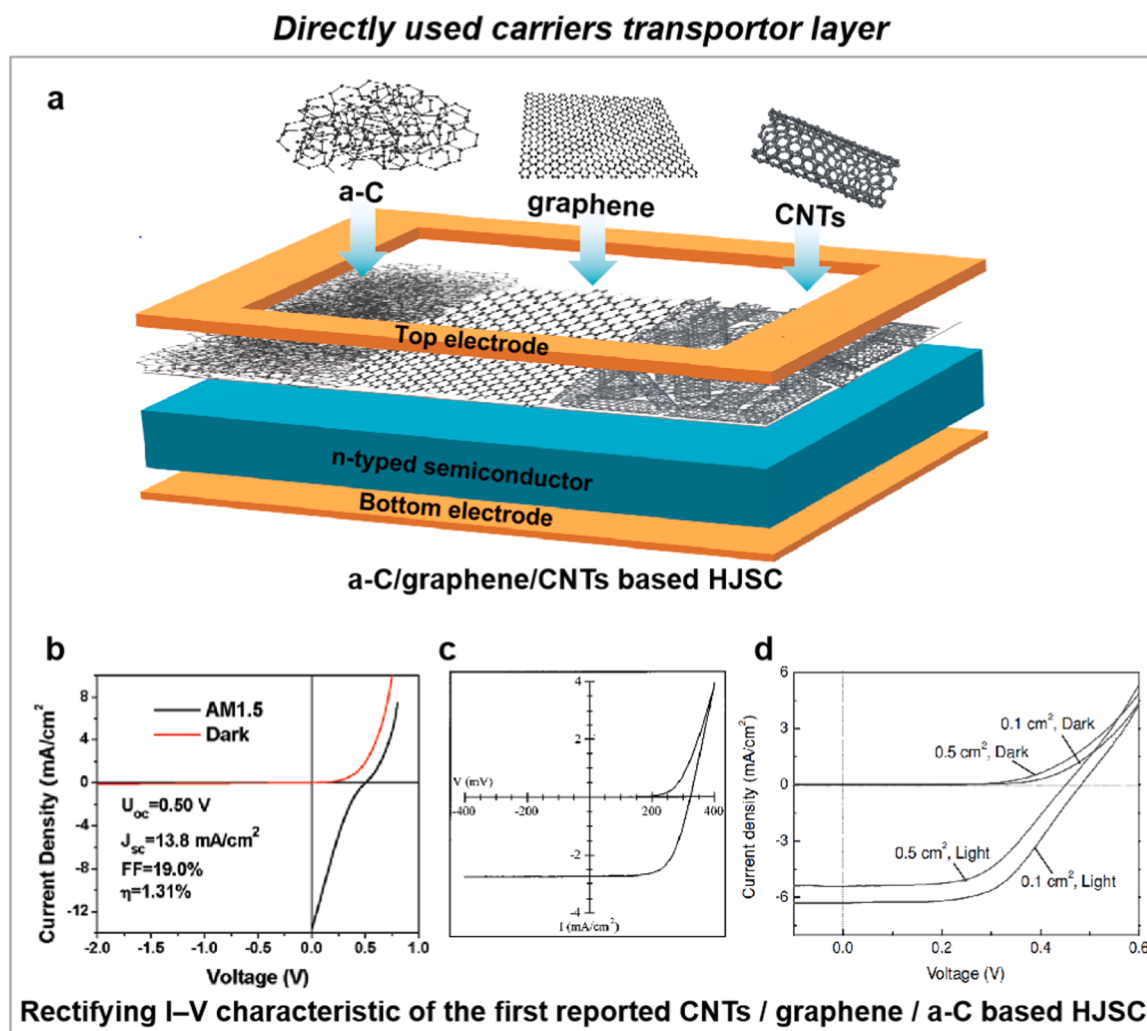


Fig. 2. (a) Schematic diagrams and rectifying J-V characteristic of (b) CNTs [18], (c) graphene [19] and (d)  $a\text{-C}$  [53] used in SCs.

Reproduced with permission. [18] Copyright 2007, American Chemical Society. Reproduced with permission. [19] Copyright 1996, AIP Publishing. Reproduced with permission. [53] Copyright 2010, John Wiley and Sons.

directly on Si substrate in 1996. The Si/*a*-C HJSC displayed a rectifying J-V characteristic in Fig. 2d and showed that the open circuit voltage ( $V_{oc}$ ), short-circuit current density ( $J_{sc}$ ), fill factor (FF) and PCE of 0.325 mV, 2.73 mA cm<sup>-2</sup>, 65% and 3.8%, respectively [53]. Kim et al. designed Schottky junction using Ag nanowires loaded with N-doped *a*-C, annealing at 900 °C to form SCs with a PCE of 6.17%, further improving to 7.67% of 0.2 wt%-Ag nanowires-C<sub>N</sub>-Si SCs. Ag nanowires network can effectively accelerate the desperation of carriers and reduce the interface resistance, demonstrating the effectiveness of the *a*-C application for Schottky junction preparation [54].

Moreover, GaAs with a wider band gap is used to replace Si substrate for achieving high PCE, such as GaAs/graphene HJSC (PCE=13.7%) modified by P3HT insertion layer [55] and their PCE reached 15.9% by employing self-assembled alkyl sulfur generation single molecular layer for inhibiting GaAs surface oxidation [27]. The highest value recorded for GaAs/graphene HJSC is 18.5% by depositing the Al<sub>2</sub>O<sub>3</sub> dielectric layer and applying electronic gating [22]. Otherwise, the PCE of the GaAs/CNT heterojunction is then found to be 3.8%. The n-GaAs/CNT heterojunction reveals a strong rectifying behaviour under the illumination, while ohmic-like contact formed in the p-GaAs/CNT heterojunction, which demonstrates the potential for n-GaAs/SWNT heterojunction in PVs field [56]. However, the research of GaAs/CNTs HJSCs is mainly focusing on the physical device modeling and PV characteristics simulation, which may be ascribed to the limitation of GaAs substrate and commercialization of CNT films. Recently, GaAs/CNTs van der Waals HJSC was fabricated by transferring p-type (6,5)-enriched SWCNT film onto the n-GaAs substrate, a pristine PCE of 7.23% is further enhanced to 11.24% by introducing Nafion as a highly

effective dopant [57]. On the other hand, graphene is also used as electron transportor and combined with the p-Si substrate to form HJSCs with a record PCE of 12.5% after depositing AlO<sub>x</sub> ARC and chemical doping [58]. InP with a suitable bandgap of 1.34 eV combined with graphene to form HJSC with a PCE of 3.3% in 2015 and a final PCE of 5.6% was obtained by Fermi level tuning of graphene [59]. Compared to electron transportor, the PCE performance of carbon materials/n-typed semiconductor HJSCs seems to be better. For bulk semiconductor-based HJSCs, studies on CNTs film-based are longer and the PCE is the highest. These studies indicate that simple coating on semiconductor processes is promising for realizing practical and efficient graphene/semiconductor Schottky junction SCs.

### 2.1.3. Carbon materials as additive for functional layer in SCs

Compared to conductive polymers or carbon materials such as graphene and CNTs, although metal oxides have good environmental stability, their poor conductivity is insufficient to prepare carrier transportor in high-efficiency SCs. However, due to their lower conductivity, polymers' direct contact with the active layer would significantly hinder the charge transportation, which brings about free carrier recombination and photocurrent losses. Thus, CNTs, CQD and fullerene are applied to be a dopant for the composite layer to solve the problem mentioned above.

To prepare the hole transport layer, CNTs have been developed for usage as an ingredient in polymers and metal oxides. The addition of CNTs can slightly improve the current density of Si/CNTs/Nafion HJSCs, like the CNTs/Nafion composite layer (Fig. 3a), and a high PCE (21%) is shown to be stable for just 20 min [23]. Using a simple encapsulation by

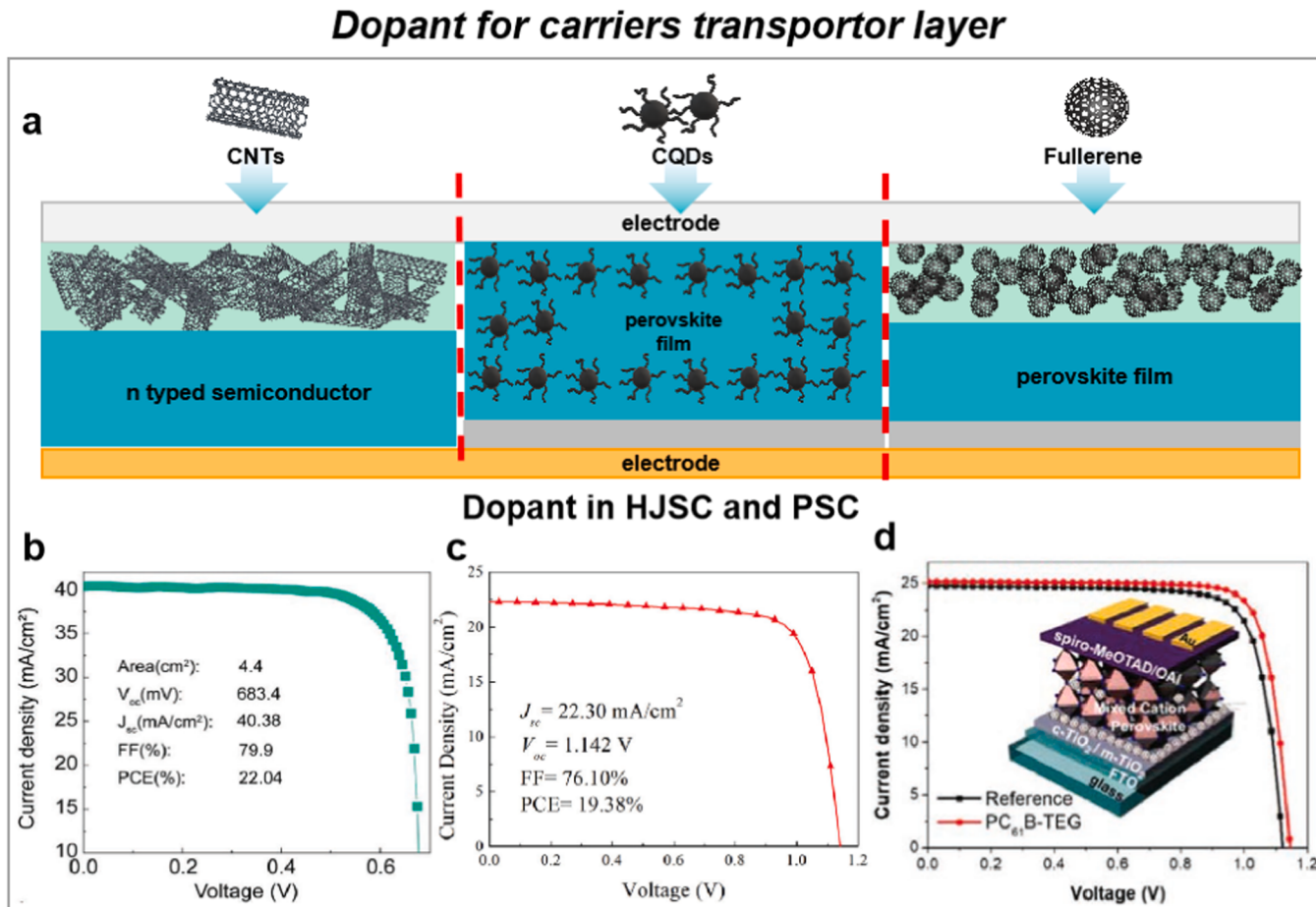


**Fig. 3.** (a) Schematic diagrams and J-V curves of (b) CNTs [23], (c) CQDs [78] and (d) Fullerene [79] used as dopants for Si SC, PSC and PSC, respectively. Reproduced with permission [23]. Copyright 2021, Wiley-VCH GmbH. Reproduced with permission. [78] Copyright 2021, Elsevier. Reproduced with permission [79]. Copyright 2022, John Wiley and Sons.

Nafion, the stability of CNT:Nafion mixed systems are studied by varying the content of water within the film and humidity of the external environment. A record PCE of 22%, a high FF of 83.4% and stable performance are achieved (Fig. 3b)[23]. Moreover, CNTs have attracted considerable attention for fabricating efficient PSCs by incorporating into Cu<sub>2</sub>ZnSnS<sub>4</sub> hole transport layer to enhance efficiency and stability of devices[60,61] or serve as a dopant to optimise the electrical performance of carrier transporter. Such as ZnO electron transport layer [62], NiO<sub>x</sub> [63] and MoS<sub>2</sub>[64] hole transport layer. The addition of CNTs would have an influence on the covalent and conduct band, together with the lowest unoccupied molecular orbital and highest occupied molecular orbital of MAPbI<sub>3</sub> to form a good pn junction. The huge band gap between CNTs decorated hole transport layer and perovskite thus forms the bigger potential barrier to inhibit the transition of electron, effectively forcing the separation and transportation of photogenerated carriers. Furthermore, as a potential nano-dopant candidate, CNTs could be mixed with polymers hole transport layer such as PEDOT:PSS or P3HT to enhance the photovoltaic performances of PSCs [65], OSCs [66] and organic/Si SCs [67].

CQDs, as a new frontier in the field of fluorescent nanomaterials, have found applications in SCs, LEDs and other related areas due to magnetic properties such as biocompatibility, low toxicity, eco-friendliness, good water solubility and photostability. The amorphous shell of CQDs, consisting of various functional groups (oxygen, amino-based groups or polymer chains, etc.), denies its unique optical properties and its ability to act as an electron-donor/acceptor and hole/electron transporter in energy conversion system [68], such as Si-based HJSCs [69], OSCs [70], polymer SCs [71], PSCs [72] and DSSCs [73]. The role of CQDs in PSCs are similar to CNTs introduced above, which can enhance the conductivity of active films and inhibit the combination of carriers while speeding up charge transport (Fig. 3a). The functional group on CQDs can react with Pb ions in the perovskite film for passivating the internal defects [24]. To inhibit the formation defects at the perovskite surface and grain boundaries, CQDs are originally introduced as an additive for the stabilization of MAPbI<sub>3</sub>. Lower trap-state density and better optoelectronic properties are obtained. A typical PCE increases from 17.59% to 18.81%, while the PCE of the optimised champion PSCs reaches 19.38% (Fig. 3c). This is achieved under ambient atmosphere without controlling the humidity for 4 months, which could be ascribed to the strong and stable interactions between CQDs and perovskite, and the contact between water and MAPbI<sub>3</sub> is blocked after introducing CQDs [72].

Additionally, the idea of doping CQDs to improve photo-excitation performance and electron concentration offers a viable application concept for increasing the performance of DSSCs at a reasonable cost. For example, the maltitol conversion of S-CQDs by a mild solution strategy and electrodeposition onto transparent metal selenide counter electrode for the fabrication of high-performance bifacial DSSCs. The bifacial DSSCs yield maximised front and rear efficiencies of 9.15% and 6.26%, respectively, ascribed to the significantly enhanced catalytic ability of S-CQDs tailored counter electrode, as the boost of photo-excitation and the increased electron density at electrode surfaces[74]. Similarly, N-CQDs are prepared by strawberry powders via mild hydrothermal method. Using co-sensitisation of nitrogen N-CQDs with N719 dye to make high-performance DSSCs featured by wide-spectral absorption and fast charge extraction. Higher PCE of 9.29% under one sun illumination is obtained due to the up-conversion and hole extraction behaviours of N-CQDs[75]. CQDs with varying Stokes shifts: blue-, green- and red-emissive CQDs could be obtained by modulating the surface states, which is achieved by varying the synthesis solvents. Red-emissive CQDs with the largest Stokes shift and better electrocatalytic activity are combined with CNTs for providing multi-dimensional charge transport channels, thereby preventing aggregation-induced quenching of the electrocatalytic activity and enhancing the conductivity. Finally, a record PCE of 9.4% is obtained for CQDs in DSSCs[73].

Moreover, the CQD interlayer could serve as both an electron blocking layer and hole transport layer to reduce the carrier recombination in Si/graphene HJSCs[76]. CQD/vinyl acetate-ethylene composite, a luminescent, transparent and strong cohesive film, could tune the solar absorption spectra and contribute to the PCE enhancement for mini crystalline Si module (17.86%), which contributes to strong UV absorption and consequential downshifting fluorescence of CQD/VAE [69]. For hole transportation, CQDs embedded in the P3HT:PC<sub>61</sub>BM layer as ternary components also provides a promising way for ternary OSCs [70]. In addition, Zhang *et al.* reported a solution-processable ZnO/CQDs electron extraction layer for polymer SCs, the application of CODs-based bilayer electron transport layer can suppress the exciton quenching by passivating the surface of ZnO. The reduced charge recombination and more efficient charge extraction probability can enhance the PCE to 9.64%, which is > 27% higher than that of the pristine cell (~7.59%)[71]. Similarly, N,S-CQDs is prepared by a simple hydrothermal treatment and lead to downconversion and excitation-dependent photoluminescence character for OSCs[77]. The cells with N,S-CQDs-modified ZnO electron transport layer showed a high PCE of 9.31%, which is attributed to the ZnO surface defect passivation by N,S-CQDs. The embedding of the N,S-CQDs can effectively facilitate the transportation and collection of photogenerated carriers by reducing the roughness and surface energy of the ZnO layer.

Fullerene and its derivatives have been seen as an additive (Fig. 3a) and are widely used in OSCs[80] and PSCs[81], all-polymer SCs[82] because of their excellent properties such as low-temperature preparation good electron mobility, energy level matching and defect passivating ability. For OSCs, in the past few years, the PCE of non-fullerene OSCs has been increased to beyond 17%. However, the PCE of conventional OSCs based on fullerene derivatives as acceptors cannot reach the former level [83]. For example, a new donor polymer named D18-Cl can achieve high-performance non-fullerene OSCs with a wide range of molecular weight, and the addition of less PC<sub>71</sub>BM can significantly enhance  $J_{sc}$  so that the D18-Cl:Y6:PC<sub>71</sub>BM OSCs can achieve a significantly improved efficiency of 17.97% [83]. The design of fullerene and non-fullerene functional layer provides a promising strategy for scale-up, high-performance and low-cost OSCs.

For PSCs, because the defects in the interface will reduce the efficiency and stability of PSCs, it is necessary to use passivator for inhibiting the generation of interface defects. However, most passivators with poor conductivity are not conducive to the transmission of photo-generated electrons in the adjacent layer [84]. There are still some challenges in the applications of PCBM in PSCs limitations. For example, the limited solubility of PCBM in an orthogonal solvent may cause higher energy loss due to the formation of films with a high degree of energy disorder and incomplete coverage on the perovskite layer. Another disadvantage is the poor passivation ability of PCBM. The absence of heteroatoms/groups containing lone pair electrons made it unable to heal the positive vacancy that accounts for the majority of surface defects. Furthermore, PCBM with weak intermolecular interactions and disordered orientation could not form stronger adhesion with the perovskite surface, thus suffering severe self-aggregation under continuous illumination or heating [85].

The modification and optimisation of PCBM in PSCs are necessary to address the aforementioned shortcomings. A small amount of the bathophenanthroline is introduced into PCBM as the interlayer can largely stabilise the PCBM under UV and natural light exposure. The state-of-art planar n-i-p PSCs prepared on the PCBM:Bphen interlayer achieved a PCE of 23.09% (certified 22.85%)[86]. After that, the highest PCE of 23.34% is achieved among the fullerene additives-used PSCs, which is certified by a national laboratory[79]. In a previous report[79], triethylene glycol monomethyl ether (TEG) chains to fullerene moiety (PC<sub>61</sub>B-TEG) to greatly enhance its miscibility. The advanced formamidinium/methylammonium mixed cation lead halide (FA<sub>0.65</sub>MA<sub>0.35</sub>PbI<sub>3.8</sub>Cl<sub>0.2</sub>) and PC<sub>61</sub>B-TEG are directly mixed to the perovskite precursor, simultaneously overcoating on mesoporous (m)-TiO<sub>x</sub>. The

final PCE of 23.34% is reached, which is substantially higher than that of the reference devices (Fig. 3b). It is the first time that miscible fullerene derivatives have been used to describe the formation of a vertical gradient within the perovskite active layer, which represents a significant novelty in this sector.

## 2.2. Carbon Material-based Heterojunction Structure Design

The concept of HJSCs is proposed in 1951, significant advances in the development of bulk-heterojunction SCs have been made [88]. Based on the key role of carbon materials, graphene, CNTs, fullerene and *a*-C have potential as candidate functional layers for conventional homogenous junction device. Owing to the advantages in flexible, large surface area, high carrier mobility, chemical stability, and optoelectronic properties, they could meet the requirements of the heterojunction design, and combine with polymers or semiconductors to achieve band gap matching for efficient generation and separation of photon-generated carriers [89]. Bulk-heterojunction SCs, generated in inorganic/organic blends, composites, and hybrid materials, could gather advantages of both materials in one system, which are considered to be one of the most promising ways to lower the cost of SCs. Except for the polymers, the common light-harvesting materials include Si (1.1 eV) [89], GaAs (1.42 eV) [90], InP (1.34 eV) [59], Sb<sub>2</sub>S<sub>3</sub> (1.4–1.8 eV) [91], CdS (2.4 eV) [92], CdSe (1.74 eV) [93], Zn<sub>3</sub>P<sub>2</sub> (1.5 eV) [94], or metal oxides, such as ZnO (3.3 eV), CuO (1.2 eV), Cu<sub>2</sub>O (2.1 eV) [95], TiO<sub>2</sub> (3.2 eV) and Co<sub>3</sub>O<sub>4</sub> (1.9 eV) [96].

The research of carbon materials in first generation SCs mainly focuses on Si-based HJSCs, such as Si/*a*-C, Si/fullerene, Si/CNTs and Si/

graphene. Based on Shockley-Queisser limit, Si is currently regarded as an ideal substrate due to its abundant content and low-cost, high-efficient design for SC, achieving a great progress in PV market. Fig. 4 shows the evolution and representative results of carbon materials-based heterojunctions and HJSCs. The first reported Si/*a*-C, Si/fullerene and Si/CNTs heterojunction was studied in 1979 [15], 1994 [97] and 1999 [98], respectively. Subsequently, their corresponding HJSCs were first reported in 1996 [53], 1996 [99] and 2007 [18]. The PCE of Si/*a*-C (3.8% in 1996 [53]) is further improved to 7.9% in 2001 [100] and 7.67% in 2021 [54]. The difficulty in rapidly improving their efficiency is attributed to its material properties of the disordered phase containing atoms in different hybridization states and a mixture of sp<sub>2</sub> and sp<sub>3</sub> sites [101], a severe recombination on the surface and inside may be caused by relatively high resistances of *a*-C films [54]. Notably, CNTs with a dual electrical property of semiconducting and metallic are combined with Si substrate to obtain HJSC with a PCE exceeding 1%. Moreover, graphene, firstly reported in 2004 [102], possesses remarkable electronic and mechanical properties that enable it to be applied in the field of PVs. The Si/graphene HJSC with a PCE of 1.5% was first reported in 2010 [19]. Since then, there has been a substantial increase in the fundamental research on the heterojunction structure design, the recorded highest PCE of Si/graphene HJSC is 15.8%. CNTs re-inspired the research on carbon material-based HJSCs, with a PCE of Si/CNT HJSCs up to 18.9% by back-junction design [48]. The PCE is up to 21.4% by applying CNTs/Nafion ink as an inorganic-passivation free carrier selective contact [25] and further enhancement to 22% after encapsulation [23], showing great potential in future high-performance PVs.

SCs with the advantages of lighter weight, flexible shape, versatile

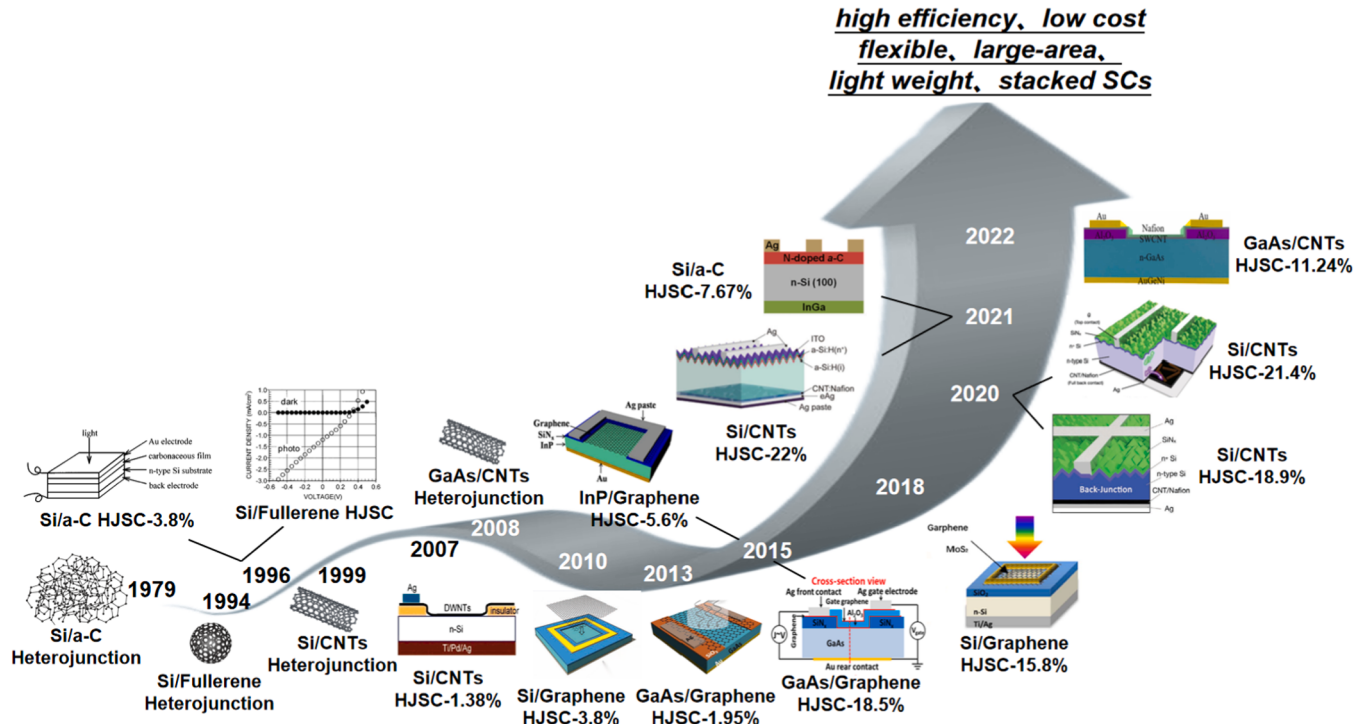


**Fig. 4.** Schematic diagrams of the evolution and representative results of carbon material-based heterojunctions and HJSCs: Si/*a*-C Heterojunction [15], Si/Fullerene Heterojunction [97], Si/*a*-C HJSC-3.8% [53], Si/Fullerene HJSC [99], Si/CNTs Heterojunction [98], Si/CNTs HJSC-1.38% [18], GaAs/CNTs Heterojunction [56], Si/graphene HJSC-3.8% [19], GaAs/graphene HJSC-1.95% [20], InP/graphene HJSC-5.6% [59], GaAs/graphene HJSC-18.5% [22], Si/graphene HJSC-15.8% [50], Si/CNTs HJSC-18.9% [48], Si/CNTs HJSC-21.4% [25], Si/*a*-C HJSC-7.67% [54], Si/CNTs HJSC-22% [23] and GaAs/CNTs HJSC-11.24% [57].

Reproduced with permission. [53] Copyright 1996, AIP Publishing. Reproduced with permission. [99] Copyright 1996, AIP Publishing. Reproduced with permission. [18] Copyright 2007, American Chemical Society. Reproduced with permission. [19] Copyright 2010, John Wiley and Sons. Reproduced with permission. [20] Copyright 2013, AIP Publishing. Reproduced with permission. [59] Copyright 2015, Elsevier. Reproduced with permission. [22] Copyright 2015, Elsevier. Reproduced with permission. [50] Copyright 2018, Elsevier. Reproduced with permission. [48] Copyright 2020, John Wiley and Sons. Reproduced with permission. [25] Copyright 2020, John Wiley and Sons. Reproduced with permission. [54] Copyright 2021, Elsevier. Reproduced with permission. [23] Copyright 2021, Elsevier. Reproduced with permission. [57] Copyright 2023, Elsevier.

material synthesis, simple device fabrication techniques and low cost in large-scale industrial production have been widely recognized as the third generation of SCs, and contain OSCs, DSSCs, QDSCs, inorganic-organic PSCs etc [103]. The details of polymer-based HJSCs are concluded and illuminated by the group of Heeger *et al.* in 1995 [104]. Among them, organic parts help to provide stability against temperature, moisture, and chemical degradation in SCs, while inorganic parts offer higher efficiency, higher environmental stability, and higher mechanical strength [105]. Processable functionalized carbon materials, such as fullerenes and their derivatives (PC<sub>61</sub>BM, PC<sub>70</sub>BM, bis-PC<sub>61</sub>BM, ICBA, etc.) could be used as electron-acceptor (n-type). Electron-donor materials (p-type) include P3HT, P3OT, P3ATs, P3DDT, PTV and PF [106]. The active layer of the bulk-heterojunction structure needs to have strong carriers mobility and light absorption, suitable band gap match between the highest occupied molecular orbital and lowest unoccupied molecular orbital of the donor/acceptor, and an appropriate device architecture and active layer configuration for efficient exciton diffusion and charges separation [107]. CNTs [108] and solution-processable functionalized graphene material [107] are introduced into OSCs as acceptor to facilitate carrier transportation. However, there are still challenging issues, mainly derived from the impurity, insolubility and bundling structure of CNTs, as well as aggregation in the polymers matrix. Otherwise, PCBM is not necessarily the optimum structure for efficient solution-processable OSCs. Numerous efforts have been made, such as optimizing the preparation method or solvent, incorporating additives and replacing PCBM with other fullerene derivatives or small molecules [109].

As the represent III-V compound for stacked SCs, GaAs with the advantages of direct and wide band gap, high optical absorption coefficient and a high electron mobility of  $8000 \text{ cm}^2 \text{V}^{-1} \text{s}^{-1}$ , become the optimal choice to reach the highest PCE, and has been extensively studied in the field of HJSCs. Such as GaAs/graphene HJSC with a PCE of 1.95% in 2013 [20]. In our previous work, graphene/GaAs modified by interface engineering reached a PCE of 15.9% [27], and the recorded highest PCE is further enhanced to 18.5% via electronic gating [22]. CNTs have been systematic studied in Si-based HJSCs and achieve a high PCE over 22% [23], however, the PCE of GaAs/CNTs heterojunction is found to be only 11.24% in 2022 [57]. Future development trend of carbon materials in HJSCs may focuses on the light weight, high efficiency tandem MJSCs with carbon material-based heterojunction. Based on the evolution of carbon materials/semiconductor HJSCs in Fig. 4, it is obvious that their promotion depends mainly on technological progress and the champion efficiency is achieved by CNT-based SCs system. However, there is still have to make more efforts to make up for the disparity with Si-based or GaAs-based homogenous SCs. As the most promising carbon materials in the study of HJSCs, the optimization strategies and technologies of CNT-based HJSCs need to be systematic studied for providing the fundamental theory support on the further promotion of carbon material-based HJSCs.

### 2.3. Work mechanism of carbon material-based HJSCs

Carbon material-based HJSCs primarily comprise carrier transportor, functional layer and charge collector. Carbon material/semiconductor heterojunction, as one of the most promising structures, has been extensively studied since 1979 [15]. As the representative carbon materials for the bulk semiconductor HJSCs, graphene and CNTs combined with n-type or p-type substrates to form the heterojunction have been studied systematically, such as the above mentioned Si-based and GaAs-based HJSCs. Their corresponding energetic band scheme of heterojunction is shown in Fig. 5. The semiconductor substrate absorbs most of the incident light due to the high transparency of graphene and CNT film and generates electron-hole pairs, which would be separated by the built-in potential ( $V_{bi}$ ) at the interface and collected by carbon material transporter [110]. Transferring CNTs or graphene on semiconductor substrates can induce an asymmetric current flowing channel,

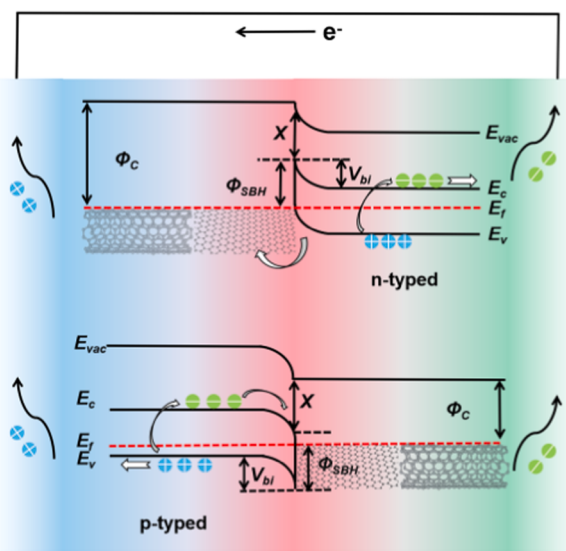


Fig. 5. Energetic band scheme of the carbon material-based heterojunction.

named rectifying junction similar to a pn or Schottky diode. Graphene, as a semimetal, combined with n-type semiconductors such as n-Si [111], n-GaAs [27], n-GaN [112] and n-ZnO [113] to form graphene/n-type semiconductor heterojunction can be defined as a minority device with similar pn junction like devices [17]. In this system, the Fermi level of graphene lies near the Dirac point and shows weakly p-type doped holes collected by graphene and electrons transported through the thick n-semiconductor layer. However, a p-type semiconductor/graphene with a forward bias is exerted on the graphene side. For example, in p-InP/graphene [59] and p-Si/graphene [58], electrons are collected by graphene and holes are separated by the semiconductor. Such heterostructure can be defined as a majority carrier device, similar to conventional Schottky diode [17].

For semiconductor/graphene, its heterojunction model has been developed and takes better account of graphene with linear energy-wavevector relations and its effective ‘zero mass’. Zero gaps (semimetal) conduction/valence band structure, and the typical J-V data of such heterojunction show strong rectification behaviour that current would pass under the negative bias of semiconductor while becoming highly resistive under the positively bias [17]. The formation of a depletion region in carbon materials/semiconductors is an indispensable condition to achieve a junction with rectifying behaviour. The two layers of opposite charge in the interface assemble a thin parallel plate capacitor with an electric field and a potential, which would prevent the charge diffusion. Schottky-Mott model [49] state that any semiconductor with electron affinity ( $X$ ) has a work function that is less than the metal ( $\Phi_M$ ), resulting in rectification with a schottky barrier height, where  $\Phi_{SBH} = \Phi_M - X$ . Similarly, the energy barrier against the electron diffusion from carbon materials to an n-type semiconductor can be obtained as  $\Phi_{SBH, n} = \Phi_C - X_S - \Delta_C$ , where  $\Phi_C$ ,  $X_S$  and  $\Delta_C$  are defined as the work function of carbon materials, electron affinity of the semiconductor and the Fermi level shift of carbon material, respectively. Based on this equation, higher  $\Phi_{SBH, n}$  can be obtained by decreasing  $\Delta_C$  with suppressed charge transfer [17]. For p-type semiconductor [59], the  $E_c$  and  $E_v$  bend to reach an equilibrium after contacting with graphene, and their Fermi levels are aligned by injecting holes from the semiconductor to graphene. The built-in electric field separates the generated electron-hole pairs, and the electrons are collected by a p-type semiconductor, which can be optimized by tuning the work function of graphene and modulating the electrical behaviours of heterojunction.

### 3. Surface/interface modulation of carbon material-based heterojunction SCs

In order to weaken the uncontrollability of doping concentration and the increased lattice mismatch and cost with increasing junction number, HJSCs such as p-type or n-type semiconductors combined with carbon materials (graphene[27], CNTs[114]), conductive polymers (PEDOT:PSS[27], P3HT[115]) and metal oxides (NiO<sub>x</sub> [116], ZnO [117]) are designed to simplify the fabrication process and reduce the cost while remaining high PV performance. As mentioned above, CNTs, graphene and their composites could be used as hole transport agents due to the adjustable band gap alignment. After contacting with semiconductor, the energy band distortion occurs at the contact interface, which further realizes the generation and transportation of photo-generated carriers. When the built-in field is formed, the hole carriers are transferred through the hole transport layer and finally collected by the electrode, as shown in Fig. 6a. Based on the photo-electric conversion mechanism, aiming at the poor PV performance caused by imperfect energy level matching and severe interfacial recombination, several optimization techniques for CNT-based HJSCs are discussed in depth, including surface optical engineering, Fermi level tuning, morphological design, conductivity optimization for transporter, and interface engineering.

First of all, during surface optical engineering, the propagation path and reflection of incident light are commonly adjusted by the incorporation of ARC and plasmonic nanoparticles, and an inverted pyramid structure to reduce the reflectivity and lengthen the propagation path of incident light, as shown in Fig. 6b. Otherwise, the micro-nano design of substrate surface is also considered as an efficient way for light management, such as nanowires[115] and nanosized structure [118]. Then, Fermi level adjustment and film conductivity optimization for hole transport layer through doping and morphological design could realize the regulation of barrier and the enhancement of carrier transportation, such as molecular absorption, electronic gating, solid-state functionalization and surface electrical property tuning. After that, surface optical management and hole transport layer optimization are not sufficient to gain high-quality devices due to the presence of defects and impurities in the interface, which would cause a reduction of current density. Therefore, the insertion layer at the interface of heterojunction is

necessary to suppress the carrier recombination and enhance the barrier height of the band alignment. In Fig. 6b, inserting an appropriate interlayer between CNT hole transport layer and substrate could effectively block the electron transport in the hole transport layer without affecting the continuous transportation of holes, thereby facilitating the efficient and rapid separation of photo-generation electrons and holes. On the other hand, interface passivation is significant for suppressing the carrier recombination, and also further enhances the band bending in the interface. In this section, several optimization techniques would be discussed in detail through CNT-based HJSCs.

#### 3.1. Surface Optical Property Tuning

##### 3.1.1. Antireflection coating

For HJSCs, although an antireflection structure [119] is used instead of a polished substrate to reduce light absorption, it inevitably leads to the degraded contact between absorption layer and carrier transporter [120]. Alternatively, the design of ARC for SCs becomes the lowest cost but effective strategy. Metal oxides, such as TiO<sub>2</sub> [121], ZnO [111] and MoO<sub>x</sub> [122], could be applied as ARC in Si/CNTs HJSCs. As shown in Table 2, the Si/CNTs HJSCs with TiO<sub>2</sub> ARC shows an excellent PCE of 15.1%. Herein, TiO<sub>2</sub> ARC could reduce light reflection from the device surface to below 10%, thus enhancing the  $J_{sc}$  and external quantum efficiency (EQE) in the visible region. In addition, the utilization of TiO<sub>2</sub> ARC by a simple spin-coating method could fully cover and fill the porous area of the CNT network, thereby generating good adhesion between the substrate and active materials[121].

Similarly, MoO<sub>x</sub> has been reported as ARC in CNT-based HJSCs due to its environmentally friendly, durable and inexpensive features. The spin-coating of MoO<sub>x</sub> not only reduces the light reflection, but also serves as a carrier transporter, which could tune the energy band alignment for efficient separation and transportation of photogenerated carriers [111]. There is  $\phi_B$  between CNTs layer and Au electrode, and the elimination of  $\phi_B$  after inserting MoO<sub>x</sub> is higher than the ionization energy of the CNTs due to the work function of the MoO<sub>x</sub> layer is close to the Fermi level of the CNT film, which can achieve efficient hole transportation [111]. Compared to the high temperature evaporation of metal oxide-based ARC, direct spin-coating method seems to be more convenient and has less chance to induce damage to the substrate, as

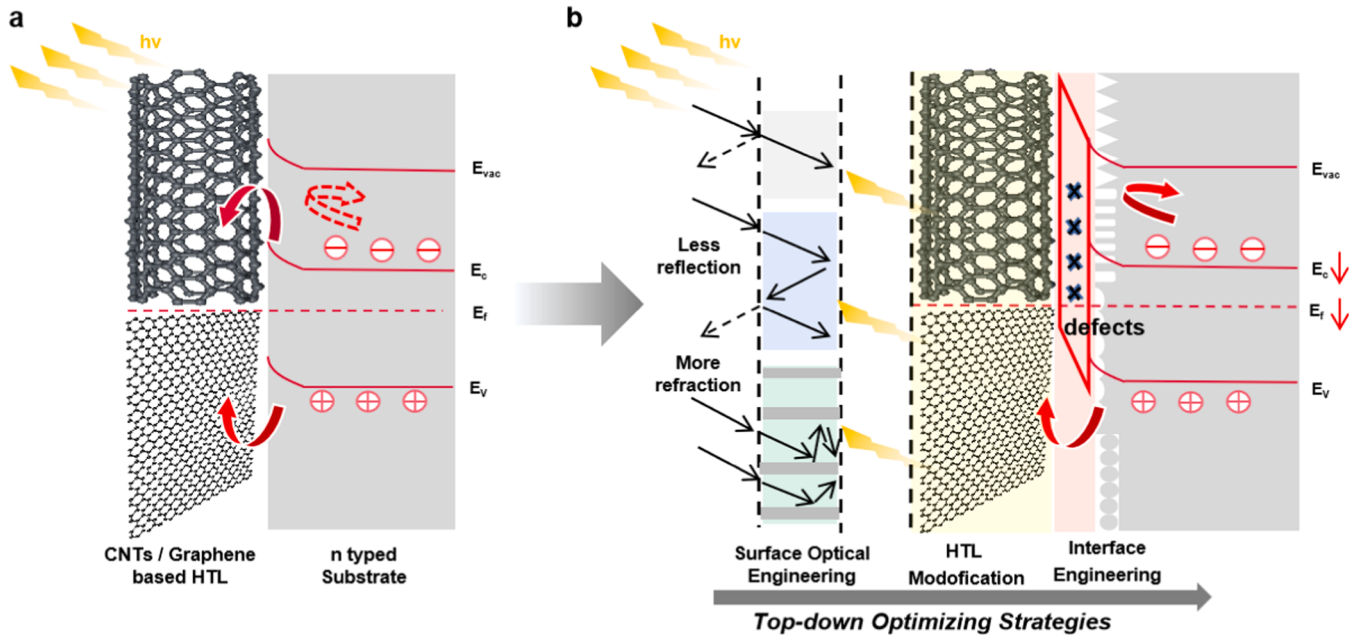


**Fig. 6.** Schematic diagram of (a) energy band alignment and (b) Top-down optimizing strategies includes surface optical engineering, hole transport layer modification and interface engineering.

**Table 2**

Comparison of Si/CNTs HJSCs with different ARCs.

Si/CNTs HJSCs with different ARC	Working area ( $\text{cm}^2$ )	$J_{\text{sc}}$ ( $\text{mA}/\text{cm}^2$ )	$V_{\text{oc}}$ (V)	FF (%)	PCE (%)	Retention of initial PCE (%)	Year	Refs.
Si/CNTs-HNO <sub>3</sub> /PDMS	0.09	29	0.56	67.6	10.9	83.49% after 20 days	2011	[124]
Si/CNTs/TiO <sub>2</sub>	0.15	32	0.61	77	15.1	-	2012	[121]
Si/CNTs/MoO <sub>x</sub>	0.008	36.6	0.59	78	17	-	2015	[111]
Si/CNTs/PS	0.079	24.2	0.51	63	7.8	~50% after 1 week	2015	[125]
Surface-texturing Si/CNTs	0.03	26.3	0.58	63	9.57	-	2016	[119]
Si/PEDOT:PSS-CNTs	0.09	28.6	0.548	65.4	10.2	-	2016	[126]
Si/PEDOT:PSS-CNTs	1	25.3	0.502	60.79	9.05	-	2020	[67]
Si/CNTs/MoO <sub>x</sub>	0.0314	31.1	0.56	58	10	80% after 2 months	2021	[122]
Si/CNTs-PSS/Nafion	0.0314	34.5	0.55	75	14.1	94.33% after 1000h	2021	[26]
Si/CNTs/GQD/PVP/HNO <sub>3</sub>	0.09	35.58	0.598	70.22	14.94	~100% after 1 week	2021	[127]
Si/CNTs/WO <sub>3</sub> /TiO <sub>2</sub> /HNO <sub>3</sub>	0.09	36.77	0.638	80.19	18.52	-	2021	[123]
GaAs/CNTs/Nafion	0.09	24.7	0.64	71	11.24	71.35% after 47 days	2022	[57]

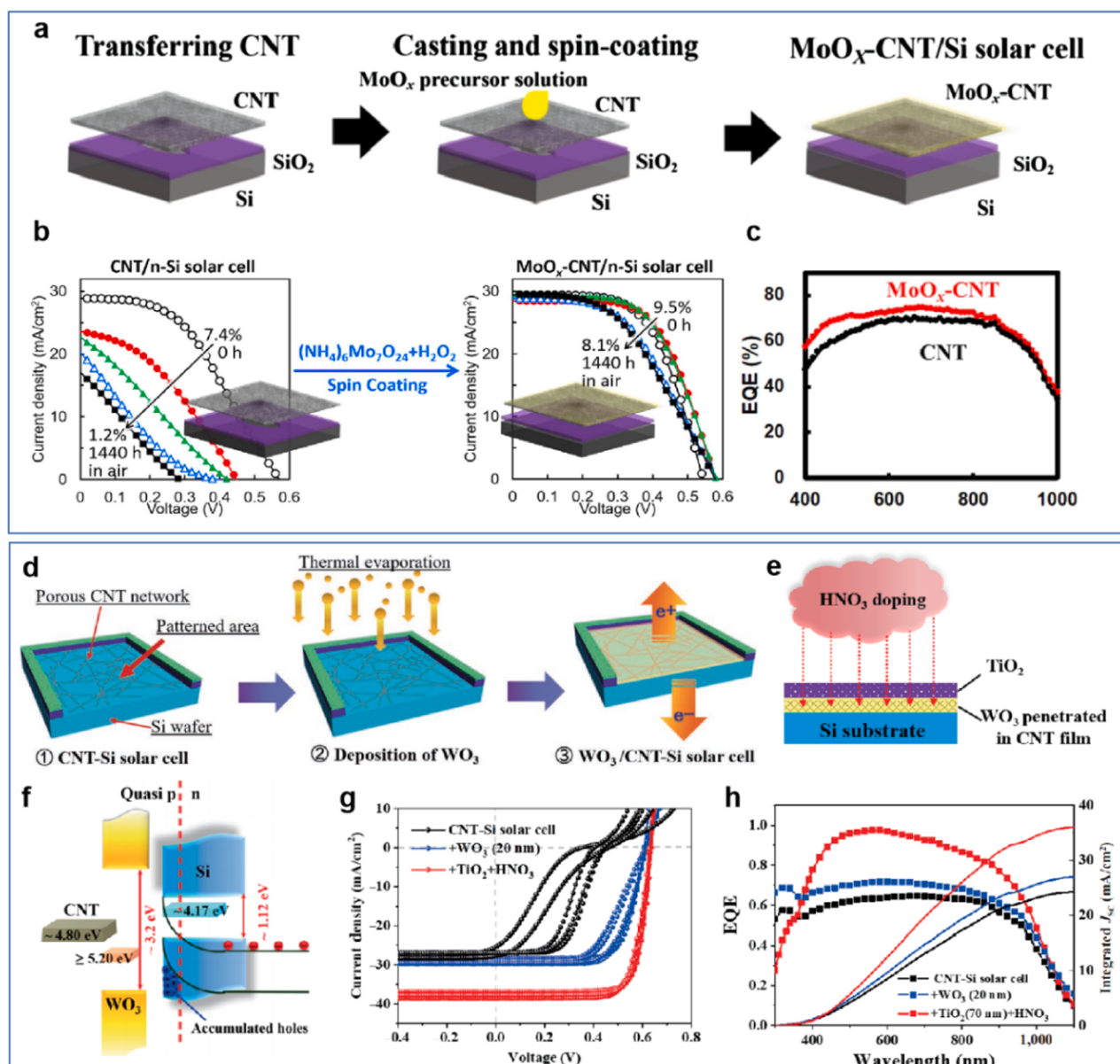


**Fig. 7.** (a) Schematics of the fabrication process of the Si/CNTs/MoO<sub>x</sub> SC. (b) Comparison of the J-V characteristics and (c) EQE spectra of the Si/CNTs SC with/without MoO<sub>x</sub> [122]. Schematics of the fabrication process of the Si/CNTs SC with (d) WO<sub>3</sub> coating and (e) TiO<sub>2</sub> coating and HNO<sub>3</sub> doping. (f) Schematic energy diagram of Si/CNTs/WO<sub>3</sub> SC. (g) J-V curves and (h) EQE curves of Si/CNTs SC with/without WO<sub>3</sub> or TiO<sub>2</sub>/HNO<sub>3</sub>.

(c) Reproduced with permission. [122] Copyright 2021, Elsevier. (f) Reproduced with permission. [123] Copyright 2021, Springer Nature.

shown in Fig. 7a and c. The addition of  $\text{MoO}_x$  ARC leads to lower sheet resistance ( $R_s$ ), a higher  $J_{sc}$  and a higher performance in EQE ranging from 400 to 800 nm. The PCE is increased from 7.2% to 10%, along with improved stability in air [122].  $\text{WO}_3$  with a high work function and wide bandgap is connected to a porous CNT network via thermal evaporation method (Fig. 7d and e) to form a synergistic system that consists of light absorption management of the  $\text{WO}_3$  coating, carrier separation and charge collection by CNT network [123]. As shown in Fig. 7f, the direct contact between  $\text{WO}_3$  and Si results in a large-offset, and thus a strong upward band bending, which leads to the accumulation of holes on the proximal side of Si, while electrons are extracted to the  $\text{WO}_3$  to generate a quasi p-n junction near the Si surface. Combining  $\text{TiO}_2$  coating and  $\text{HNO}_3$  doping, the optimized cell can reach 18.52% at an active area of  $0.09 \text{ cm}^2$ , and the values of  $J_{sc}$  and FF are enhanced significantly, further verified by their EQE measurement (Fig. 7g and h).

Insulating polymer materials, such as PDMS [124], PMMA [125], PS [125], PEDOT:PSS [126] and Nafion [26], could be spin-coated as ARC and surface protection layer to reduce light reflection and improve the stability. The spin-coating of PDMS in Si/CNTs HJSCs could cover the conductive blind zone and achieve a PCE of 10% for the final cell, showing a great potential application prospects [124]. Similarly, PEDOT:PSS is used to combine with CNT film for Si-based HJSC with a PCE of 10.2%, much higher than 5.5% of Si/PEDOT:PSS and 6.1% of Si/CNTs HJSC. These results demonstrated that the presence of PEDOT:PSS could maintain high transmittance and low  $R_s$  for fast carrier transportation [126]. Furthermore, the CNT filter in PEDOT:PSS would improve the mechanical strength of composite film, which could offer the possibility for the fabrication of flexible QSCs and PSCs [67].

Recently, CNT composite film with light transparency of 90% and low  $R_s$  of  $\sim 115 \Omega/\text{sq}$  is fabricated via a solution process using PSS [26] as both dispersant and dopant. The schematics diagram of Si/CNTs-PSS/Nafion HJSC is shown in Fig. 8a. Based on the band alignment of Si/CNTs-PSS in Fig. 8b, PSS doping can also increase the work function of CNT film, leading to a diode with a larger  $V_{bi}$  and higher barrier height. The increased barrier height is beneficial for separating and collecting electron-hole pairs, preventing the reverse electron flow and suppressing the interface recombination. The performance of Si/CNTs HJSC is improved from the pristine 7.7–11.7% after the addition of PSS and Nafion ARC. Nafion shows better reflectance and conversion performance than PMMA (Fig. 8c and d), which is attributed to the fact that the PMMA ARC would penetrate into the pores of CNTs-PSS, thereby replacing the PSS-doping and weakening p-doping and conductivity of composite film. Nafion could be used as ARC in SCs, and also passivator and encapsulation material. In Fig. 8e, the PCE of Si/CNTs-PSS, Si/CNTs-PSS/PMMA and Si/CNTs-PSS/Nafion HJSC decreased from 11.4% to 9.9%, 13.0–12.2%, and 14.1–13.3% after 1000 h, respectively, indicating a higher stability after the encapsulation in Nafion [26]. In addition, Nafion could also serve as p-type dopant and surface passivator for CNTs film. Chen et al. reported a GaAs/CNTs HJSCs with an initial PCE of 7.23% and the highest PCE of 11.24% was achieved after adding Nafion layer. With the Nafion ARC, the  $J_{sc}$  is value increases significantly from  $21.83 \text{ mA cm}^{-2}$  to  $24.70 \text{ mA cm}^{-2}$ . And their PL results indicate a fast charge separation and extraction between p-type SWCNT film and n-type GaAs, which demonstrate the porous SWCNT films filled with Nafion layer can expand the transportation paths of photo-generated holes and reduce the recombination probability [57].

As shown in Fig. 8f, a multifunctional solid coating with well-preserved fluorescence is prepared through embedding graphene quantum dots (GQDs) with photon down-conversion function in poly-vinyl pyrrolidone (PVP) matrix with anti-reflection function [127]. In this low-cost optical managing system, GQDs could convert UV light to green light, while PVP matrix could further reduce the loss of visible light absorption. As can be seen from Fig. 8g, the spectrum of GQDs/PVP solid film is red-shifted compared to the GQDs solution, indicating that the formation of hydrogen bonding between GQDs and polymer matrix

contributed to the reduction of emission energy. The photon down-conversion of GQDs is also verified by the EQE results in Fig. 8h, in which an obvious enhancement of EQE in the UV region (300–400 nm) indicated the conversion of the lower-energy photons from high energy UV photons to improve the quantum efficiency. The special cell design showed a PCE of 14.94% and excellent air stability, demonstrating a low-cost and versatile strategy for optoelectronic and PV devices. Si/CNTs HJSCs with the optimization of ARC displayed PCEs around 10%–18% over the past decade (Table 2), far from the theoretical PCE of Si-based HJSCs, demonstrating that light management with ARC alone is not enough. Therefore, the optimization of CNT film and the contact interface between carriers transportor and substrate are also of great significance.

### 3.1.2. Plasmonic nanoparticles

Currently, how to decrease the  $R_s$  between Si and CNT film remains a challenge. The introduction of metal nanoparticles with a light scattering behaviour, which is caused by localized surface plasma resonance under conditions of light scattering at the plasma resonance frequency, could be used to enhance the photocurrent of SCs. Ag [128] and Au [129] nanoparticles have been prepared on the surface of Si/CNTs HJSCs with a PCE of only 1.32% and 1.15%, respectively. Au nanoparticles doped with a CNTs/graphene hybrid film for Si-based HJSCs have a PCE of 8.8%. Especially, the Fermi level can be shifted down after Au doping thus enhancing work function [130]. However, using plasmonic nanoparticles to boost the PCE of cells is limited. For example, Pt nanoparticles (3–5 nm) are uniformly decorated on a CNT film would result in the reduction of the  $R_s$ , while the optical transmittance of a composite film at 550 nm decreased from 91.01% to 61.88% [131]. Moreover, the prepared cells achieved a final PCE of only 7.423% after doping with  $\text{HNO}_3$ . The improved current density and PCE demonstrated that the introduction of metal nanoparticles greatly reduces the  $R_s$  of hybridized CNT film. Except for the plasmonic nanoparticles mentioned above, others such as Al, Ni, Mg, and In have been regarded recently as alternatives in the application of light trapping. Furthermore, the plasmonic alloys of earth abundant materials, such as Al-Cu, Al-Au, Al-Ni, Al-In, and Al-Mg, have also attracted attention because of their plasmonic tunability, high corrosion resistance, and low cost [132]. Therefore, for these reasons, the alloys of plasmonic nanoparticles show promise for light management in CNT-based HJSCs.

### 3.2. Fermi level tuning

Recently, adsorption doping has been regarded as an efficient way to optimize the photoelectrical properties of CNT film. The lower  $R_s$  after doping is attributed to the decrease in the Schottky barriers between CNT film and charge injection from the dopant [133]. At the same time, electrochemical doping, induced by an electrical double layer on the CNT film/electrolyte interface under the applied potential, is designed to address the existing problem of the heterogeneity and irreversibility of absorption doping by solvent evaporation or spin-coating. Undoped CNT film might not be suitable for band alignment in HJSCs because of their lower free carrier concentration than that of bulk metals, which is significant for shifting the Fermi level of CNT film with the enhanced electrical conductivity by doping, such as molecular absorption doping, electronic gating, and solid-state functionalization, which could effectively increase the charge carrier density in CNT film [120].

#### 3.2.1. Molecular absorption

To improve the PCE, chemical doping and gas absorption are applied to CNTs to adjust their Fermi level and carrier concentration. Si/CNTs HJSCs with the chemical doping and gas absorption displayed PCEs over 10% are listed in Table 3. For example, the  $\text{H}_2\text{O}_2$  doping method is reported to improve Si/CNTs HJSCs to a PCE of 10.3%. By adding dilute  $\text{H}_2\text{O}_2$  and participating in the reaction and formation of  $\text{SiO}_x$  in the Si/CNTs interface, the  $R_s$  of the cells dropped from  $12.5 \Omega$  to  $3.3 \Omega$  and the

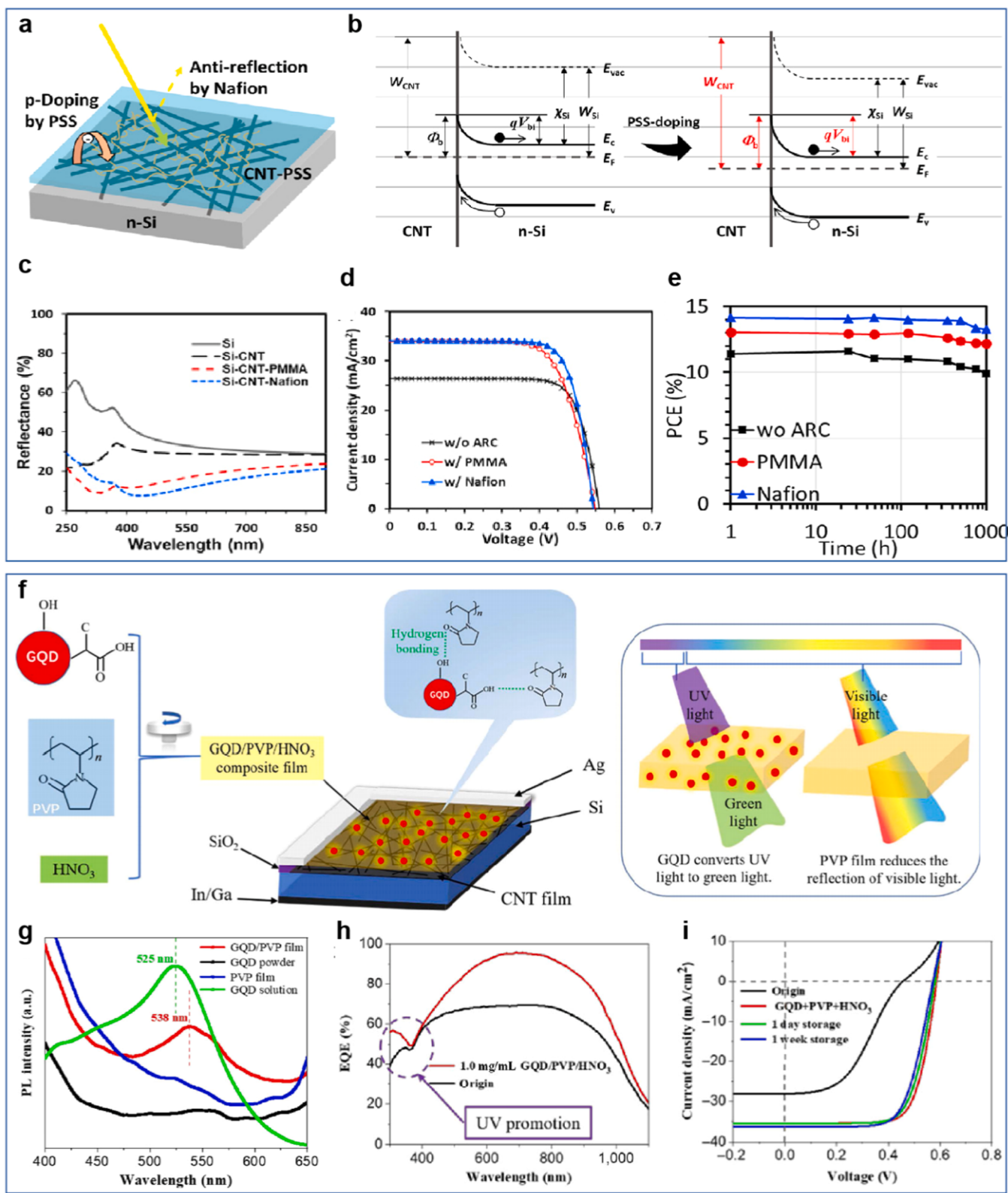


**Fig. 8.** Schematics diagram of (a) Si/CNTs-PSS/Nafion SC device and (b) band alignment of Si/CNTs SC before/after PSS doping. (c) The reflectance of Si, Si-CNTs, Si-CNTs-PMMA and Si-CNTs-Nafion. (d) J-V curves and (e) stability of Si/CNTs, Si/CNTs/PMMA and Si/CNTs/Nafion SC [26]. (f) Schematics of the fabrication process of the Si/CNTs SC coated with GQD/PVP/HNO<sub>3</sub> composite film, EDS mechanism of GQDs and anti-reflection effects of PVP film. Comparison of (g) PL spectra, (h) EQE curves and (i) J-V curves of the Si/CNTs SC with/without GQD/PVP/HNO<sub>3</sub>.

(e) Reproduced with permission. [26] Copyright 2021, Elsevier. (i) Reproduced with permission. [127] Copyright 2021, Springer Nature.

**Table 3**

Comparison of Molecular absorption of Si/CNTs HJSCs.

Molecular absorption of Si/CNTs HJSCs	Working area (cm <sup>2</sup> )	$J_{sc}$ (mA/cm <sup>2</sup> )	$V_{oc}$ (V)	FF (%)	PCE (%)	Retention of initial PCE (%)	Year	Refs.
Si/CNT-H <sub>2</sub> O <sub>2</sub>	0.09	29.3	0.55	64.4	10.3	-	2012	[134]
Si nanowires/CNT-NO <sub>2</sub>	0.24	22.2	0.55	54.4	8.4	-	2016	[137]
Si/GOCNT-HNO <sub>3</sub>	0.087	26.83	0.588	72	11.38	70% after 10 days	2017	[135]
Si/GOCNT-HClO <sub>4</sub>	0.087	26.69	0.59	72	11.35	65% after 10 days		
Si/GOCNT-H <sub>2</sub> SO <sub>4</sub>	0.087	26.42	0.589	71	11.02	35% after 5 days		
Si/GOCNT-HCl	0.087	26.13	0.575	60	8.99	65% after 10 days		
Si/GOCNT-SOCl <sub>2</sub>	0.087	26.36	0.588	66	10.26	65% after 10 days		
Si/CNT-NO <sub>2</sub>	0.09	-	-	-	7.6	-	2020	[138]
Si/CNT-XeF <sub>2</sub>	0.09	31.3	0.593	73.2	13.6	91.91% after 1 month	2020	[139]
Si/CNTs/lactic acid	0.09	32.58	0.543	57.9	10.3	-	2022	[136]

PCE showed an ~70% improvement after doping [134]. Yu *et al.* reported a graphene oxide (GO)/CNT (GOCNT) film with highly transparency and conductivity by p-type doping, such as HCl, HNO<sub>3</sub>, HClO<sub>4</sub>, H<sub>2</sub>SO<sub>4</sub> and SOCl<sub>2</sub>. The HNO<sub>3</sub>-doped GOCNT/Si HJSCs showed the highest PCE of 11.38%, which is attributed to chemical doping-induced shifts of the Fermi level, allowing further increases in the density of charge carriers and reduction in the Schottky barrier height between Si and the GOCNT film [135]. Han *et al.* used acetic acid, formic acid, lactic acid, and citric acid as the p-dopant for the CNT film, and proved that lactic acid is the best choice for Si/CNTs HJSC with an adequately strong p-doping effect and stable doping durability. A pristine PCE of 8.2% can

be enhanced to 10.3% after doping lactic acid, which is ascribed to the p-doping and antireflection effect [136]. In addition to chemical doping, gas doping is also a feasible method to improve SC performance, such as NO<sub>2</sub> molecular doping[137]. The photoelectric performance of Si nanowires/CNTs HJSC reached 8.4% after NO<sub>2</sub> gas doping, which also demonstrated a self-powered gas detection sensitivity for the Si/CNTs heterojunction based gas sensor.

A recent study [138] reported that the exposure to a few ppm of NO<sub>2</sub> significantly enhanced the performance of Si/CNTs HJSCs from 5.6% to 9.7%. By contrast, NH<sub>3</sub> exposure is detrimental to the PCE. As seen in curves I-V in Fig. 9a and b, the positive effect of NO<sub>2</sub> exposure might be

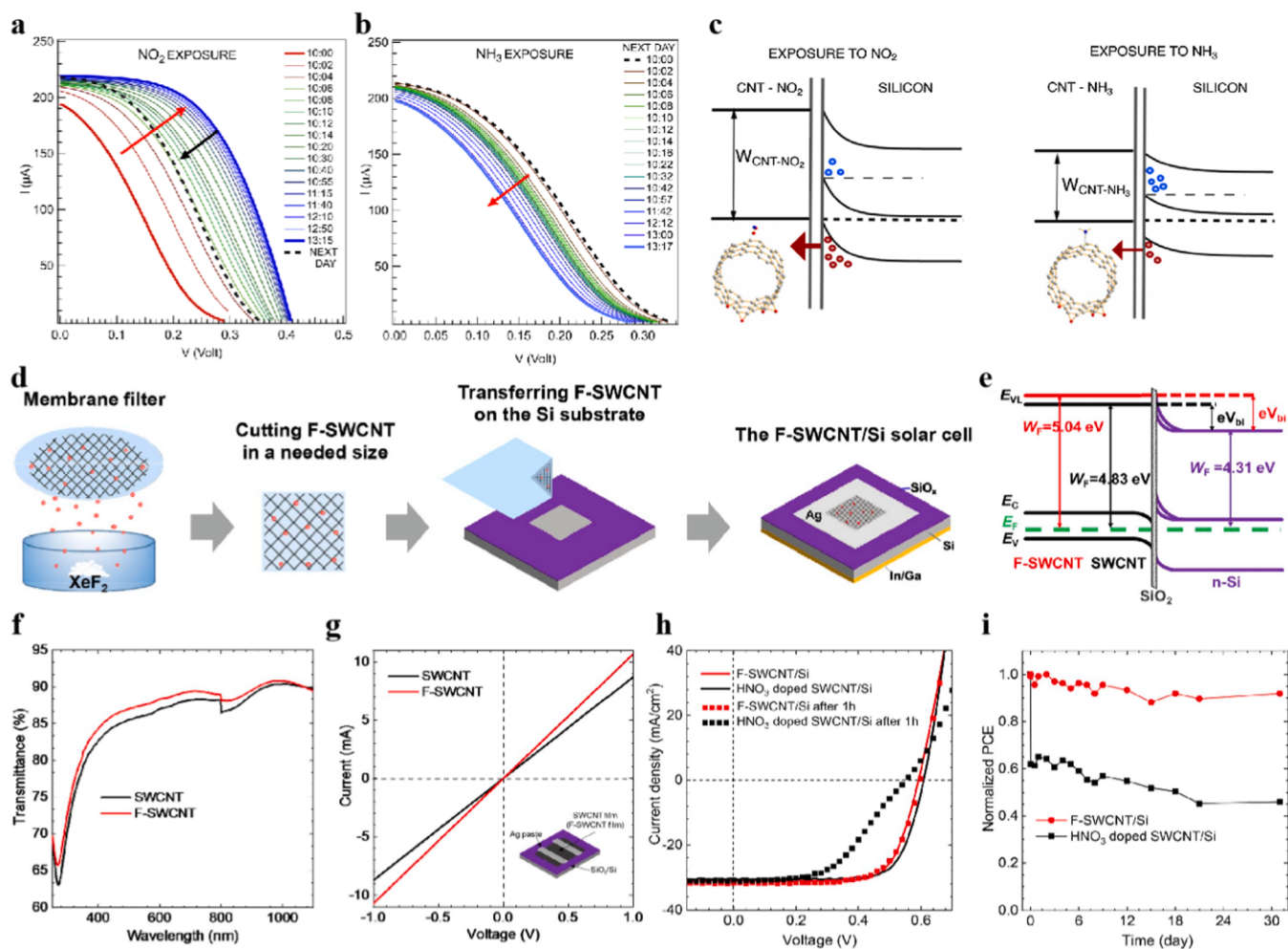


**Fig. 9.** I-V curves of Si/CNTs SC collected at different delay time upon (a) NO<sub>2</sub> and (b) NH<sub>3</sub> exposure [138].(d) Schematics of the fabrication process and (e) band alignment of the Si/CNTs-XeF<sub>2</sub> SC. (f) Optical transmittance, (g) I-V curves, (h) J-V curves and (i) normalized photovoltaic efficiency degradation of the pristine and fluorinated SWCNT SCs [139].

(c) Reproduced with permission. [138] Copyright 2020, Elsevier. (i) Reproduced with permission. [139] Copyright 2020, Elsevier.

attributed to an additional p-doping of CNT film and to the modification of the potential barrier at the Si/CNTs interface.  $\text{NH}_3$  exposure decreased the work function of CNT film, producing a  $V_{oc}$  reduction and an increase in electron density, thus leading to an increase in the recombination probability of the carriers, corresponding to the energy band alignment shown in Fig. 9c. Moreover, the cell performance was reduced on the next day (Fig. 9a) because of the presence of different covalently bound chemical groups formed by  $\text{NO}_2$  molecules and CNTs, which caused many defects in the exposed area. At the same time,  $\text{XeF}_2$  gas is used to prepare fluorinated CNT film by direct exposure at room temperature. As seen in schematics of the fabrication process in Fig. 9d,  $\text{XeF}_2$  gas doping improved the electronic conductivity and enlarged the work function, leading an enhanced areal density and reduced surface roughness. Based on the results of UPS measurement and band energy alignment shown in Fig. 9e, the  $V_{bi}$  for fluorinated Si/CNTs heterojunctions is 0.73 V, which is higher than that of Si/CNTs (0.52 V). A higher  $V_{bi}$  is beneficial to improve the capacity to collect photogenerated

carriers. After fluorination, CNT films show higher light transmittance (Fig. 9f) and lower  $R_s$  (Fig. 9g), which is attributed to the smaller film thickness, lower surface roughness, and the presence of ionic C-F bonds, in which F acts an electron acceptor. Therefore, as seen in Fig. 9h, the PCE of fluorinated Si/CNTs HJSC reached 13.6%, but only 13.7% after  $\text{HNO}_3$  doping. Also, cells without acid doping seem to be more stable in the air atmosphere, the ~8% decrease of the fluorinated Si/CNTs HJSCs was much lower than the ~54% for  $\text{HNO}_3$ -doped cells (Fig. 9i). To prepare the CNT film with high work function and conductivity in HJSCs, and even in OSCs or PSCs, the use of gas adsorption in CNT-based PV devices deserves further consideration and systematic exploration.

### 3.2.2. Electronic gating

Electronic gating for barrier modulation in a Schottky diode was reported in 1997 [140], and recent studies demonstrated that carbon materials, such as graphene [22] and CNTs [141], have Fermi levels that can be readily shifted via electronic gating, which could realize the contact

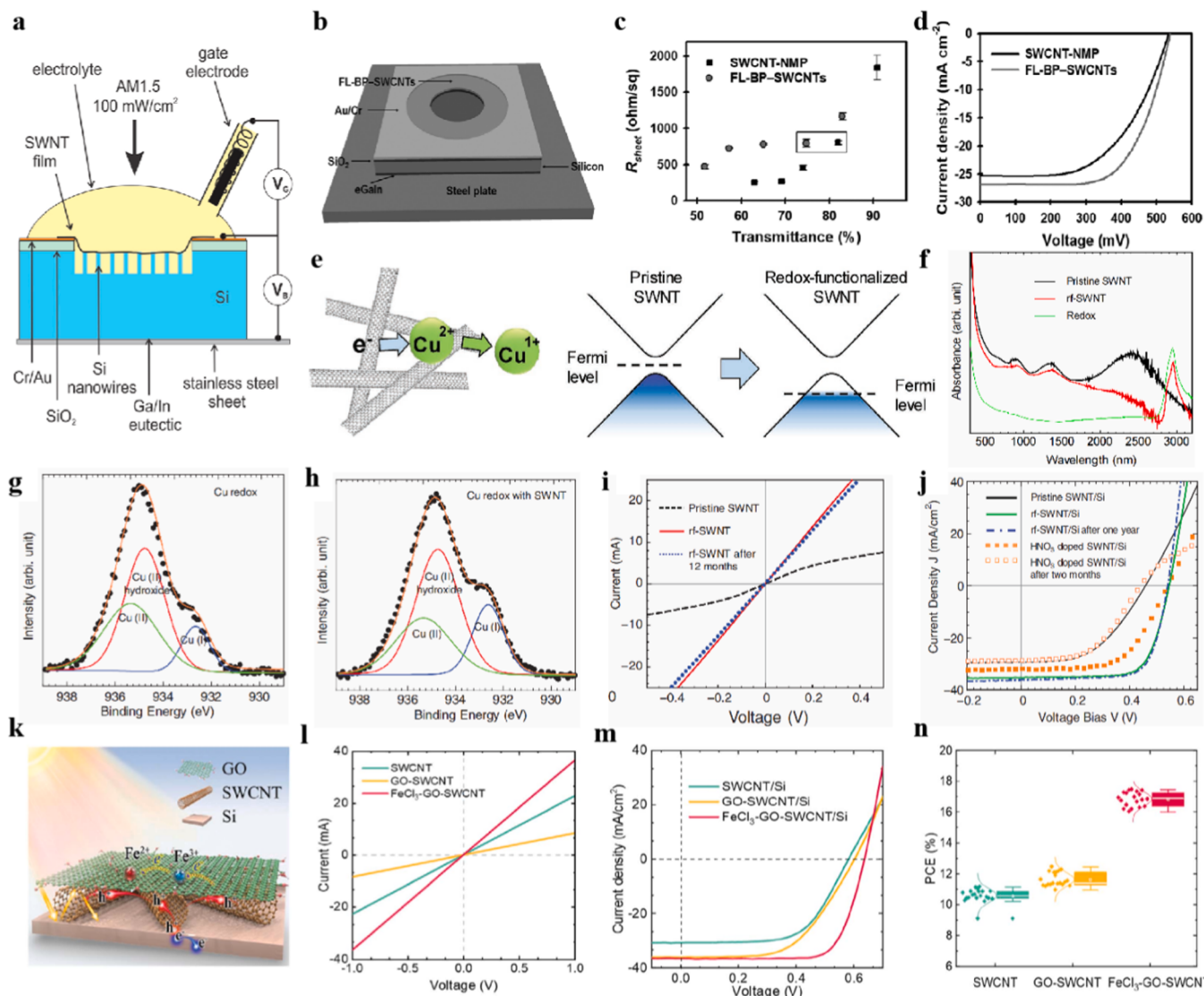


**Fig. 10.** Schematic of (a) Si nanowires/CNTs SC with electronic gating [141] and (b) Si/CNTs SC with FL-BP sheets. (c)  $R_s$  versus transmittance of different thicknesses and (d) J-V curves of CNT films with NMP and FL-BP [146]. (e) Schematics of the charge transfer mechanism in  $\text{CuC}_2/\text{Cu}(\text{OH})_2$  redox-CNTs. (f) UV-vis-NIR absorption spectra, (g, h) XPS spectra and (i) Four-point probe measurement of sheet resistance of CNT films. (j) J-V curves of the pristine Si/CNTs,  $\text{HNO}_3$  doped Si/CNTs and Si/rf-SWCNT SCs [145]. (k) Schematic of the working mechanism of Si/CNT-GO- $\text{FeCl}_3$  SC. (l) I-V curves, (m) J-V curves and (n) distributions of the PCE values of the Si/CNTs, Si/CNTs-GO and Si/CNTs-GO- $\text{FeCl}_3$  solar cells.

(d) Reproduced with permission. [141] Copyright 2015, American Chemical Society. Reproduced with permission. [146] Copyright 2017, John Wiley and Sons. (j) Reproduced with permission. [145] Copyright 2017, John Wiley and Sons. (n) Reproduced with permission. [150] Copyright 2022, The Royal Society of Chemistry.

barrier and  $V_{bi}$  control. The basic cell architecture with electronic gating is shown in Fig. 10a, which consists of Si nanowires/CNTs, an electrolyte and a gate electrode. Over the past decade, Wadhwa et al. have successfully enhanced the performance of designed Si/CNTs HJSCs from 10.9% [142] to 12% [143] by exploiting electrolyte gating, which was further improved to 15% by Maureen et al. [141]. In this system, an inversion layer would be induced on the Si surface by the electrolyte, which remedies the degradation of trapped charge in metal-insulator-semiconductor SCs [144]. Thus, the two principle mechanisms for electronic gating mainly involve modulation of the contact barrier through modulating the Fermi level of CNT film and the modulation of the electric field induced via the direct contact with the electrolyte. Significantly, the application of electrolyte for electronic gating provides a new opportunity in HJSCs design.

### 3.2.3. Solid-state functionalization

Doping could increase the conductivity of CNT film and modulate the contact barrier between the CNT film and the semiconductor or metallic electrode. However, as representative p-type dopants, inorganic/organic oxidizing agents are unstable at ambient temperature, such that the cell performance decrease quickly, and metal oxide dopants require vacuum conditions and a high-temperature annealing process. This makes it difficult to use substrates with a low working temperature, which would increase production costs in large-scale applications [145]. Few-layer black phosphorus (FL-BP), with an ultrathin 2D configuration and p-type dominated semiconducting characteristics, has been studied in the application of HJSCs [146]. N-methyl-2-pyrrolidone (NMP)-based FL-BP sheets incorporated in CNTs remain stable, and the fabricated Si/BP-CNT HJSCs (Fig. 10b) showed an improvement in the PCE from 7.52% to 9.37%, corresponding to the J-V curves in Fig. 10d. As shown in Fig. 10c, the film transmittance decreased with the increasing filtered volume of the CNT solution; however, the  $R_s$  was lower. Therefore, it is necessary for an ideal device to keep a high transmittance and low  $R_s$  at the same time.

CuI is usually used as hole-injector, collector and transportor in SCs because of its good electrical conductivity [147]. CuI particles could enhance the hole-collecting and transporting ability of Si/CNTs HJSCs; however, some particles do not contact with the Si surface directly, such that the cell performance declined quickly and only achieved a PCE of 6% [148]. Similarly, CuCl<sub>2</sub>-doping is also used as an effective method to modify the graphene oxide hole transport layer in SCs [149]. In CNT-based HJSCs, drop-casting/spin-coating CuCl<sub>2</sub>/Cu(OH)<sub>2</sub> colloidal ethanol solution on the CNT film is also an effective strategy to further reduce production costs and realize a scalable and room-temperature solid-state redox functionalization process [145]. That study showed that redox functionalized SWCNTs (rf-SWCNTs) could decrease the Fermi level from 4.83 V to 5.06 V (Fig. 10e), which was attributed to the electron shift in SWCNTs induced by the charge transportation between the redox reaction of Cu<sup>2+</sup> and Cu<sup>+</sup>. This result was confirmed by the UV-vis-NIR optical absorbance spectroscopy shown in Fig. 10f, in which the suppression of interband optical absorption is related to the shift of the Fermi level. In addition, the XPS spectra shown in Fig. 10g and demonstrate that the ratio of Cu<sup>2+</sup>/Cu<sup>+</sup> in rf-SWCNTs decreased, which was attributed to the electrons extracted from the SWCNTs being involved in the charge transportation of the redox reaction. Especially, the addition of CuCl<sub>2</sub>/Cu(OH)<sub>2</sub> could cover the blank area of CNT film on Si to reduce the  $R_s$  and increase stability, as shown in Fig. 10i and j. In addition, the redox dopant also serves as an ARC, finally obtaining stable Si/rf-SWCNT HJSCs with a PCE of 14.09%, which is much higher than that of HNO<sub>3</sub>-doped SCs (10.17%). However, certain problems remain, such as, for the CuI particle dopant mentioned above, the indirect contact between the bulk dopant and substrate might be a limitation for the improvement of PCE.

Similarly, redox FeCl<sub>3</sub>-functionalized Si/CNTs-GO HJSCs was achieved using a simple drop-casting method [150]. The working mechanism is shown in Fig. 10k. The introduction of GO and FeCl<sub>3</sub> could lead to increased light harvesting and decrease the resistance of CNTs-GO

composite film (Fig. 10l), respectively. The ferric ions are reduced by receiving electrons, thus facilitating the electron shift in the carrier transporting bridge formed by FeCl<sub>3</sub> and GO. The disappearance of the blind area significantly enhanced the current density for Si/CNTs-GO (Fig. 10m and n), and the addition of FeCl<sub>3</sub> significantly improved the FF to a high value of 73.9 ± 2.01%, and the final PCE to 17.5%, which was higher than that of Si/CNTs (11.1%) and Si/CNTs-GO (12.3%). This is the most efficient solid-state functionalization for Si/CNTs HJSCs reported in recent years (Table 4).

### 3.3. Surface electrical property tuning

The 1D tubular structure and high ratio surface area of CNTs mean that morphological design would have a dramatic impact on film conductivity. For CNT film, the common preparation methods include solution spraying [151], immersion [152], vacuum solution treatment [153], electrodeposition [154], and chemical vapor deposition (CVD) [155]. These processes involve surfactant-assisted ultrasonic dispersion, deposition, removal, and transfer, which inevitably lead to contamination of the prepared film and impairment of its optical transmittance and interlayer resistance.

In 2013, Di et al. proposed an undoped and transparent aligned CNT film that functioned as a charge-collecting electrode as well as a heterojunction, using multilayer aligned CNT film that could fill up the gaps between adjacent CNTs and inhibit the carrier recombination caused by the long migration path. The current density and PCE reached 33.4 mA cm<sup>-2</sup> and 10.5%, respectively, which were higher than those of the pristine random CNT-based SCs [156]. Besides the multilayer design, adding conductive materials such as graphene [157], GO [158] or Ag nanowires [159] to CNTs seems to promote carrier migration (Table 5). Hybrid CNTs/graphene films are prepared by electrophoretic methods [130] or CVD [157] to increase the PCE of Si-based HJSCs, which is mainly attributed to their improvement conductivity. For CNT-embroidered graphene (CeG) grown by CVD (Fig. 11a and b), the prepared HJSCs achieved a better PCE of 15.2% after adding TiO<sub>2</sub> ARC and chemical doping, and especially, the FF and  $J_{sc}$  were enhanced (Fig. 11c) [157]. In addition, direct transfer to assemble the hybrid CNTs/graphene film [160] is also a good choice for SC fabrication: the  $R_s$  values of the direct transfer-obtained CNT/graphene film and CVD-grown G-CNT films were 190 Ω sq<sup>-1</sup> and 210 Ω sq<sup>-1</sup>, respectively. However, the G-CNT-based SC showed a better PCE of 7.9% and finally reached 9.1% after coating with PMMA ARC. Similarly, spin-coating Ag nanowires on Si/CNTs heterojunctions achieved a PCE of 10.8% and the final PCE was still > 10% in 49 mm<sup>2</sup> SCs, which was attributed to the high transparency hybrid film and the lower  $R_s$  [159]. These works revealed the new aspects for charge collectors and the potential for HJSCs.

Interestingly, CNT strips are used to replace conventional metal grids as the top electrode on to CNT film, improving the PCE from 3.97% to 6.52%, which finally reached 10.11% after coating with TiO<sub>2</sub> ARC in > 2 cm<sup>2</sup> cells (Fig. 11d). A CNT film floated on ethanol is picked up to make a CNT strip and then laid on the cell surface, as shown in Fig. 11e and f. Controlling the number of strips can effectively enhance carrier transportation and collection at the CNTs side, without introducing a contact barrier [37]. To enhance the photogenerated carrier density, optimizing the conductivity of the CNT film could be considered. Unlike extra additives such as graphene, Ag NW, and CNT strip electrodes mentioned above, O<sub>3</sub> doping [114] with various treatment times, a dry gas doping for decorating the morphology of CNT film, could donate holes to CNT film to increase their work function, thus enhancing the  $V_{bi}$  and Schottky barrier at the heterojunction. As seen in Fig. 11g, under ozone treatment, CNTs would become thinner by lifting off layer by layer and transferring into amorphous carbon. However, the increasing treatment time and its transparency would lead to increased defects in CNTs. Five minutes of ozone treatment balanced the impact of surface destruction and the p-doping effect, increasing the PCE from 5.29% to

**Table 4**

Comparison of solid-state functionalization of Si/CNTs HJSCs.

Solid-state functionalization of Si/CNTs HJSCs	Working area (cm <sup>2</sup> )	<i>J</i> <sub>sc</sub> (mA/cm <sup>2</sup> )	<i>V</i> <sub>oc</sub> (V)	FF (%)	PCE (%)	Retention of initial PCE (%)	Year	Refs.
Si/CNT-CuI	0.09	20.6	0.5	58.4	6	-	2012	[148]
Si/BP-SWCNTs	0.079	26.9	0.538	65	9.37	-	2017	[146]
Si/rf-SWCNTs	0.09	36.1	0.54	72.3	14.09	102.32% after one year	2017	[145]
Si/CNT-GO-FeCl <sub>3</sub>	0.09	36.7	0.637	74.6	17.5	90% after 15 days	2022	[150]

**Table 5**

Comparison of Si/CNTs HJSCs with morphology design.

Si/CNTs HJSCs with morphology design	Working area (cm <sup>2</sup> )	<i>J</i> <sub>sc</sub> (mA/cm <sup>2</sup> )	<i>V</i> <sub>oc</sub> (V)	FF (%)	PCE (%)	Retention of initial PCE (%)	Year	Refs.
Si/Aligned CNTs	~0.12	33.4	0.54	58.3	10.5	-	2013	[156]
Si/SWNT/Ag nanowires	0.49	31	0.51	69	10.8	-	2014	[159]
Si/CNTs /graphene/ HNO <sub>3</sub> /TiO <sub>2</sub>	0.141	32.6	0.62	75.5	15.2	40% after 17 min	2015	[157]
Si-CNT-CNT strip/ HNO <sub>3</sub> /TiO <sub>2</sub>	2	29.7	0.6	48	10.34	90.8% after 2 days	2016	[37]
Si/CNT-graphene (PMMA)	2.15	25.32	0.63	52	10.11	-	2018	[160]
Si/GOCNT	0.09	25.5	0.48	64.5	7.9 (9.1)	94% after 15 days	2018	[158]
Si/CNTs-O <sub>3</sub> treatment	0.087	33.75	0.573	68	13.01	-	2019	[114]
Si/CNTs-O <sub>3</sub> treatment	0.09	36.95	0.625	75.61	17.46%	61.13% after 21 days	2019	[114]

12.7%, which finally reached 17.46% after HNO<sub>3</sub> doping and adding TiO<sub>2</sub> ARC. Compared with chemical doping or conductive additives, gas doping seems to be a more effective, eco-friendly, and easier method to scale up low-cost SC manufacture.

### 3.4. Interface engineering

Conventional Si-based HJSCs employ a thin dielectric passivation interlayer, such as intrinsic hydrogenated amorphous Si (a-Si:H(i)), SiO<sub>2</sub>, or SiN<sub>x</sub>, to passivate the interlayer defects. For example, SiO<sub>2</sub> was first introduced into Si/CNTs HJSCs in 2012 and improved the PCE from 0.5% to 8.8% [161]. Despite the better performance of these designed cells, the complicated manufacturing steps, involving high temperature processes, such as thermal oxidation, plasma enhanced CVD, and atomic layer deposition, led to high costs. A quick annealing process under a vacuum (1 min, 500–550 °C, < 5 × 10<sup>-4</sup> Pa) was developed to reduce the passivation time and cost. The PCE of the prepared Si/SiO<sub>2</sub>/CNTs HJSCs increased from 6.61% to 8.52%, which revealed a promising method for the facile fabrication of Si-based HJSCs [162]. By contrast, recent research has begun to develop “dopant-free carrier-selective heterocontacts” using thermal evaporation, and spin-coating or sputtering, including electron-selective contacts such as LiF<sub>x</sub> [163], MgO<sub>x</sub> [164] and TiO<sub>x</sub> [165], whereas MoO<sub>x</sub> [166], NiO<sub>x</sub> [167], WO<sub>x</sub> [168], PEDOT [169] and P3HT [170] have been shown to be hole-selective. Several studies reported that the performance of Si/CNTs HJSCs could be improved by introducing the additional interlayer of conductive polymers, such as PANI placed between Si and CNTs. A higher PCE than Si/PANI could be achieved because of the limited lateral current-carrying capacity of polymer film after acid doping, which could significantly improve the PCE to 9.66% [171]. Also, while PEDOT:PSS and P3HT serve as conducting interlayer of the system, their PCEs are 7.73% and 6.52%, respectively, which indicates that the existence of conductive polymer could protect the Si surface from oxidation. The performance of the Si/PEDOT:PSS/CNTs HJSCs could be further enhanced to 8.66% after adding PS ARC [172]. Similarly, spi-ro-OMeTAD [173], NAP, BPV, and PEDOT:PSS [174] have been applied as hole transporting interlayers for Si/GOCNT HJSCs, with final PCE of 12.83%, 10.57%, 10.68%, and 12.05%, respectively (Table 6). The significant enhancement can be attributed to the addition of the conductive polymer layer, which dramatically minimizes recombination at the heterojunction interface and enhances cell stability.

Compared with metal oxide-based hole selection, the application of conductive polymers is more convenient and milder, but still cannot

satisfy the manufacturing requirement of both conductive performance and the passivation effect. Interestingly, Nafion (a sulfonated tetrafluoroethylene-based fluoropolymer-copolymer) has been proposed for use as interface passivator in Si-based HJSCs, which combines with high conductive polymers to form the hole selective composite. The excellent passivation effect of Nafion has been demonstrated in 2107, the direct spin-coating of Nafion on the c-Si surface at room temperature was reported to produce a better passivation value of ~9.6 ms [175], which increased to 12 ms by 2019 [176]. As a non-reactive polymer with a strongly acidic Lewis value, the addition of Nafion can form a high density of fixed charges on the Si surface, at around two orders of magnitude higher than that of conventional passivators. It is worth noting that the Nafion passivator works through forming fixed charges rather than chemical modification of the overhang bonds; therefore, complex instruments are not required, and its large-scale application is promising.

Although Nafion is an ideal passivator, it is unlikely that one component would possess both an excellent defect passivating effect and carrier transporting ability simultaneously. Thus, conductive-passivating carrier-selective contact was proposed, and PEDOT:PSS combined with Nafion to form a thin composite film was constructed [177]. As shown in Fig. 12a, common passivators such as SiO<sub>2</sub>, SiN<sub>x</sub>, and Al<sub>2</sub>O<sub>3</sub> have excellent defect state passivation, but poor conductivity, while conductive polymers, such as PEDOT:PSS, have poor passivation ability. The relationship between the ratio of Nafion/PEDOT:PSS and carrier lifespan is shown in Fig. 12b. According to the corresponding SEM images, the adhesive quality achieved in PEDOT:PSS increased with the increasing dose of Nafion. This result was supported by the reduced moist angle of PEDOT:PSS (the inserted images of Fig. 12b (a-f)). In the schematic diagram of band alignment in Fig. 12c, the excellent passivating effect of the composite film originates from a thin Si-O-R layer formed between the sulfonic group in the Nafion molecule and the Si surface by electrochemical grafting of O groups, thus creating carrier-selective contact for majority carriers and a blockade barrier for minority carriers [177].

Nafion was also used for p-doping, ARC, and encapsulation coating to enhance the PCE of Si/CNTs HJSC from 9.5% to 14.4%, leading to unprecedented device stability of more than 120 days under a serving environment [179]. Furthermore, the performance of Nafion-decorated CNT HJSCs was characterized by Qian *et al.* and breakthrough PCEs of 17.2% and 15.5% were obtained at 1 cm<sup>2</sup> and 5 cm<sup>2</sup>, respectively [178]. The results indicated that combining a new dopant and advanced substrate design is more efficient than the CuCl<sub>2</sub>/Cu(OH)<sub>2</sub> colloidal ethanol

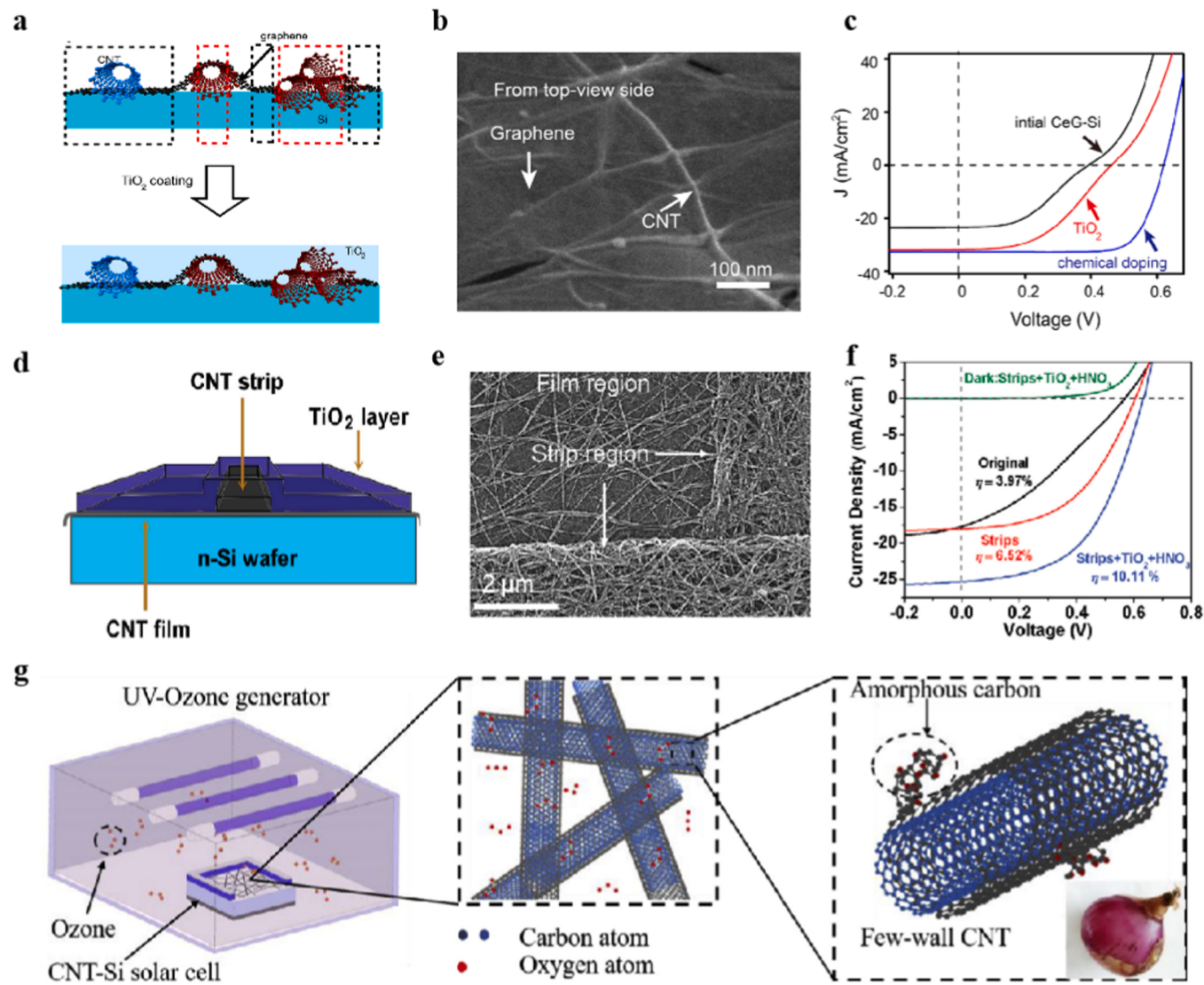


**Fig. 11.** (a) Schematic, (b) SEM image and (c) J-V curves of Si/CNTs/graphene SC [157]. (d) Schematic, (e) SEM image and (f) J-V curves of Si-CNTs-CNTs strip SC [37]. (g) Schematics of the fabrication process of Si/CNTs-O<sub>3</sub> SC[114].

(c) Reproduced with permission. [157] Copyright 2015, Elsevier. (f) Reproduced with permission. [37] Copyright 2016, John Wiley and Sons. (g) Reproduced with permission. [114] Copyright 2019, (c) Reproduced with permission. [157] Copyright 2015, Elsevier. (f) Reproduced with permission. [37] Copyright 2016, John Wiley and Sons. (g) Reproduced with permission. [114] Copyright 2019, Elsevier.

solution as a dopant in a previous report[145]. An Si substrate with an antireflective texture (Fig. 12d) might not be suitable for combination with CNT film and colloidal dopant because of their poor interface contact, which can be seen in Fig. 12g (a-d). Meanwhile, adding Nafion could form significantly more conformal coating and could fill the blank area between the substrate and the CNT film. Nafion also exhibits more reflective than colloidal behaviour (Fig. 12f), based on the assumption that the back scattering center is caused by non-contact between colloids and the Si surface because of the crossing web net of CNTs. A texture-compatible dopant for CNT film is beneficial to photogenerated carrier transportation, such as obtaining a higher  $J_{sc}$  and PCE (Fig. 12e), which is why Nafion is more effective in a large-area device.

The requirement for large-scale SC devices is increasing, which might benefit from recent progress reported for Si/CNTs/Nafion HJSCs, with a PCE of 17.2% and 15.5% for an active area of 1 cm<sup>2</sup> and 5 cm<sup>2</sup>, respectively [178], and a PCE of 14.4% [179] for 0.09 cm<sup>2</sup>, which are better than those reported in previous studies of Si/CNTs HJSC with a small active area, such as Si/SiO<sub>x</sub>/CNTs (8.8% [161] for 0.09 cm<sup>2</sup>, 8.52%[162] for 0.0314 cm<sup>2</sup>), Si/PANI/CNTs-HF/HCl (9.66% for

0.08 cm<sup>2</sup>)[171], Si/PANI/CNTs (7.1% for 0.079 cm<sup>2</sup>)[172], Si/PEDOT: PSS/GOCNT (9.9% for 0.089 cm<sup>2</sup>)[174] and Si/spiro-OMeTAD/GOCNT (12.83% for 0.087 cm<sup>2</sup>) [173] (Table 6). The results indicate that the excellent passivating performance of Nafion makes it very suitable for use in p-doping, ARC, and encapsulation coating in the preparation of large-scale devices. Nafion was used as a passivator in back-junction design on purpose, and the cross-sectional schematics of Si/CNTs/Nafion HJSCs with front-junction and back-junction designs are shown in Fig. 13a[48]. The front-junction design is the same as that in a previous study, in which the CNTs/Nafion composite film served as the hole transport layer and Nafion served as the p-dopant and ARC, producing promising PCEs of 15.2% and 8.8% for an effective area of 1 cm<sup>2</sup> and 16 cm<sup>2</sup>, respectively (Fig. 13b). By comparison, placing the CNT film and spin-coating Nafion on the rear of the Si substrate in back-junction architecture, which reduced the loss of incident light and ignored the shading effect of the surface active layer, further improved the PCE to 18.9% and 17% for 3 cm<sup>2</sup> and 16 cm<sup>2</sup> devices, respectively (Fig. 13c), showing a better stability in scale-up device application.

Such a back-junction design is more meaningful for other HJSCs by

**Table 6**

Comparison of interface engineering of Si/CNTs HJSCs.

Interface engineering of Si/CNTs HJSCs	Working area ( $\text{cm}^2$ )	$J_{sc}$ ( $\text{mA}/\text{cm}^2$ )	$V_{oc}$ (V)	FF (%)	PCE (%)	Retention of initial PCE (%)	Year	Refs.
Si/SiO <sub>x</sub> /CNTs	0.09	24.32	0.54	67	8.8	16.36% after 1 year	2012	[161]
Si/PANI/CNTs-HF/HCl	0.08	27.38	0.52	68	9.66	-	2013	[171]
Si/PANI/CNTs	0.079	21.5	0.55	61	7.1	~38% after 1 week	2015	[172]
Si/P3HT/CNTs	0.079	21.1	0.53	58	6.52	~50% after 1 week		
Si/PEDOT:PSS/CNTs	0.079	20	0.54	72	7.73	~48% after 1 week		
Si/PEDOT:PSS/CNTs/PS	0.079	24.5	0.54	66	8.66	64.43% after 1 week		
Si/PEDOT:PSS/GOCNT	0.087	28.13	0.577	61	9.9	-	2017	[174]
Si/NAP/GOCNT		27.92	0.525	49	7.08	-		
Si/BPV/GOCNT		27.24	0.53	61	8.81	-		
Si/spiro-OMeTAD/GOCNT	0.087	28.1	0.575	75	12.83	90% after 2 weeks	2017	[173]
Si/SiO <sub>x</sub> /CNTs	0.0314	26.53	0.55	58	8.52	82.28% after ~1000 h	2019	[162]
Si/CNTs/Nafion	0.09	36.7	0.549	71.2	14.40%	98.61% after 120 days	2020	[179]
Si/CNTs/Nafion	1	32.77	0.661	79	17.20%	81.4%-84.3% after 1 week	2020	[178]
Si/CNTs/Nafion-Front-junction	1	32.75	0.639	72.6	15.50%	-	2020	[48]
Back-junction	16	34	0.6	43.1	8.80%	-		
Si/CNTs@Nafion-Back-junction	3	38.8	0.631	77.2	18.90%	-		
Si/CNTs@Nafion-Back-junction	16	37	0.638	72.1	17%	-		
Si/CNTs@Nafion-Back-junction	4.8	39.9	0.654	82	21.40%	-	2020	[25]
Si/CNTs-PSS/Nafion	245.71	39.5	0.646	78.9	20.1	-		
Si/CNTs@Nafion/eAg-Back-junction	0.0314	34.5	0.55	75	14.10%	94.33% after 1000 h	2021	[26]
Si/CNTs@Nafion/eAg-Back-junction	4	40.38	0.683	79.9	22.04%	~118% after 1600 min	2021	[23]

forming a hybrid passivated charge selective rear contact to increase the photogenerated carriers, resulting in low-cost and simplified industrial application. Based on the achievements introduced above, Chen *et al.* reported mixing CNTs and Nafion to prepare an ink that was placed on the rear surface of the Si substrate, which used the surface texture and an SiN<sub>x</sub> passivator to reduce light loss and carrier recombination, as shown in Fig. 13d. Compared with the back-junction design in a study of Si/CNTs/Nafion HJSCs [48], the CNTs/Nafion ink [25] could be spin coated directly onto Si and was more beneficial for the preparation of a large-area device, achieving a higher PCE of 21.4% for an area of 4.8  $\text{cm}^2$  and a PCE of 20.1% after expanding the wafer area to 245.71  $\text{cm}^2$  (Fig. 13e). The formation of “passivated charge selective contact” by combining both carrier selective transporter and passivator in a single layer, thereby removing the need for a thin dielectric interlayer, and the addition of CNTs in ink, could enhance the conductivity of Nafion, thus obtaining a higher PCE. For CNTs/Nafion ink, the carrier lifetime would be directly influenced by changing of the CNT content, as shown in Fig. 13f, and we would have to combine the results of electroluminescence intensity maps to balance the quality of CNTs/Nafion. In Fig. 13g, the higher CNT content caused higher mapping intensity, indicating that CNTs are responsible for electrical contact with Si and hole extraction. The photoluminescence intensity map of CNTs/Nafion with wafer size of 245.71  $\text{cm}^2$  is shown in Fig. 13h.

The CNTs/Nafion ink showed a homogenous contrast because of its minimal variation of composition, which demonstrated the great potential for such advanced design in industrial applications. However, the Si/CNTs/Nafion HJSCs with a back-junction design and the organic passivated interface are not stable, which can be attributed to the CNT network providing a channel for water molecules at the interface. The Si/CNTs/Nafion HJSC structure was further optimized by Chen *et al.* [23], a thin Ag film was evaporated following the spin-coating of CNTs/Nafion on the Si back side, as shown in Fig. 13i. A record high PCE of 22.04%, a  $V_{oc}$  of 683.4 mV, a  $J_{sc}$  of 40.38  $\text{mA}/\text{cm}^2$ , and an FF of 79.9% were obtained after adding Ag encapsulation (eAg) (Fig. 13j). Based on the performance values recorded and in comparison with devices with and without encapsulation, the Si/CNTs/Nafion with Ag film encapsulation showed better stability and PCE performance (Fig. 13k). In particular, the FF of Si/CNTs/Nafion/eAg HJSCs reached 83.4%, revealing an advantage of the passivating contact and encapsulation

technology and providing a new direction for the development of large-area and high performance carbon material-based HJSCs.

#### 4. Towards large-area and flexible heterojunction SCs

##### 4.1. Large-area heterojunction SCs

The optimization methods mentioned above demonstrate new opportunities for HJSCs with high efficiency, large-area and long-term stability. Besides, the adoption of flexible materials with excellent mechanical flexibility and robustness provides flexibility to the device. Most of the design and fabrication in the investigations on CNT-based HJSCs in the past decade exhibited an active area of less than 1  $\text{cm}^2$ , as listed in Tables 2–6. The general design of CNT film is directly transferred to the light absorber surface and covered with metal grids to form electrode window. Various optimization ways have been applied in the system from top to bottom for device, such as surface optical management, electrical and chemical modulation and interface engineering. With reasonable modulation in optical, electrical and chemical properties, a high PCE over 20% could be achieved on such small area. However, the designed cell structure severely limited the development of large-area devices due to the instabilities and indeterminate factors. As shown in Fig. 14, the Si/CNTs HJSC with an active area of 2.15  $\text{cm}^2$  and a PCE of only 10.11% is obtained with the incorporation of CNT strips instead of metal grids for charge collection [37]. After introducing Nafion, both the passivation and large-area production are achieved with PCE further enhanced to 15.5% [178] at 5  $\text{cm}^2$ . The combination of Nafion/CNTs composite and back-junction structure design showed a huge potential in large-area process, with a PCE of 17% at 16  $\text{cm}^2$ , much higher than that of front-junction design (8.8%) [48]. For further improvement, a solution-processed Nafion/CNTs ink is used as a substitute for Nafion/CNTs composite film [25], having a PCE of 21.4% at 4.8  $\text{cm}^2$  and 20.1% at 245.71  $\text{cm}^2$ . After adding the encapsulation on Nafion/CNTs, a record PCE of 22.02% at 4  $\text{cm}^2$  is obtained [23], demonstrating a new passivator design and device structure design for industrial large-area fabrication. Although large-area device has achieved higher PCE, the high requirements for materials still severely limited the large-area production in other device, such as graphene-based HJSCs.

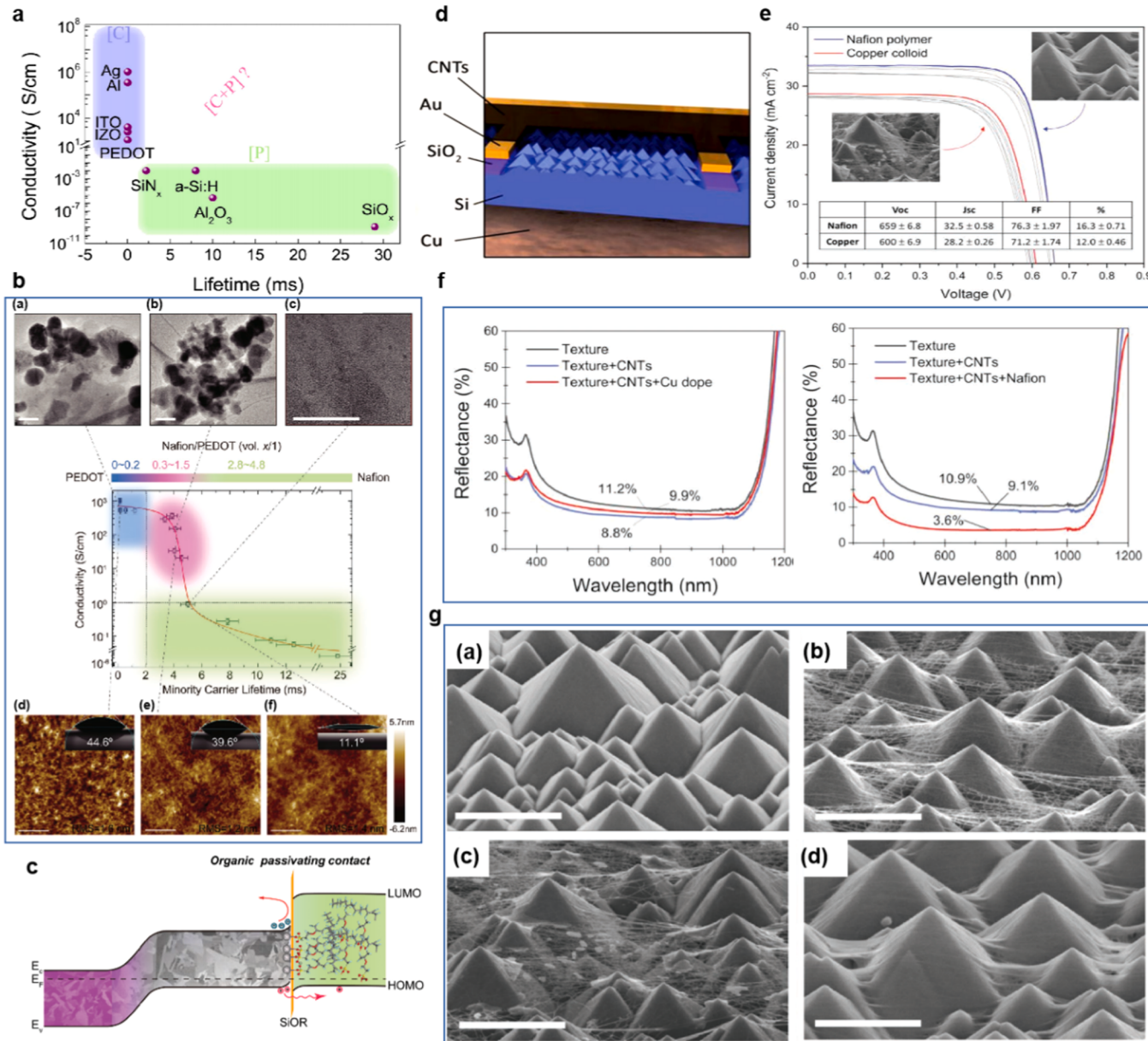


**Fig. 12.** (a) Curves of conductivity versus minority carrier lifetime for different metals, conducting polymers and dielectric passivation materials. (b) a-c) TEM images of Nafion/PEDOT, d-f) AFM images and contact angles, and the center curve plots conductivity versus minority carrier lifetime for Nafion, Nafion/PEDOT and PEDOT. (c) Schematic of band alignment and electrochemical grafting mechanism [177]. (d) Schematic of Si/CNTs HJSC. (e) J-V curves of Si/CNTs/Nafion and Si/CNTs/CuCl<sub>2</sub>/Cu(OH)<sub>2</sub> SC. (f) Reflectance changes with addition of CuCl<sub>2</sub>/Cu(OH)<sub>2</sub> colloidal dopant and Nafion polymeric acid dopant. (g) SEM images of a) random pyramid texture, b) with CNTs, c) CNTs/CuCl<sub>2</sub>/Cu(OH)<sub>2</sub> and d) Nafion [178].

(c) Reproduced with permission. [177] Copyright 2020, John Wiley and Sons. (g) Reproduced with permission. [178] Copyright 2019, John Wiley and Sons.

#### 4.2. Flexible heterojunction SCs

The flexibility of HJSCs enables itself to a variety of applications, such as portable power generators for wearable electronics, power-generated textiles and building-integrated PV systems. Owing to its long-term stability, high transparency, high conductivity and excellent mechanical flexibility, carbon materials have also attracted much attention in the fields of electrode, carriers transport and photoactive layer for different generation of flexible SCs, such as flexible DSSCs, OSCs, PSCs and Si-based HJSCs [180]. Graphene and CNTs with a lower  $R_s$  and negligible change in resistance under various flexible conditions are commonly used as the substitutes for Pt counter electrodes in DSSCs. Since their catalytic performance is lower than that of Pt electrode for I<sub>3</sub> reduction, there are several optimization methods to generate new

catalytic sites, such as plasma treatment to improve the hydrophilicity of CNTs [181], heteroatom doping of graphene [182], complexation with metal oxides [183], metal sulfides [184] and conductive polymers [185]. Besides, they have also been reported as photoanode in DSSCs to overcome the brittleness of pristine TiO<sub>2</sub> by virtue of their flexibility. And CNTs is used as both counter electrode and photoanode in flexible and stable fiber-shaped DSSCs [186]. Given that most DSSCs with the use of liquid electrolytes, it is still not considered to be the most desirable target for flexible and stable device. Fullerenes and their derivatives with tunable energy levels and high electron affinity have been developed as electron acceptor in OSCs. In addition, fullerenes and their derivatives are further introduced as electron transport [187], and CNTs and graphene are reported as transparent electrode [188]. However, flexible OSCs suffers poor efficiency and much lower PCE than PSCs

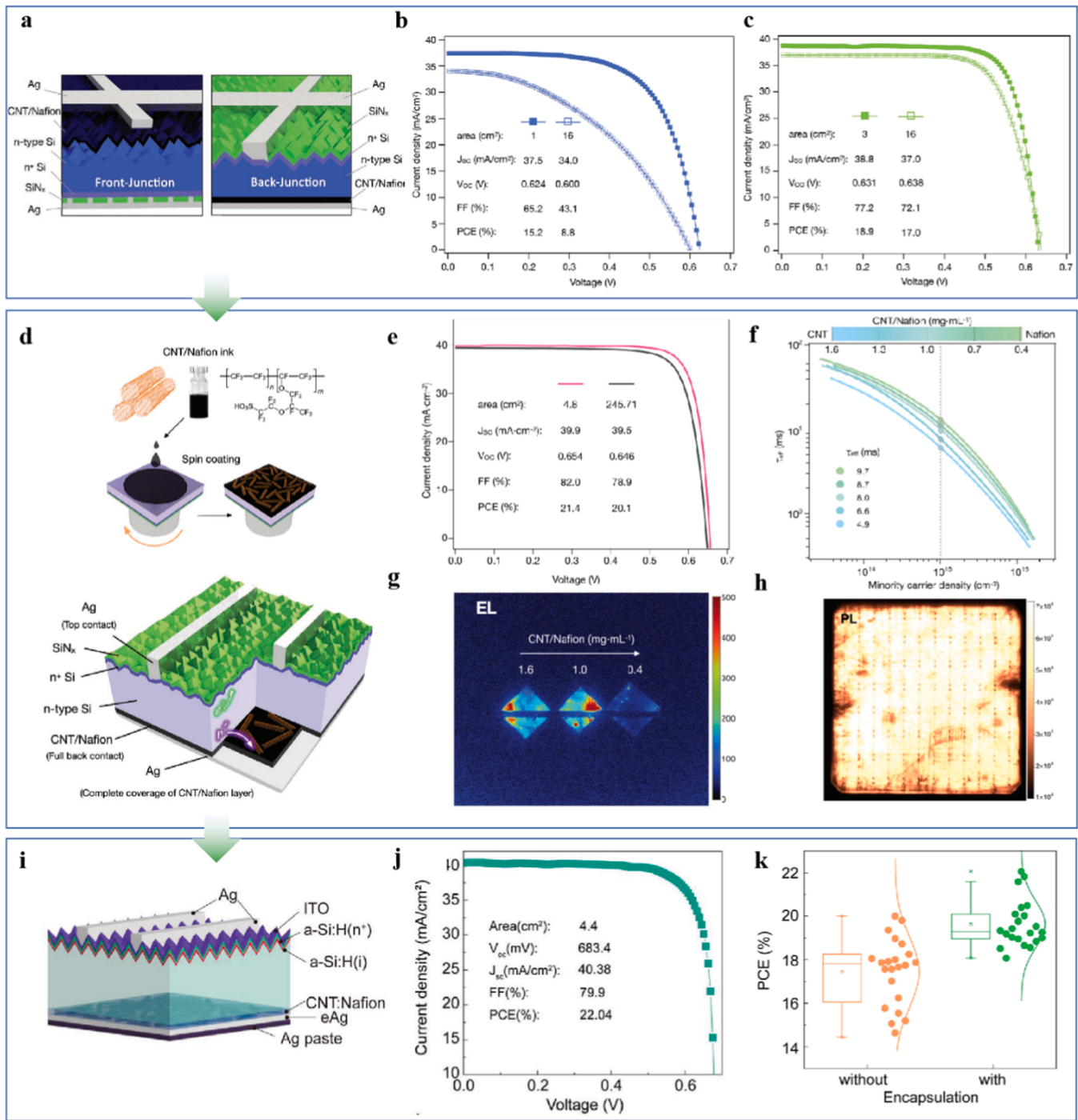


**Fig. 13.** (a) Schematic of Si/CNTs/Nafion HJSC with front-junction and back-junction design. J-V curves of Si/CNTs/Nafion HJSC with (b) front-junction and (c) back-junction design [48]. (d) Schematic of Si/CNTs/Nafion HJSC prepared by spin coating CNTs/Nafion ink. (e) J-V curves of Si/CNTs/Nafion SC with device areas of 4.8 and 245.71 cm<sup>2</sup>. (f) Transient photoconductance decay measurements, (g) electroluminescence intensity maps and (h) photoluminescence intensity map of CNTs/Nafion film [25]. (i) Schematic, (j) J-V curves and (k) PCE distribution of Si/CNTs@Nafion/eAg HJSC with Back-junction.

(c) Reproduced with permission. [48] Copyright 2020, John Wiley and Sons. (h) Reproduced with permission. [25] Copyright 2020, John Wiley and Sons. (j) Reproduced with permission [23]. Copyright 2021, Wiley-VCH GmbH.

which typically show relatively high PCE over 22% [189]. Similarly, fullerenes and their derivatives display excellent electron extraction as transportor, while CNTs and graphene are commonly used as front/back electrode and hole transportor in flexible PSCs. For the newest generation SCs, there is still a urgent need for the systemic research of the various roles of carbon materials in flexible DSSCs, OSCs and PSCs. On the contrary, Si-based HJSCs, as the first-generation SCs, still have a strong competitiveness with its greater promotion and price advantage

in the application of flexible device.

Although numerous studies about CNT-based HJSCs with high PCE have been reported, the PCE of their flexible devices is still lower than those of commercial bulk SC modules [190]. Conventional Si-based flexible SCs are typically based on Si wafer with a thickness of around 160–240 μm, which strictly limits the reduction of fabrication cost. Moreover, due to the indirect bandgap and insufficient optical absorption of Si, thinner absorber would lead to a reduced light trap. Further

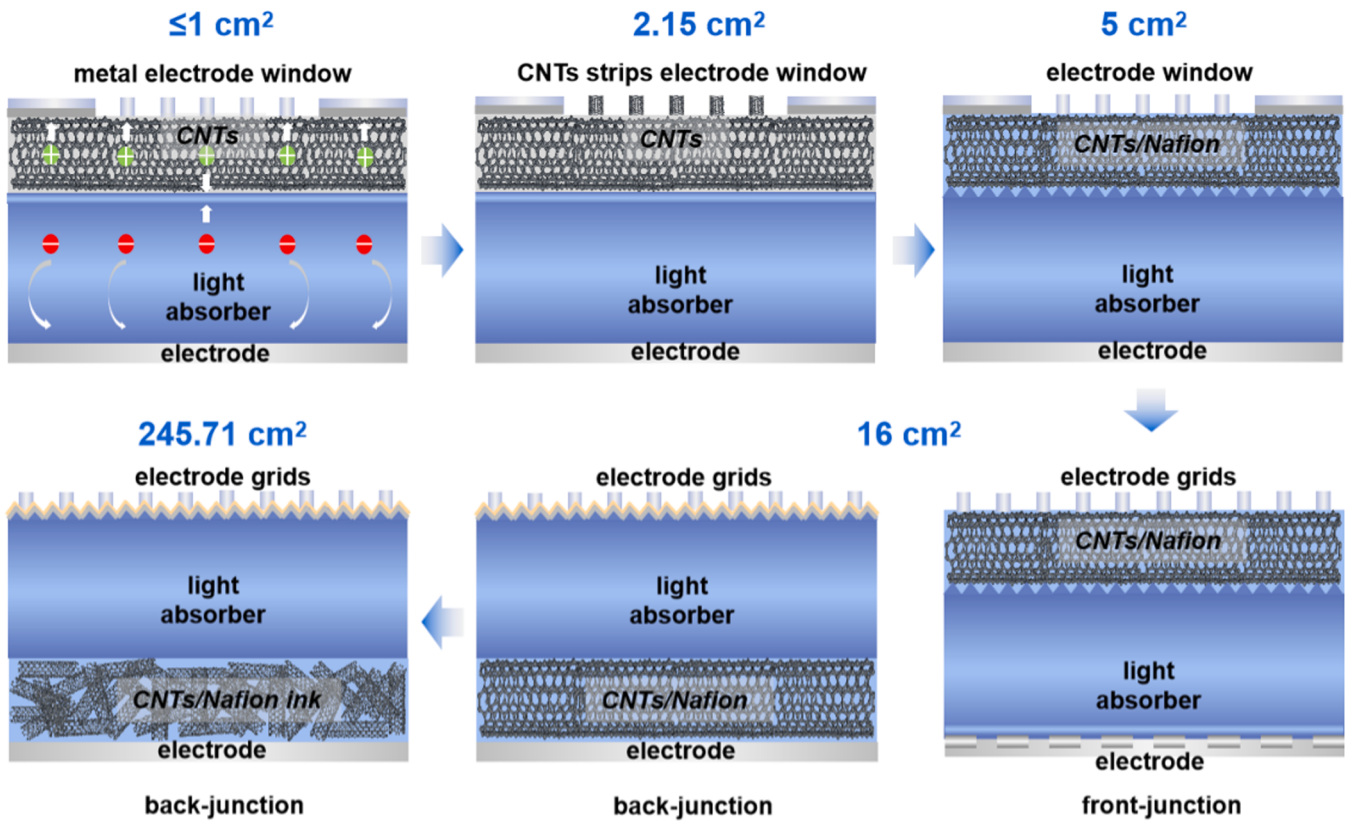


Fig. 14. Schematic of evolution of Si/CNTs HJSC with large area design.

optimization steps involve lightgraphy, etching, ion implantation and high temperature annealing, which would significantly increase the cost [191]. Hybrid design system, such as Si/carbon materials [192] or Si/conducting polymers [193], offer a cost-effective approach for flexible HJSCs. The PCE and FF of pristine Si/Graphene flexible HJSCs without modification are only 1.3% and 25.2%, respectively, due to its thinner absorber with a thickness of only 10.6  $\mu\text{m}$ . Notably, the PCE and FF are enhanced to 5.09% and 60.4% after adding PMMA, respectively [194]. Sonali *et al.* proposed an all-dielectric approach, comprising lossless spherical silica and titania nanoparticle bilayers to simulate leaf-inspired biomimetic omnidirectional photon management and their light trapping mechanism, and fabricated flexible Si/graphene HJSC [192]. As shown in Fig. 15a and b, leaf-focusing and waveguiding, and scattering are performed, and the incident light is managed through whispering gallery modes and subsequent forward scattering. The top-to-bottom configuration would increase the incident light path length and allow for omnidirectional absorption, behaving as a waveguide to trap and scatter the light. The cell design includes a 20  $\mu\text{m}$  Si substrate,  $\text{Al}_2\text{O}_3$  interface passivator, and  $\text{TiO}_2$  and Si nanoparticles, without any micro-nano modification of Si surface, thus avoiding the optical management profits offset by interface recombination losses. The J-V curves in Fig. 15c show an increase in PCE from 6.8% to 8.8% after optical management, and the pseudo J-V curves indicate that the apparent FF loss may be caused by the  $R_s$ . Moreover, the reduction of incident radiation by the cosine effect is estimated. The angle-dependent current density of cells with and without optical management in Fig. 15d show a minimal  $I_{sc}$  deviation of bio-inspired SC as an angle tuning, which confirms that the effectiveness of bi-layer nanoparticles for omnidirectional ARC [192].

Despite the excellent roughness of flexible Si/graphene HJSCs, the PCE is still relatively low due to insufficient light absorbs of ultrathin Si substrate. CNTs have been reported to have intrinsic mobility over  $10^5$

$\text{cm}^2/(\text{V.s})$ , high electrical conductivity up to  $10^6 \text{ S/cm}$ , Young's modulus of 1–2 TPa, tensile strength of 10–100 GPa, elongation at breaking of 6–12% and specific surface areas of  $1600 \text{ m}^2/\text{g}$ , which provides a solid foundation for their applications in flexible SCs [180]. The better photon absorption of CNTs shows a great potential to improve the performance of flexible HJSCs. Thin flexible Si/CNTs HJSCs composed of Si thin film with less than 50  $\mu\text{m}$  has been investigated with a PCE of 3–5% for initial cell. The thickness of Si is reduced from 235 to 20  $\mu\text{m}$  through KOH wet-etching, with the  $V_{oc}$  decreasing from 540 to 472 mV, and the PCE reducing from 5.1% to 4.2%. Thinner Si substrate, longer etching time and tougher Si surface, thus serious surface recombination between Si and CNTs limits the breakthrough in the PCE for thin flexible HJSCs.

Despite an impressive PCE of flexible Si/CNTs HJSC (6%) is obtained after doping with  $\text{HNO}_3$ , it is still lower than of Si/CNTs bulk HJSCs (~7%), especially a lower  $I_{sc}$  [190]. Combining p-type CNT film (<20 nm) and n-type Si wafer ( $\leq 50 \mu\text{m}$ ), the fabricated flexible hybrid Si/CNTs HJSCs exhibit an intrinsic PCE of ~7.5% with any additional light-trapping structures [191]. The fabrication steps of sandwich flexible Si/CNTs HJSCs involving lithographic process, CNTs deposition and PET encapsulation. The devices with 50  $\mu\text{m}$  thickness of c-Si revealed a higher current rectification ratio ( $>10^4$  at  $\pm 1 \text{ V}$ ) and lower ideality factors (1.1–1.3), implying a reduction of recombination in the junction, and resulting in a higher PCE (7.37%) than that of the previous report (3–5%) [190]. Due to the reduced thickness dependence, the PCE decreased by 47% after the thickness is reduced to 12  $\mu\text{m}$ , and increased to 8.61% after the addition of  $\text{TiO}_2$  ARC. To sum up, the PCE of graphene and CNT-based flexible HJSCs is severely limited, mainly including insufficient light absorption of flexible thin substrate and lack of effective surface/interface modification. Based on the optimization approaches summarized above, graphene and CNTs with excellent properties could be further utilized to realize cost-effective and high-efficiency flexible HJSCs.

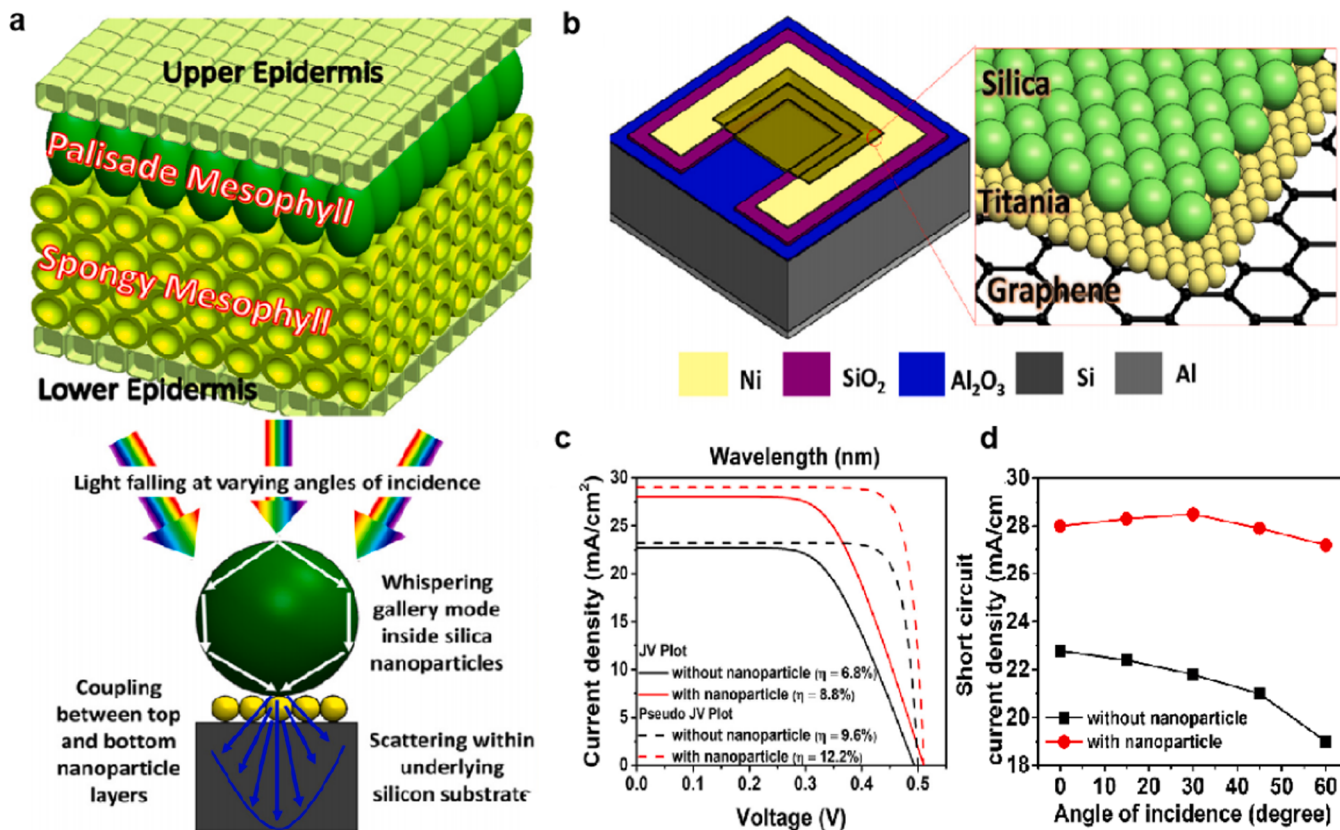


**Fig. 15.** (a) Schematic of leaf anatomy and their corresponding light trapping mechanism and (b) flexible Si/graphene HJSC. (c) Comparison of J-V curves and pseudo J-V curves, and (d) angle of incidence-I<sub>sc</sub> plot of the flexible Si/graphene HJSCs [192]; Reproduced with permission. [192] Copyright 2019, Elsevier.

#### 4.3. Roadmap of carbon material-based heterojunction SCs

To date, the shortcomings of CNT-based HJSCs, as reported in a comprehensive overview [110] of state-of-the-art Si/CNTs heterojunction devices, have been addressed. CNTs, as a representative carbon material, have been systemic studied in the HJSCs field. The previously

mentioned limited active area of HJSCs (less than 1 cm<sup>2</sup>) has been increased to 245.71 cm<sup>2</sup>, while maintaining a promising PCE of 20.1% [25]. In addition, the performance of Si/CNTs HJSCs is largely affected by the  $R_s$  of CNT films. Connecting CNTs and PSS can further reduce the  $R_s$  from  $\sim 200 \Omega \text{ sq}^{-1}$  [195] to  $\sim 115 \Omega \text{ sq}^{-1}$  [26] at a light transparency of 90%. Although lower  $R_s$  and a larger active area are obtained,

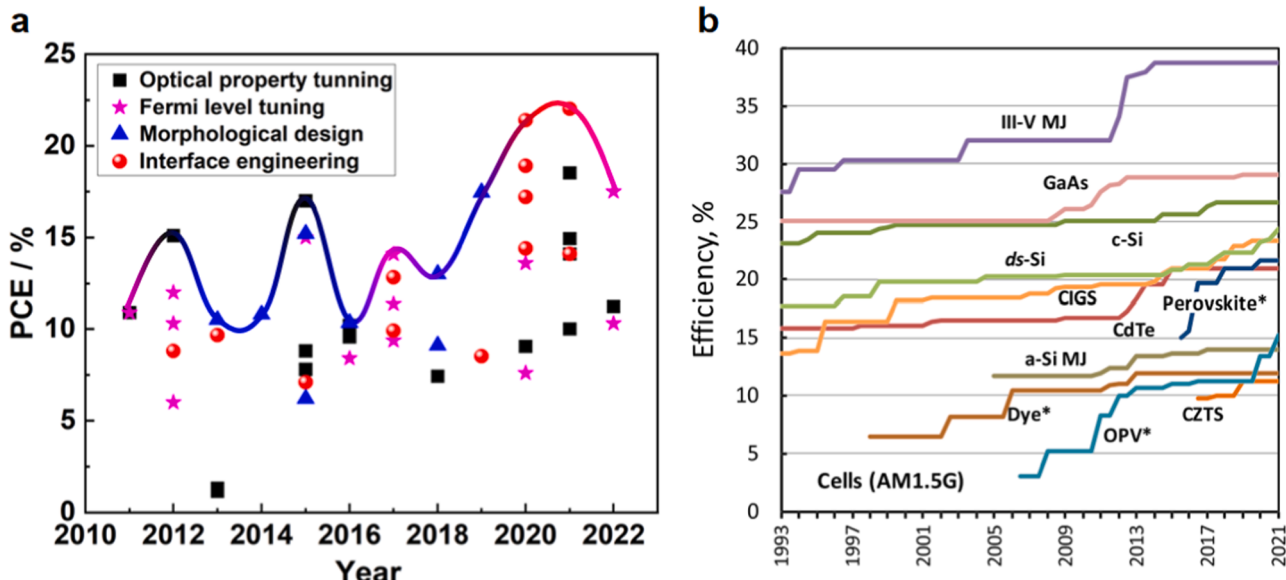


**Fig. 16.** (a) A decade of development of CNTs-based HJSCs; (b) Twenty-eight years of progress of SCs [200]. (b) Reproduced with permission. [200] Copyright 2020, John Wiley and Sons.

considerable obstacles still exist that hinder the improvement and commercialization of CNT-based HJSCs, such as tube chirality, the Fermi level, and the device structure. As displayed in Fig. 16a, several optimization methods have been adopted for Si/CNTs HJSCs over the past decade, including optical property tuning, Fermi level tuning, morphological design and interface engineering, which have dramatically enhanced incident light absorption, forced the separation of photogenerated carriers, and reduced carrier recombination. However, CNT film composed of numerous randomly entangled tubes offered many interconnected sections and blank areas, which inevitably lead to higher  $R_s$  [110]. According to the progress in morphological design, it is probable that the combination of the additives such as Ag nanowires [159] and graphene [157] for the preparation of composite films will not achieve a breakthrough, and the PCE will remain at 10–15%, which can be attributed to the loss of incident light. Conversely, O<sub>3</sub> etching of CNTs can change the intrinsic resistance of the film, thereby enhancing the PCE to 17.46% [114]. In addition, adjustment of the Fermi level could increase the work function of CNT film and enhance the junction barrier height, thereby further increasing the carrier concentration at the interface. Molecular absorption and solid-state functionalization has been used to achieve p-doping. However, the highest PCE was around 15% because of the instability of the gaseous or chemical compound molecular dopants. Therefore, there is an urgent need to develop an efficient way, such as B-/N-doping [196], to realize the optimization or doping of CNT film to obtain high-performance, long-term stable CNT-based HJSCs.

Starting from the first reported Si/CNTs HJSCs with a PCE of 1.4% [18] and GaAs/CNTs HJSCs with a PCE of 3.8% [56], excellent PCE over 22% [23] has been achieved through interface engineering. Although Si/CNTs HJSCs with great potential for industrial application exhibited high performance close to the predicted value of ~23% [197], there is still a certain gap between them and the heterojunction interdigitated back contact Si-based SCs (26.6%) [198] and the Shockley-Quiesser limit of the c-Si SCs (~29.43%) [199]. In future work, CNT-based SCs should be developed to be lighter, with a lower cost, a large area, and a flexible and integrated design. The design of CNT-based heterojunctions is ongoing, aiming to increase the device quality and simplify the preparation process by replacing conventional homogeneous SCs. The efficiency comparison of different types of SCs [200] is shown in Fig. 16b. Compared with Si/CNTs heterojunctions, GaAs has a direct band gap of 1.42 eV, and a higher optical absorption coefficient and electron mobility, permitting the optimum harvesting and conversion of incident light [201]. Thus, the addition of GaAs to HJSCs could theoretically achieve higher PCE, and a thinner GaAs absorption area could make the device lighter. Moreover, CNT film shows great potential for assembling flexible devices because of their excellent flexibility and structural stability, as well as the solution processability of CNT/polymer composites, which offers the possibility of simplifying the preparation process and reducing the cost.

Although progress has been made, research on CNT-based HJSCs should focus on multi-mechanism synergistic optimization. On the one hand, p-doping has been confirmed as an efficient optimization method for CNT film, such as acid doping [135] and gas molecular absorption [139]. However, it is still not stable enough, which severely limit performance improvement. On the other hand, the redox functionalization of CNTs with the CuCl<sub>2</sub>/Cu(OH)<sub>2</sub> dopant and its redox reaction (Cu<sup>2+</sup>/Cu<sup>+</sup>) [145] not only reduces the Fermi level of CNT film, but also maintains one year stability in air. However, the characteristic of solid-state dopants do not appear to be suitable for surface micro/nano configuration for light management because of their colloidal-like nature and heterogeneity, which has been demonstrated in a comparative study [178]. Interestingly, a design of “Solid-state photoelectrochemical SCs” and a Schottky junction formed with an embedded polyvinyl alcohol (PVA) based solid electrolyte (PVA+H<sub>2</sub>SO<sub>4</sub>) has been proposed, which demonstrated that a hybrid working mechanism combining chemical modification and electronic coupling is a feasible and

convenient approach for HJSCs [202]. Owing to their flexibility and simplicity of assembly, PVA-based solid electrolytes have been widely used in solid-state supercapacitors [203]. PVA/acid solid electrolytes were proven to be beneficial for the enhancement of the PCE, which is attributed to acid doping and the photochemical effect [202]. Therefore, in addition to acidic additives, combining PVA and redox additives, such as Fe<sup>2+</sup>/Fe<sup>3+</sup> [204], I<sup>-</sup> [205], Br<sup>-</sup> [206] or VOSO<sub>4</sub> [207], could enhance the photochemical effect by exploiting the electrochemical effect of reversible redox reactions, thereby accelerating the photogenerated carrier separation using charge transfer. Such a design could realize both acid doping of carbon materials and electrochemical/photochemical synergistic effect of carrier transportors, with a hybrid working mechanism being regarded as an efficient method to produce carbon material-based HJSCs.

In addition, the PCE of single junction SCs are limited by the finite sunlight absorption spectrum, whereas multi-junction tandem SCs like Si/III-V [208] and Si/perovskite [209] could expand the light absorption range with different wavelengths contrarily, resulting in a higher PCE. For homogeneous MJSCs, the continuous growth of multi-layers might lead to severe lattice mismatch, leading to the defects that limit the optimization of a device. Advanced methods, such as direct wafer bonding [210], intermetallic bonding [211], and smart stack technology [208] have been adopted to fabricate the hybrid MJSCs, which could further simplify the process and reduce the cost. Indeed, more effort is required to investigate carbon material-based heterojunction in MJSCs, which have shown great potential application in large-area and flexible PVs.

## 5. Conclusion

The remarkable development of carbon allotropes as versatile materials in the PV industry has attracted much attention, especially in the development of HJSCs. The key roles of carbon materials in the PV field and excellent top-down optimization strategies for HJSC performance are summarized, including surface optical engineering, Fermi level tuning, surface electrical property tuning for the carbon materials layer, and interface engineering between the carbon materials and the semiconductor substrate. The CNT-based HJSCs with the highest PCE of 22.02% and the largest active area are expected to reach an industrial level of up to 245.17 cm<sup>2</sup>, while maintaining a PCE above 20%. Thus, there is plenty of room for HJSCs performance optimization and industrialization.

Firstly, pushing high-efficiency heterojunction devices to the theoretical limit is one of the biggest challenges. There are still difficulties in manufacturing high quality carrier transportors with extremely high conductivity to realize perfect heterojunctions and excellent junction structure. Research on carbon material-based HJSCs is mostly limited to Si-based devices. Heterojunctions composed of absorber with high photoabsorption coefficients and ideal band alignments remain the dominant factor responsible for high PCE.

Secondly, although the existing optimization methods, such as acid doping and solid-state functionalization, could significantly enhance cell performance, a strategy for long-term stable devices is still lacking. The desired device stability requires not only advanced absorber and transportor layers, but also an appropriate device frame and encapsulation design. Nevertheless, more effort is required to explore multi-mechanism optimization strategies to further promote the optimization of HJSCs.

Thirdly, insufficient efficiency and stability still limit the development of large-area and flexible HJSCs that are cost-effective and can be manufactured on a large scale.

In conclusion, this review analyzed the current application of carbon materials in the field of HJSCs, their advanced optimization strategies and designs, and their main scientific challenges. To achieve high-performance HJSCs with a large area and excellent flexibility, it is necessary to develop material optimization strategies, novel junction

structures, and advanced device design. Therefore, we suggest that future research should focus on the following directions:

- (71) Firstly, more basic research on HJSCs is required, including that on functional layers, junction design, and optimization mechanisms of SCs. The direct application of carbon materials for junction preparation might result in poor interfacial connection, leading to sluggish carrier kinetics and weakened stability. Therefore, the development of new functional layers for heterojunctions is imperative. Moreover, exploring new interface passivators and the corresponding techniques to fabricate state-of-art heterojunctions will provide an alternative pathway to produce highly efficient carbon material-based HJSCs.
- (72) Secondly, overcoming the instability of HJSCs is a long-overlooked issue. Poor cell performance is not only related to the design of the functional layers, their junction design, and band alignment, but also is influenced by the device encapsulation design and technology. Thus, based on optimized transportors and junctions, and their interfaces, there is an urgent need to develop functional layers and cost-effective encapsulation techniques to prevent the decay of SC performance, from internal recombination inhibition to external oxidation aging.
- (73) Finally, cutting edge research on the design of novel HJSCs could not only maximize light utilization, but also enhance economic benefits and expand their application. The development of large-area and flexible devices places high demand on material preparation, cell efficiency, and stability. Novel designs of HJSCs include hybrid carbon material-based HJSCs, multiple working mechanisms, and multi-junction tandem techniques. Furthermore, multi-device module integration of HJSCs with other electronic devices, such as supercapacitors and sensing elements, is also crucial from an economic perspective.

#### CRediT authorship contribution statement

Profs. Guoqiang Li and Wenliang Wang proposed the project. Profs. Guoqiang Li and Wenliang Wang supervised the project. Youtian Mo wrote and revised the manuscript. Xi Deng, Peixin Liu and Jiansen Guo provided the information support and assisted with the manuscript revision. All authors made contributions to the discussions and interpretations.

#### Declaration of Competing Interest

The authors declare no competing financial or non-financial interests.

#### Data Availability

No data was used for the research described in the article.

#### Acknowledgments

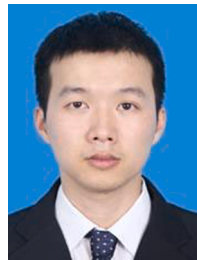
This work was supported by the National Key Research and Development Program of China (No. 2022YFB3604500), the Distinguished Youth Foundation of Guangdong Scientific Committee (No. 2021B1515020001), the Sail Plan of Guangdong Province (No. 2017YT05C007), the Technology Development Project of Shanxi-Zheda Institute of Advanced Materials and Chemical Engineering (No. x2cl/D8225310), the Development Fund of Changchun Institute of Optics, Fine Mechanics and Physics, CAS (No. x2cl/B7210410), and the Key Area Research and Development Project of Guangdong Province (No. 2020B010170001).

#### References

- [1] H. Hanaei, M.K. Assadi, R. Saidur, *Renew. Sust. Energ. Rev.* 59 (2016) 620–635.
- [2] M.R. Khan, M.T. Patel, R. Asadpour, H. Imran, N.Z. Butt, M.A. Alam, *J. Phys. D Appl. Phys.* 54 (2021), 323001.
- [3] D. Luo, X. Li, A. Dumont, H. Yu, Z.H. Lu, *Adv. Mater.* 33 (2021) 2006004.
- [4] B. Chen, N. Ren, Y. Li, L. Yan, S. Mazumdar, Y. Zhao, X. Zhang, *Adv. Energy Mater.* 12 (2021) 2003628.
- [5] D. Devadiga, M. Selvakumar, P. Shetty, M.S. Santosh, *J. Electron. Mater.* 50 (2021) 3187–3206.
- [6] D. Zhang, M. Stojanovic, Y. Ren, Y. Cao, F.T. Eickemeyer, E. Socie, N. Vlachopoulos, J.-E. Moser, S.M. Zakeeruddin, A. Hagfeldt, M. Gratzel, *Nat. Commun.* 12 (2021) 1777.
- [7] L. Zhu, M. Zhang, J. Xu, C. Li, J. Yan, G. Zhou, W. Zhong, T. Hao, J. Song, X. Xue, Z. Zhou, R. Zeng, H. Zhu, C.-C. Chen, R.C.I. MacKenzie, Y. Zou, J. Nelson, Y. Zhang, Y. Sun, F. Liu, *Nat. Mater.* 21 (2022) 656.
- [8] V. Karade, A. Lokhande, P. Babar, M.G. Gang, M. Suryawanshi, P. Patil, J.H. Kim, *Sol. Energy Mater. Sol. Cells* 200 (2019), 109911.
- [9] J.-R. Wu, D. Thakur, S.-E. Chiang, A. Chandel, J.-S. Wang, K.-C. Chiu, S.H. Chang, *Nanomaterials* 9 (2019) 1269.
- [10] W. Shockley, H.J. Queisser, *J. Appl. Phys.* 32 (1961) 510–519.
- [11] Y. Zhang, H. Liu, *J. Phys. D* 53 (2020), 233001.
- [12] Z. Zhang, Z. Li, L. Meng, S.-Y. Lien, P. Gao, *Adv. Funct. Mater.* 30 (2020) 2001904.
- [13] J. Zhao, J. Zha, Z. Zeng, C. Tan, *J. Mater. Chem. A* 9 (2021) 18887–18905.
- [14] M.A. Deshmukh, S.-J. Park, B.S. Hedau, T.-J. Ha, *SoEn* 220 (2021) 953–990.
- [15] G.K. Bhagavat, K.D. Nayak, *Thin Solid Films* 64 (1979) 57–62.
- [16] Y. Liu, Y. Li, Y. Wu, G. Yang, L. Mazzarella, P. Procel-Moya, A.C. Tamboli, K. Weber, M. Boccard, O. Isabella, X. Yang, B. Sun, *Mater. Sci. Eng. R. Rep.* 142 (2020), 100579.
- [17] S. Lin, Y. Lu, J. Xu, S. Feng, J. Li, *Nano Energy* 40 (2017) 122–148.
- [18] J. Wei, Y. Jia, Q. Shu, Z. Gu, K. Wang, D. Zhuang, G. Zhang, Z. Wang, J. Luo, A. Cao, D. Wu, *Nano Lett.* 7 (2007) 2317–2321.
- [19] X. Li, H. Zhu, K. Wang, A. Cao, J. Wei, C. Li, Y. Jia, Z. Li, X. Li, D. Wu, *Adv. Mater.* 22 (2010) 2743–2748.
- [20] W. Jie, F. Zheng, J. Hao, *Appl. Phys. Lett.* 103 (2013), 233111.
- [21] Y. Song, X. Li, C. Mackin, X. Zhang, W. Fang, T. Palacios, H. Zhu, J. Kong, *Nano Lett.* 15 (2015) 2104–2110.
- [22] X. Li, W. Chen, S. Zhang, Z. Wu, P. Wang, Z. Xu, H. Chen, W. Yin, H. Zhong, S. Lin, *Nano Energy* 16 (2015) 310–319.
- [23] J. Yan, C. Zhang, H. Li, X. Yang, L. Wan, F. Li, K. Qiu, J. Guo, W. Duan, A. Lambertz, W. Lu, D. Song, K. Ding, B.S. Flavel, J. Chen, *Adv. Sci.* 8 (2021) 2102027.
- [24] S. Li, Y. Li, K. Liu, M. Chen, W. Peng, Y. Yang, X. Li, *J. Colloid Interface Sci.* 600 (2021) 691–700.
- [25] J. Chen, L. Wan, H. Li, J. Yan, J. Ma, B. Sun, F. Li, B.S. Flavel, *Adv. Funct. Mater.* 30 (2020) 2004476.
- [26] R. Xie, H. Sugime, S. Noda, *Carbon* 175 (2021) 519–524.
- [27] L. Wen, F. Gao, Y. Yu, Z. Xu, Z. Liu, P. Gao, S. Zhang, G. Li, *J. Mater. Chem. A* 6 (2018) 17361–17370.
- [28] T.-S. Chen, Y.-C. Hsueh, S.-E. Chiou, S.-T. Shiue, *Sol. Energy Mater. Sol. Cells* 137 (2015) 185–192.
- [29] Z. Li, L. Zheng, V. Saini, S. Bourdo, E. Dervishi, A.S. Biris, *J. Exp. Nanosci.* 8 (2013) 565–572.
- [30] Z. Li, S.A. Kulkarni, P.P. Boix, E. Shi, A. Cao, K. Fu, S.K. Batabyal, J. Zhang, Q. Xiong, L.H. Wong, N. Mathews, S.G. Mhaisalkar, *ACS Nano* 8 (2014) 6797–6804.
- [31] A.B. Cook, J.D. Yuen, A. Zakhidov, *Appl. Phys. Lett.* 103 (2013), 163301.
- [32] T.A. Shastry, M.C. Hersam, *Adv. Energy Mater.* 7 (2017) 1614–6832.
- [33] L. Kavan, Exploiting Nanocarbons in Dye-Sensitized Solar Cells, in: M. Marcaccio, F. Paolucci (Eds.), *Making And Exploiting Fullerenes, Graphene, And Carbon Nanotubes*, vol 348, 2014, pp. 53–93.
- [34] W. Li, S. Zhang, Q. Chen, Q. Zhong, *Catal. Sci. Technol.* 11 (2021) 2745–2752.
- [35] B. Farhadi, M. Naseri, *Optik* 127 (2016) 6224–6231.
- [36] K.J. Singh, T.J. Singh, D. Chettri, S.K. Sarkar, *Optik* 135 (2017) 256–270.
- [37] W. Xu, S. Wu, X. Li, M. Zou, L. Yang, Z. Zhang, J. Wei, S. Hu, Y. Li, A. Cao, *Adv. Energy Mater.* 6 (2016) 1600095.
- [38] X. Zhao, D. Wang, S. Liu, Z. Li, J. Meng, Y. Ran, Y. Zhang, L. Li, *Mater. Res. Bull.* 125 (2020), 110800.
- [39] D.S. Hecht, L. Hu, G. Irvin, *Adv. Mater.* 23 (2011) 1482–1513.
- [40] M. Aftabuzzaman, C.K. Kim, H. Zhou, H.K. Kim, *Nanoscale* 12 (2020) 1602–1616.
- [41] X. Wang, Y. Xie, Y. Jiao, K. Pan, B. Bateer, J. Wu, H. Fu, J. Mater. Chem. A 7 (2019) 10405–10411.
- [42] J. Qiu, D. He, H. Wang, W. Li, B. Sun, Y. Ma, X. Lu, C. Wang, *Electrochim. Acta* 367 (2021), 137451.
- [43] B. Pang, M. Zhang, C. Zhou, H. Dong, S. Ma, J. Feng, Y. Chen, L. Yu, L. Dong, *Chem. Eng. J.* 405 (2021), 126944.
- [44] K. Zhao, Y. Zhao, M. Hao, X. Li, S. Liu, L. Li, W. Zhang, *Electrochim. Acta* 399 (2021), 139441.
- [45] D.M. Mitin, A.D. Bolshakov, V. Neplokh, A.M. Mozharov, S.A. Raudik, V. Fedorov, K.Y. Shugurov, V.Y. Mikhailovskii, P.M. Rajanna, F.S. Fedorov, A. G. Nasibulin, I.S. Mukhin, *Energy Sci. Eng.* 8 (2020) 2938–2945.
- [46] Y. Mo, H. Zhou, B. Zhang, X. Du, Z. Lin, W. Li, H.-Y. Liu, Y.-W. Mai, *Appl. Surf. Sci.* 465 (2019) 23–30.
- [47] G.L. Che, B.B. Lakshmi, C.R. Martin, E.R. Fisher, *Langmuir* 15 (1999) 750–758.

- [48] J. Chen, D.D. Tune, K. Ge, H. Li, B.S. Flavel, *Adv. Funct. Mater.* 30 (2020) 2000484.
- [49] A. Di Bartolomeo, *Phys. Rep.* 606 (2016) 1–58.
- [50] J. Ma, H. Bai, W. Zhao, Y. Yuan, K. Zhang, *SoEn* 160 (2018) 76–84.
- [51] S.-H. Hwang, R. Iwamoto, T. Okumura, K. Kamataki, N. Itagaki, K. Koga, T. Nakatani, M. Shiratani, *Thin Solid Films* 729 (2021), 138701.
- [52] R.A. Ismail, W.K. Hamoudi, K.K. Saleh, *Mater. Sci. Semicond. Process.* 21 (2014) 194–199.
- [53] H.A. Yu, Y. Kaneko, S. Yoshimura, S. Otani, *Appl. Phys. Lett.* 68 (1996) 547–549.
- [54] J.-H. Kim, H.-G. Kim, L.-K. Kwac, *CAP* 26 (2021) 1–8.
- [55] H. He, X. Yu, Y. Wu, X. Mu, H. Zhu, S. Yuan, D. Yang, *Nano Energy* 16 (2015) 91–98.
- [56] C.W. Liang, S. Roth, *Nano Lett.* 8 (2008) 1809–1812.
- [57] Y. Chen, X. Shi, D. Zhou, H. Wei, G. Yang, L. Zhang, M. Zhu, H. Yin, L. Sun, Y. Su, *J. Alloy. Compd.* 932 (2023), 167624.
- [58] S. Yavuz, E.M. Loran, N. Sarkar, D.P. Fenning, P.R. Bandaru, *ACS Appl. Mater. Interfaces* 10 (2018) 37181–37187.
- [59] P. Wang, X. Li, Z. Xu, Z. Wu, S. Zhang, W. Xu, H. Zhong, H. Chen, E. Li, J. Luo, Q. Yu, S. Lin, *Nano Energy* 13 (2015) 509–517.
- [60] Z. Shadrok, S. Sousani, S. Gholipour, Y. Abdi, *SoEn* 201 (2020) 908–915.
- [61] J. Raiguru, P. Mahanandia, B. Subudhi, *Opt. Mater.* 111 (2021), 110612.
- [62] M.K.A. Mohammed, M. Dehghanipour, U. Younis, A.E. Shalan, P. Sakthivel, G. Ravi, P.H. Bhoite, J. Pospisil, *N. J. Chem.* 44 (2020) 19802–19811.
- [63] J. Ryu, S. Yoon, J. Park, S.M. Jeong, D.-W. Kang, *Appl. Surf. Sci.* 516 (2020), 146116.
- [64] Y. Qian, S. Seo, I. Jeon, H. Lin, S. Okawa, Y. Zheng, A. Shawky, A. Anisimov, E. I. Kauppinen, J. Kong, R. Xiang, Y. Matsuo, S. Maruyama, *Appl. Phys. Express* 13 (2020), 075009.
- [65] W. Zhang, F. Bu, W. Shen, X. Qi, N. Yang, M. Chen, D. Yang, Y. Wang, M. Zhang, H. Jiang, P. Strizhak, J. Tang, *RSC Adv.* 10 (2020) 24847–24854.
- [66] D. Khan, Z. Ali, D. Asif, M.K. Panjwani, I. Khan, *Ain Shams Eng. J.* 12 (2021) 897–900.
- [67] K.K. Markose, M. Jasna, P.P. Subha, A. Antony, M.K. Jayaraj, *SoEn* 211 (2020) 158–166.
- [68] P. Kumar, S. Dua, R. Kaur, M. Kumar, G. Bhatt, *RSC Adv.* 12 (2022) 4714–4759.
- [69] D. Dai, X. Tu, X. Li, T. Lv, F. Han, *Prog. Photovoltaic Res. Appl.* 27 (2019) 283–289.
- [70] W. Fan, H. Li, H. Zhang, L. Cai, J. Wang, X. Wang, Y. Wang, Y. Tang, Y. Song, *J. Mater. Sci. Mater. Electron.* 32 (2021) 2293–2301.
- [71] R. Zhang, M. Zhao, Z. Wang, Z. Wang, B. Zhao, Y. Miao, Y. Zhou, H. Wang, Y. Hao, G. Chen, F. Zhu, *ACS Appl. Mater. Interfaces* 10 (2018) 4895–4903.
- [72] Q. Guo, F. Yuan, B. Zhang, S. Zhou, J. Zhang, Y. Bai, L. Fan, T. Hayat, A. Alsaedi, *Za Tan, Nanoscale* 11 (2019) 115–124.
- [73] M. Ali, A.S. Anjum, R. Riaz, A. Bibi, K.C. Sun, S.H. Jeong, *Carbon* 181 (2021) 155–168.
- [74] Y. Zhang, Y. Zhao, J. Duan, Q. Tang, *Electrochim. Acta* 261 (2018) 588–595.
- [75] Y. Zhao, J. Duan, B. He, Z. Jiao, Q. Tang, *Electrochim. Acta* 282 (2018) 255–262.
- [76] C. Geng, Y. Shang, J. Qiu, Q. Wang, X. Chen, S. Li, W. Ma, H.-J. Fan, A.-A.-A. Omer, R. Chen, *J. Alloy. Compd.* 835 (2020), 155268.
- [77] Y. Wang, L. Yan, G. Ji, C. Wang, H. Gu, Q. Luo, Q. Chen, L. Chen, Y. Yang, C.-Q. Ma, X. Liu, *ACS Appl. Mater. Interfaces* 11 (2019) 2243–2253.
- [78] D. Xia, Z. Zhang, C. Zhao, J. Wang, J. Xia, G. Chen, S. Li, Z. Tang, S. You, W. Li, *J. Colloid Interface Sci.* 601 (2021) 70–77.
- [79] K. Kim, Z. Wu, J. Han, Y. Ma, S. Lee, S.K. Jung, J.W. Lee, H.Y. Woo, I. Jeon, *Adv. Energy Mater.* 12 (2022) 2200877.
- [80] J. Deng, B. Huang, W. Li, L. Zhang, S.Y. Jeong, S. Huang, S. Zhang, F. Wu, X. Xu, G. Zou, H.Y. Woo, Y. Chen, L. Chen, *Angew. Chem. -Int. Ed.* 61 (2022), e202202177.
- [81] X. Zhou, W. Zhang, S. Wang, F. Wen, Q. Chen, X. Shen, X. Hu, C. Peng, Z. Ma, M. Zhang, Y. Huang, S. Yang, W. Zhang, *Sci. China Mater.* 65 (2022) 2325–2334.
- [82] Y. Sun, R. Ma, Y. Kan, T. Liu, K. Zhou, P. Liu, J. Fang, Y. Chen, L. Ye, C. Ma, H. Yan, K. Gao, *Macromol. Rapid Commun.* (2022) 2200139.
- [83] A. Zeng, X. Ma, M. Pan, Y. Chen, R. Ma, H. Zhao, J. Zhang, H.K. Kim, A. Shang, S. Luo, I.C. Angunawela, Y. Chang, Z. Qi, H. Sun, J.Y.L. Lai, H. Ade, W. Ma, F. Zhang, H. Yan, *Adv. Funct. Mater.* 31 (2021).
- [84] T. Zheng, B. Fan, Y. Zhao, B. Jin, L. Fan, R. Peng, *J. Colloid Interface Sci.* 598 (2021) 229–237.
- [85] Y. Jiang, J. Wang, H. Zai, D. Ni, J. Wang, P. Xue, N. Li, B. Jia, H. Lu, Y. Zhang, F. Wang, Z. Guo, Z. Bi, H. Xie, Q. Wang, W. Ma, Y. Tu, H. Zhou, X. Zhan, *J. Am. Chem. Soc.* 144 (2022) 5400–5410.
- [86] P. Hang, J. Xie, C. Kan, B. Li, Y. Zhang, P. Gao, D. Yang, X. Yu, *Adv. Mater.* 33 (2021) 2006910.
- [87] H. Movla, S. Ghaffari, E. Rezaei, *OQE* 48 (2016) 390.
- [88] S. Beaupre, M. Leclerc, *J. Mater. Chem. A* 1 (2013) 11097–11105.
- [89] X. Li, Z. Lv, H. Zhu, *Adv. Mater.* 27 (2015) 6549–6574.
- [90] Z. Zhang, J. Lin, P. Sun, Q. Zeng, X. Deng, Y. Mo, J. Chen, Y. Zheng, W. Wang, G. Li, *J. Mater. Chem. A* 9 (2021) 16160–16168.
- [91] J. Chen, R. Liu, L. Zhu, W. Chen, C. Dong, Z. Wan, W. Cao, X. Zhang, R. Peng, M. Wang, *Mater. Lett.* 300 (2021), 130190.
- [92] Z. Li, J. Wei, P. Li, L. Zhang, E. Shi, C. Ji, J. Liu, D. Zhuang, Z. Liu, J. Zhou, Y. Shang, Y. Li, K. Wang, H. Zhu, D. Wu, A. Cao, *Nano Res* 5 (2012) 595–604.
- [93] Y. Ye, L. Gan, L. Dai, Y. Dai, X. Guo, H. Meng, B. Yu, Z. Shi, K. Shang, G. Qin, *Nanoscale* 3 (2011) 1477.
- [94] O. Vazquez-Mena, J.P. Bosco, O. Ergen, H.I. Rasool, A. Fathalizadeh, M. Tosun, M. Crommie, A. Javey, H.A. Atwater, A. Zettl, *Nano Lett.* 14 (2014) 4280–4285.
- [95] S. Sathiеш Kumar, S. Vairam, N. Neelakandeswari, S. Aruna, *SoEn* 166 (2018) 195–202.
- [96] S. Sathiesh Kumar, S. Vairam, N. Neelakandeswari, S. Aruna, *Mater. Lett.* 220 (2018) 249–252.
- [97] K.M. Chen, Y.Q. Jia, S.X. Jin, K. Wu, X.D. Zhang, W.B. Zhao, C.Y. Li, Z.N. Gu, *J. Phys.: Condens. Matter* 6 (1994) L367–L372.
- [98] J.T. Hu, M. Ouyang, P.D. Yang, C.M. Lieber, *Nature* 399 (1999) 48–51.
- [99] K. Kita, C. Wen, M. Ihara, K. Yamada, *J. Appl. Phys.* 79 (1996) 2798–2800.
- [100] Z.Q. Ma, B.X. Liu, *Sol. Energy Mater. Sol. Cells* 69 (2001) 339–344.
- [101] B. Gupta, A. Kapoor, R.M. Mehra, T. Soga, T. Jimbo, M. Umeno, *Sol. Energy Mater. Sol. Cells* 79 (2003) 305–311.
- [102] K.S. Novoselov, A.K. Geim, S.V. Morozov, D. Jiang, Y. Zhang, S.V. Dubonos, I. V. Grigorieva, A.A. Firsov, *Science* 306 (2004) 666–669.
- [103] T.H. Chowdhury, A. Islam, A.K.M. Hasan, M.A.M. Terdi, M. Arunakumari, S. P. Singh, M.K. Alam, I.M. Bedja, M.H. Ruslan, K. Sopian, N. Amin, M. Akhtaruzzaman, *Chem. Rec.* 16 (2016) 614–632.
- [104] G. Yu, J. Gao, J.C. Hummelen, F. Wudl, A.J. Heeger, *Science* 270 (1995) 1789–1791.
- [105] E. Singh, H.S. Nalwa, J. Nanosci. Nanotechnol. 15 (2015) 6237–6278.
- [106] M. Al-Ibrahim, H.K. Roth, M. Schroedner, A. Konkin, U. Zhokhavets, G. Gobsch, P. Scharff, S. Sensfuss, *Org. Electron.* 6 (2005) 65–77.
- [107] Z. Liu, Q. Liu, Y. Huang, Y. Ma, S. Yin, X. Zhang, W. Sun, Y. Chen, *Adv. Mater.* 20 (2008) 3924–3930.
- [108] V. Singh, S. Arora, M. Arora, V. Sharma, R.P. Tandon, *Phys. Lett. A* 378 (2014) 3046–3054.
- [109] B. Li, X. Yu, L. Jia, M. Zhang, W. Hu, Y. Shang, X. Li, L. Ding, J. Xu, S. Yang, *ACS Appl. Mater. Interfaces* 12 (2020) 37265–37274.
- [110] X. Hu, P. Hou, C. Liu, H. Cheng, *Nano Mater. Sci.* 1 (2019) 156–172.
- [111] F. Wang, D. Koizawa, Y. Miyachi, K. Hiraoka, S. Mouri, Y. Ohno, K. Matsuda, *Nat. Commun.* 6 (2015) 6305.
- [112] Y. Lu, Z. Wu, W. Xu, S. Lin, *Nanot* 27 (2016) 48LT03.
- [113] Z. Wu, X. Li, H. Zhong, S. Zhang, P. Wang, T.-H. Kim, S.S. Kwak, C. Liu, H. Chen, S.-W. Kim, S. Lin, *Opt. Express* 23 (2015) 18864–18871.
- [114] X. Zhao, H. Wu, L. Yang, Y. Wu, Y. Sun, Y. Shang, A. Cao, *Carbon* 147 (2019) 164–171.
- [115] H. Bi, R.R. LaPierre, *Nanot* 20 (2009), 465205.
- [116] X. Yang, J. Guo, Y. Zhang, W. Liu, Y. Sun, *J. Alloy. Compd.* 747 (2018) 563–570.
- [117] D.P. Pham, S. Lee, S. Kim, S. Chowdhury, M.Q. Khokhar, A.H. Tuan Le, Y. Kim, J. Park, J. Yi, *Mater. Sci. Semicond. Process.* 121 (2021), 105344.
- [118] Y. Liu, K. Dong, L. Bian, Z. Guan, *Crystals* 11 (2021) 459.
- [119] E. Muramoto, Y. Yamasaki, F. Wang, K. Hasegawa, K. Matsuda, S. Noda, *RSC Adv.* 6 (2016) 93575–93581.
- [120] K. Cui, S. Maruyama, *Progr. Energy Combust. Sci.* 70 (2019) 1–21.
- [121] E. Shi, L. Zhang, Z. Li, P. Li, Y. Shang, Y. Jia, J. Wei, K. Wang, H. Zhu, D. Wu, S. Zhang, A. Cao, *Sci. Rep.* 2 (2012) 884.
- [122] X. Huang, R. Xie, H. Sugime, S. Noda, *Appl. Surf. Sci.* 542 (2021), 148682.
- [123] X. Zhao, W. Xu, Y. Wu, H. Wu, Z. Xia, H. Xu, Y. Shang, J. Wei, A. Cao, *Nano Res.* 15 (2021) 2497–2504.
- [124] Y. Jia, P. Li, X. Gui, J. Wei, K. Wang, H. Zhu, D. Wu, L. Zhang, A. Cao, Y. Xu, *Appl. Phys. Lett.* 98 (2011).
- [125] L. Yu, D.D. Tunc, C.J. Shearer, J.G. Shapter, *SoEn* 118 (2015) 592–599.
- [126] Q. Fan, Q. Zhang, W. Zhou, X. Xia, F. Yang, N. Zhang, S. Xiao, K. Li, X. Gu, Z. Xiao, H. Chen, Y. Wang, H. Liu, W. Zhou, S. Xie, *Nano Energy* 33 (2017) 436–444.
- [127] X. Zhao, Y. Wu, Z. Xia, S. Chang, Y. Shang, A. Cao, *Nano Res.* 14 (2021) 3893–3899.
- [128] L. Chen, S. Zhang, L. Chang, L. Zeng, X. Yu, J. Zhao, S. Zhao, Y. Mi, D. Yang, *Nanoscale Res. Lett.* 8 (2013) 225.
- [129] L. Chen, H. He, S. Zhang, C. Xu, J. Zhao, S. Zhao, Y. Mi, D. Yang, *Nanoscale Res. Lett.* 8 (2013) 225.
- [130] L. Chen, H. Yu, J. Zhong, H. He, T. Zhang, *Electrochim. Acta* 178 (2015) 732–738.
- [131] S. Wu, L. Yang, H. Wu, Y. Yuan, Z. Ji, A. Cao, *ChemistrySelect* 3 (2018) 9736–9742.
- [132] A. Pujari, T. Thomas, *Sustain. Mater. Technol.* 28 (2021), e00250.
- [133] D.S. Kopylova, D.A. Satco, E.M. Khabushev, A.V. Bubis, D.V. Krasnikov, T. Kallio, A.G. Nasibulin, *Carbon* 167 (2020) 244–248.
- [134] X. Bai, H. Wang, J. Wei, Y. Jia, H. Zhu, K. Wang, D. Wu, *Chem. Phys. Lett.* 533 (2012) 70–73.
- [135] L. Yu, T. Grace, M. Batmunkh, M. Dadkhah, C. Shearer, J. Shapter, J. Mater. Chem. A 5 (2017) 24247–24256.
- [136] J. Han, J.S. Nam, S. Seo, A. Lee, C. Lee, S. Park, Y. Kang, H.S. Lee, D. Kim, Q. Zhang, H. Sung, E.I. Kauppinen, H. Jeong, J.W. Oh, S. Maruyama, I.D. Jung, I. Jeon, *Adv. Energy Sustain. Res.* 3 (2022) 2100155.
- [137] Y. Jia, Z. Zhang, L. Xiao, R. Lv, *Nanoscale Res. Lett.* 11 (2016) 299.
- [138] S. Freddi, S. Achilli, R. Soave, S. Pagliara, G. Drera, A. De Poli, F. De Nicola, M. De Crescenzi, P. Castrucci, L. Sangalli, *J. Colloid Interface Sci.* 566 (2020) 60–68.
- [139] X.-G. Hu, P.-X. Hou, J.-B. Wu, X. Li, J. Luan, C. Liu, G. Liu, H.-M. Cheng, *Nano Energy* 69 (2020), 104442.
- [140] M.C. Lonergan, *Science* 278 (1997) 2103–2106.
- [141] M.K. Petterson, M.G. Lemaitre, Y. Shen, P. Wadhwa, J. Hou, S.V. Vasiliyeva, I. I. Kravchenko, A.G. Rinzler, *ACS Appl. Mater. Interfaces* 7 (2015) 21182–21187.
- [142] P. Wadhwa, B. Liu, M.A. McCarthy, Z. Wu, A.G. Rinzler, *Nano Lett.* 10 (2010) 5001–5005.
- [143] P. Wadhwa, G. Seol, M.K. Petterson, J. Guo, A.G. Rinzler, *Nano Lett.* 11 (2011) 2419–2423.
- [144] W. Chen, G. Seol, A.G. Rinzler, J. Guo, *Appl. Phys. Lett.* 100 (2012), 103503.
- [145] K. Cui, Y. Qian, I. Jeon, A. Anisimov, Y. Matsuo, E.I. Kauppinen, S. Maruyama, *Adv. Energy Mater.* 7 (2017) 1700449.

- [146] M. Bat-Erdene, M. Batmunkh, S.A. Tawfik, M. Fronzi, M.J. Ford, C.J. Shearer, L. Yu, M. Dadkhah, J.R. Gascooke, C.T. Gibson, J.G. Shapter, *Adv. Funct. Mater.* 27 (2017) 1704488.
- [147] Y. Zhou, Z. Wang, T. Saito, T. Miyadera, M. Chikamatsu, S. Shimada, R. Azumi, *RSC Adv.* 6 (2016) 25062–25069.
- [148] H. Wang, X. Bai, J. Wei, P. Li, Y. Jia, H. Zhu, K. Wang, D. Wu, *Mater. Lett.* 79 (2012) 106–108.
- [149] B. Sun, D. Zhou, C. Wang, P. Liu, Y. Hao, D. Han, L. Feng, Y. Zhou, *Org. Electron.* 44 (2017) 176–182.
- [150] X.-G. Hu, Q. Wei, Y.-M. Zhao, P.-X. Hou, W. Ren, C. Liu, H.-M. Cheng, *J. Mater. Chem. A* 10 (2022) 4644–4652.
- [151] Y. Jin, T. Zhang, J. Zhao, Y. Zhao, C. Liu, J. Song, X. Hao, J. Wang, K. Jiang, S. Fan, Q. Li, *Carbon* 178 (2021) 616–624.
- [152] T. Yan, Y. Wu, W. Yi, Z. Pan, *Sens. Actuators a-Phys.* 327 (2021), 112755.
- [153] X. Li, C. Zhuang, J. Xu, L. Li, T. Xu, S. Dai, X. Wang, X. Li, Y. Wang, *Nanoscale* 13 (2021) 8199–8209.
- [154] N. Dwivedi, C. Dhand, E.C. Anderson, R. Kumar, B. Liao, R.J. Yeo, R. Khan, J. D. Carey, M.S.M. Saifullah, S. Kumar, H.K. Malik, S.A.R. Hashmi, A.K. Srivastava, S.K.R.S. Sankaranarayanan, R. Stangl, S. Duttagupta, *Adv. Electron. Mater.* 6 (2020) 2000617.
- [155] K. Wu, Y. Niu, Y. Zhang, Z. Yong, Q. Li, *Compos. Part A Appl. Sci. Manuf.* 144 (2021), 106359.
- [156] J. Di, Z. Yong, X. Zheng, B. Sun, Q. Li, *Small* 9 (2013) 1367–1372.
- [157] E. Shi, H. Li, W. Xu, S. Wu, J. Wei, Y. Fang, A. Cao, *Nano Energy* 17 (2015) 216–223.
- [158] L. Yu, M. Batmunkh, M. Dadkhah, C.J. Shearer, J.G. Shapter, *Energy Environ. Mater.* 1 (2018) 232–240.
- [159] X. Li, Y. Jung, C.-S. Huang, T. Goh, A.D. Taylor, *Adv. Energy Mater.* 4 (2014) 1400186.
- [160] S. Xiao, Q. Fan, X. Xia, Z. Xiao, H. Chen, W. Xi, P. Chen, J. Li, Y. Wang, H. Liu, W. Zhou, *Chin. Phys. B* 27 (2018), 078801.
- [161] Y. Jia, A. Cao, F. Kang, P. Li, X. Gui, L. Zhang, E. Shi, J. Wei, K. Wang, H. Zhu, D. Wu, *Phys. Chem. Chem. Phys.* 14 (2012) 8391–8396.
- [162] R. Xie, N. Ishijima, H. Sugime, S. Noda, *Sci. Rep.* 9 (2019) 12051.
- [163] W. Lin, J. Dreon, S. Zhong, V. Paratte, L. Antognini, J. Cattin, Z. Liu, Z. Liang, P. Gao, H. Shen, C. Ballif, M. Boccard, *Sol. RRL* 5 (2021) 202000771.
- [164] Y. Wan, C. Samundsett, J. Bullock, M. Hettick, T. Allen, D. Yan, J. Peng, Y. Wu, J. Cui, A. Javey, A. Cuevas, *Adv. Energy Mater.* 7 (2017) 1601863.
- [165] D. Amelot, M. Ahmadpour, Q. Ros, H. Cruguel, N. Casaretto, A. Cossaro, L. Floreano, M. Madsen, N. Witkowski, *ACS Appl. Mater. Interfaces* 13 (2021) 19460–19466.
- [166] Y. Jiang, S. Cao, L. Lu, G. Du, Y. Lin, J. Wang, L. Yang, W. Zhu, D. Li, *Nanoscale Res. Lett.* 16 (2021) 87.
- [167] S. Li, Y.-L. Cao, W.-H. Li, Z.-S. Bo, *Rare Met.* (2021) 2712–2729.
- [168] J. Kumari, P. Basumatary, M.S. Gangwar, P. Agarwal, *Mater. Today-Proc.* 39 (2021) 1996–1999.
- [169] H.-S. Lin, T. Kaneko, S. Ishikawa, I. Jeon, S. Chae, T. Yana, N. Saito, Y. Matsuo, *Jpn. J. Appl. Phys.* 60 (2021), 070902.
- [170] C. Yang, R. Yu, C. Liu, H. Li, S. Zhang, J. Hou, *ChemSusChem* 14 (2021) 3607–3613.
- [171] D.D. Tune, B.S. Flavel, J.S. Quinton, A.V. Ellis, J.G. Shapter, *ChemSusChem* 6 (2013) 320–327.
- [172] L. Yu, D.D. Tune, C.J. Shearer, J.G. Shapter, *ChemNanoMat* 1 (2015) 115–121.
- [173] L. Yu, M. Batmunkh, T. Grace, M. Dadkhah, C. Shearer, J. Shapter, *J. Mater. Chem. A* 5 (2017) 8624–8634.
- [174] L. Yu, T. Grace, H.D. Pham, M. Batmunkh, M. Dadkhah, C. Shearer, P. Sonar, J. Shapter, *Aust. J. Chem.* 70 (2017) 1202.
- [175] J. Chen, K. Ge, C. Zhang, J. Guo, L. Yang, D. Song, F. Li, Z. Xu, Y. Xu, Y. Mai, *ACS Appl. Mater. Interfaces* 10 (2018) 44890–44896.
- [176] W. Ji, Y. Zhao, H.M. Fahad, J. Bullock, T. Allen, D.-H. Lien, S. De Wolf, A. Javey, *ACS Nano* 13 (2019) 3723–3729.
- [177] L. Wan, C. Zhang, K. Ge, X. Yang, F. Li, W. Yan, Z. Xu, L. Yang, Y. Xu, D. Song, J. Chen, *Adv. Energy Mater.* 10 (2020) 1903851.
- [178] D.D. Tune, N. Mallik, H. Fornasier, B.S. Flavel, *Adv. Energy Mater.* 10 (2019) 1903261.
- [179] Y. Qian, I. Jeon, Y.-L. Ho, C. Lee, S. Jeong, C. Delacou, S. Seo, A. Anisimov, E. I. Kaupinen, Y. Matsuo, Y. Kang, H.-S. Lee, D. Kim, J.-J. Delaunay, S. Maruyama, *Adv. Energy Mater.* 10 (2020) 1902389.
- [180] X. Fu, L. Xu, J. Li, X. Sun, H. Peng, *Carbon* 139 (2018) 1063–1073.
- [181] S. He, P. Chen, L. Qiu, B. Wang, X. Sun, Y. Xu, H. Peng, *Angew. Chem. Int. Ed.* 54 (2015) 14880–14884.
- [182] I.-Y. Jeon, H.M. Kim, I.T. Choi, K. Lim, J. Ko, J.C. Kim, H.-J. Choi, M.J. Ju, J.-J. Lee, H.K. Kim, J.-B. Baek, *Nano Energy* 13 (2015) 336–345.
- [183] M.A.K.L. Dissanayake, J.M.K.W. Kumari, G.K.R. Senadeera, T. Jaseetharan, J. Weerasinghe, H. Anwar, *Mater. Sci. Eng. B-Adv. Funct. Solid-State Mater.* 273 (2021), 115440.
- [184] J. Ma, W. Shen, F. Yu, *J. Power Sources* 351 (2017) 58–66.
- [185] M.A.K.L. Dissanayake, J.M.K.W. Kumari, G.K.R. Senadeera, H. Anwar, *SoEn* 230 (2021) 151–165.
- [186] T. Chen, L. Qiu, Z. Cai, F. Gong, Z. Yang, Z. Wang, H. Peng, *Nano Lett.* 12 (2012) 2568–2572.
- [187] I.F. Dominguez, A. Distler, L. Luer, *Adv. Energy Mater.* 7 (2017) 1601320.
- [188] Z. Zhang, L. Wei, X. Qin, Y. Li, *Nano Energy* 15 (2015) 490–522.
- [189] W.S. Yang, B.-W. Park, E.H. Jung, N.J. Jeon, Y.C. Kim, D.U. Lee, S.S. Shin, J. Seo, E.K. Kim, J.H. Noh, S.I. Seok, *Science* 356 (2017) 1376.
- [190] H. Sun, J. Wei, Y. Jia, X. Cui, K. Wang, D. Wu, *Nanoscale Res. Lett.* 9 (2014) 514.
- [191] X. Li, M. Mariano, L. McMillon-Brown, J.S. Huang, M.Y. Sfeir, M.A. Reed, Y. Jung, A.D. Taylor, *Small* 13 (2017) 1702387.
- [192] S. Das, M.J. Hossain, S.-F. Leung, A. Lenox, Y. Jung, K. Davis, J.-H. He, T. Roy, *Nano Energy* 58 (2019) 47–56.
- [193] S. Li, Z. Pei, F. Zhou, Y. Liu, H. Hu, S. Ji, C. Ye, *Nano Res.* 8 (2015) 3141–3149.
- [194] T. Jiao, D. Wei, J. Liu, W. Sun, S. Jia, W. Zhang, Y. Feng, H. Shi, C. Du, *R.S.C. Adv.* 5 (2015) 73202–73206.
- [195] X.-G. Hu, P.-X. Hou, C. Liu, F. Zhang, G. Liu, H.-M. Cheng, *Nano Energy* 50 (2018) 521–527.
- [196] S.V. Sawant, A.W. Patwardhan, J.B. Joshi, K. Dasgupta, *Chem. Eng. J.* 427 (2022), 131616.
- [197] L. Wieland, H. Li, C. Rust, J. Chen, B.S. Flavel, *Adv. Energy Mater.* 11 (2020) 2002880.
- [198] K. Yoshikawa, W. Yoshida, T. Irie, H. Kawasaki, K. Konishi, H. Ishibashi, T. Asatani, D. Adachi, M. Kanematsu, H. Uzu, K. Yamamoto, *Sol. Energy Mater. Sol. Cells* 173 (2017) 37–42.
- [199] A. Richter, M. Hermle, S.W. Glunz, *IEEE J. Photovolt.* 3 (2013) 1184–1191.
- [200] M. Green, E. Dunlop, J. Hohl-Ebinger, M. Yoshita, N. Kopidakis, X. Hao, *Prog. Photovolt. Res. Appl.* 29 (2020) 3–15.
- [201] A. Polman, M. Knight, E.C. Garnett, B. Ehrler, W.C. Sinke, *Science* 352 (2016) aad4424.
- [202] X. Li, X. Zang, X. Li, M. Zhu, Q. Chen, K. Wang, M. Zhong, J. Wei, D. Wu, H. Zhu, *Adv. Energy Mater.* 4 (2014) 1400224.
- [203] Y. Mo, W. Meng, Y. Xia, X. Du, Z. Lin, W. Li, *Electrochim. Acta* 335 (2020), 135527.
- [204] Y. Mo, W. Meng, Y. Xia, X. Du, *Polymers* 11 (2019) 1357.
- [205] N. Yadav, S.A. Hashmi, *J. Mater. Chem. A* 8 (2020) 18266–18279.
- [206] Y. Tian, C. Yang, Y. Tang, Y. Luo, X. Lou, W. Que, *Chem. Eng. J.* 393 (2020), 124790.
- [207] L. Chen, C. Wu, W. Qin, X. Wang, C. Jia, *J. Colloid Interface Sci.* 577 (2020) 12–18.
- [208] K. Makita, H. Mizuno, T. Tayagaki, T. Aihara, R. Oshima, Y. Shoji, H. Sai, H. Takato, R. Müller, P. Beutel, D. Lackner, J. Benick, M. Hermle, F. Dimroth, T. Sugaya, *Prog. Photovolt. Res. Appl.* 28 (2019) 16–24.
- [209] Y.-H. Chiang, C.-C. Peng, Y.-H. Chen, Y.-L. Tung, S.-Y. Tsai, P. Chen, *J. Phys. D* 51 (2018), 424002.
- [210] S. Kim, D.-M. Geum, M.-S. Park, C.Z. Kim, W.J. Choi, *Sol. Energy Mater. Sol. Cells* 141 (2015) 372–376.
- [211] B. Hagar, I. Sayed, P.C. Colter, S.M. Bedair, *Sol. Energy Mater. Sol. Cells* 215 (2020), 110653.



Wenliang Wang received his bachelor's (2011) and Ph.D. (2016) degrees in materials science from Fuzhou University and South China University of Technology, respectively. From 2016–2021, he worked in turn at South China University of Technology, and the Hong Kong University Science and Technology, respectively. He is currently an associate professor in State Key Laboratory of Luminescent Materials and Devices, South China University of Technology. His research interests focus on the III-V compound semiconductor materials and devices, including solar cells, photodetectors.



Guoqiang Li received his Ph.D. degree from Northwestern Polytechnical University, China, in 2004. From 2004–2010, he worked in turn at GE Global Research Center in China, the University of Tokyo, Japan, and University of Oxford, UK. Since 2010, he has been a full professor in South China University of Technology, China. His research group mainly focuses on the epitaxial growth of compound semiconductor materials (particularly, III-V compounds), and fabrication of relevant optoelectronic devices (particularly, solar cells, LEDs, HEMTs and photodetectors).